

*Russian Original Vol. 59, No. 3, September, 1985*

March, 1986

FILE

SATEAZ 59(3) 715-788 (1985)

# SOVIET ATOMIC ENERGY

АТОМНАЯ ЭНЕРГИЯ  
(ATOMNAYA ÉNERGIYA)

TRANSLATED FROM RUSSIAN



CONSULTANTS BUREAU, NEW YORK

# SOVIET ATOMIC ENERGY

*Soviet Atomic Energy* is abstracted or indexed in *Chemical Abstracts*, *Chemical Titles*, *Pollution Abstracts*, *Science Research Abstracts*, *Parts A and B*, *Safety Science Abstracts Journal*, *Current Contents*, *Energy Research Abstracts*, and *Engineering Index*.

*Soviet Atomic Energy* is a translation of *Atomnaya Energiya*, a publication of the Academy of Sciences of the USSR.

An agreement with the Copyright Agency of the USSR (VAAP) makes available both advance copies of the Russian journal and original glossy photographs and artwork. This serves to decrease the necessary time lag between publication of the original and publication of the translation and helps to improve the quality of the latter. The translation began with the first issue of the Russian journal.

## Editorial Board of *Atomnaya Energiya*:

**Editor:** O. D. Kazachkovskii

**Associate Editors:** A. I. Artemov, N. N. Ponomarev-Stepnoi, and N. A. Vlasov

I. A. Arkhangel'skii	A. M. Petras'yants
I. V. Chuvilo	E. P. Ryazantsev
I. Ya. Emel'yanov	A. S. Shtan
I. N. Golovin	B. A. Sidorenko
V. I. Il'ichev	Yu. V. Sivintsev
P. L. Kirillov	M. F. Troyano
Yu. I. Koryakin	V. A. Tsykanov
E. V. Kulov	E. I. Vorob'ev
B. N. Laskorin	V. F. Zelenskii
V. V. Matveev	

Copyright © 1986, Plenum Publishing Corporation. *Soviet Atomic Energy* participates in the Copyright Clearance Center (CCC) Transactional Reporting Service. The appearance of a code line at the bottom of the first page of an article in this journal indicates the copyright owner's consent that copies of the article may be made for personal or internal use. However, this consent is given on the condition that the copier pay the flat fee of \$9.50 per article (no additional per-page fees) directly to the Copyright Clearance Center, Inc., 27 Congress Street, Salem, Massachusetts 01970, for all copying not explicitly permitted by Sections 107 or 108 of the U.S. Copyright Law. The CCC is a nonprofit clearinghouse for the payment of photocopying fees by libraries and other users registered with the CCC. Therefore, this consent does not extend to other kinds of copying, such as copying for general distribution, for advertising or promotional purposes, for creating new collective works, or for resale, nor to the reprinting of figures, tables, and text excerpts. 0038-531X/85/\$09.50.

Consultants Bureau journals appear about six months after the publication of the original Russian issue. For bibliographic accuracy, the English issue published by Consultants Bureau carries the same number and date as the original Russian from which it was translated. For example, a Russian issue published in December will appear in a Consultants Bureau English translation about the following June, but the translation issue will carry the December date. When ordering any volume or particular issue of a Consultants Bureau journal, please specify the date and, where applicable, the volume and issue numbers of the original Russian. The material you will receive will be a translation of that Russian volume or issue.

## Subscription (2 volumes per year)

Vols. 58 & 59: \$645 (domestic); \$715 (foreign)      Single Issue: \$100  
Vols. 60 & 61: \$695 (domestic); \$770 (foreign)      Single Article: \$9.50

## CONSULTANTS BUREAU, NEW YORK AND LONDON



233 Spring Street  
New York, New York 10013

Published monthly. Second-class postage paid at Jamaica, New York 11431.

Mailed in the USA by Publications Expediting, Inc., 200 Meacham Avenue, Elmont, NY 11003.

**POSTMASTER:** Send address changes to *Soviet Atomic Energy*, Plenum Publishing Corporation, 233 Spring Street, New York, NY 10013.

**SUVIET ATOMIC ENERGY**A translation of *Atomnaya Énergiya*

March, 1986

Volume 59, Number 3

September, 1985

**CONTENTS**

Engl./Russ.

Analysis of Harmonic Control Systems of Power Distribution in a Reactor - O. L. Bozhenkov and P. T. Potapenko.....	715	183
Using Time Power Series to Take Account of Nonuniform Fuel Burnup in Reactors - I. S. Akimov and F. T. Tukhvetov.....	720	187
Temperature Conditions of the Irradiation of Fuel Elements of the BOR-60 Reactor - V. D. Grachev and R. R. Mel'der.....	726	191
Irradiation Strengthening of Metals - I. V. Gorynin, S. I. Aleksandrov, and V. D. Yaroshevich.....	731	194
Gas Evolution from Absorbing Materials - I. G. Gverdtsiteli, Sh. P. Abramidze, A. G. Kalandarishvili, G. S. Karumidze, and V. A. Kuchukhidze.....	736	197
Effect of Composition and Structural State on the Radiation- Induced Swelling of High-Nickel Alloys - V. A. Nikolaev, I. P. Kursevich, O. N. Zhukov, and A. N. Lapin.....	740	200
Radiolysis of Aqueous Solutions of Gadolinium Nitrate - V. D. Ganzha, K. A. Konoplev, V. P. Mashchetov, S. P. Orlov, and V. D. Trenin.....	746	204
Selection of the Material and the Temperature Conditions of the Pickup Plate of a Fast-Ion Injector - V. G. Tel'kovskii, A. A. Pisarev, V. N. Tsyplakov, and A. N. Igritskii.....	753	209
Using the Concept of Radiation Capacity in Calculations of the Greatest Admissible Waste Release - A. L. Kononovich, N. A. Verkhovetskii, V. I. Peshkov, and S. V. Bezmenov.....	759	213
Choosing the Method of Calculating the Impurity Scattering in the Atmosphere with Normalization of the Radionuclide Emission from High Sources - N. E. Artemova.....	763	216
Distribution of $^{137}\text{Cs}$ in the Samples of Ocean Bottom Sediments of the Baltic Sea in 1982-1983 - L. I. Gedeonov, L. M. Ivanova, K. A. Kostandov, and V. M. Flegontov.....	769	221
<b>LETTERS TO THE EDITOR</b>		
Corrosion Resistance of OKh18N10T Steel in Gadolinium Nitrate Solutions in the Liquid Regulation of the Reactivity of Nuclear Reactors - V. D. Ganzha, K. A. Konoplev, V. P. Mashchetov, S. P. Orlov, and A. A. Ukhanev.....	772	224
Effect of Corrosion of Fuel-Element Jackets of Fast Reactors on Their Mechanical Properties - E. F. Davydov, F. N. Kryukov, and V. K. Shamardin.....	775	226

(continued)

Engl./Russ.

Magnetic Resonance Methods Used to Study the Mobility of Lithium Ions and the Formation of Gamma Radiolysis Products in Lithium Silicates - I. S. Pronin, A. A. Vashman, and A. S. Nikiforov.....	778	227
Measuring the Content by Volume of Deuterium in Heavy Water with Carbon Dioxide Dissolved in It - T. I. Efimova, V. F. Kapitanov, and G. V. Levchenko.....	781	229
Using the Theory of Small Perturbations in Performance Calculations of the RBMK - N. V. Isaev, Yu. V. Shmonin, L. R. Pogosbekyan, and V. E. Druzhinin.....	783	230
Changes in the Microhardness of SiC(6H) Samples in Neutron Irradiation - V. N. Brudnyi and B. T. Tolebaev.....	787	232

The Russian press date (podpisano k pechatl) of this issue was 8/26/1985.  
Publication therefore did not occur prior to this date, but must be assumed  
to have taken place reasonably soon thereafter.

ANALYSIS OF HARMONIC CONTROL SYSTEMS OF POWER DISTRIBUTION  
IN A REACTOR

O. L. Bozhenkov and P. T. Potapenko

UDC 621.039.56

An algorithm for local (zonal) control of power distribution is widely used in Soviet and non-Soviet power reactors [1-4]. Scientific and engineering problems associated with the design and implementation of a local automatic control (LAC) system for the RBMK power reactor have been successfully solved [1-3].

This paper investigates a comparatively new algorithm of harmonic (modal) control of power distribution. Harmonic automatic control (HAC) systems were described in [4, 5], and their efficiency was also considered in these references, but methods of analysis of such systems remain largely undeveloped. A digital reactor simulation program [6, 7] provided the methodological basis for our study. Our approach to power distribution control systems based on the harmonic model of the controlled reactor enabled us to establish analytical criteria and to derive qualitative estimates of stability, efficiency, and noise-tolerance of various control structures. We assume a fast-response control system (the regulating time is small compared with the time constants of nonstationary processes), which is astatic, has an arbitrary structure characterized by the observation matrix  $C$  and the control matrix  $U$ , with  $L$  control rods and  $M$  sensors, and is designed to suppress  $N$  harmonics (Fig. 1). The reactor transfer matrix has the form [7]

$$H(p) = D\tilde{W}(p)Z + S, \quad (1)$$

where  $Z$  is the static disturbance matrix - the reactivity due to the harmonics,  $\mu \times L$ ;  $D$ , static matrix of the sensor sensitivities to the harmonic amplitudes,  $M \times \mu$ ;  $W(p)$ , diagonal matrix of the transfer functions of the inertial harmonic components,  $\mu \times \mu$ ;  $S$ , matrix of influence functions representing the effect of the moving control rods on the prompt neutron power distribution,  $M \times L$ ;  $\mu$ , number of inertial harmonic components used in the model ( $\mu > N$ ).

In accordance with this model, the observability and controllability conditions for the harmonics may be written in the form

$$\text{rank}(CD) = N; \text{rank}(ZU) = N. \quad (2)$$

In what follows we assume that the conditions (2) are satisfied.

The static transfer matrices of the stable harmonic components, whose time constant is small compared with the characteristic periods of unstable deformations, may be incorporated in the influence matrix due to fast movements  $S^*$ ,

$$S^* = S + DZ_s, \quad (3)$$

where the subscript  $s$  denotes stable harmonics.

Once reference setting vector  $\Delta$  has been determined, the control  $p$  of the power distribution control system may be obtained from the equation

$$CDF_u + CS_p = \Delta, \quad (4)$$

where  $F_u$  is the amplitude vector of the unstable harmonic components. A necessary condition for nondegeneracy of the fast-movement control system is given by

$$\text{rank}(CS^*) = N. \quad (5)$$

A system with a large number of control rods ( $L > N$ ) has infinitely many solutions, yet it is effective [5] if condition (5) is satisfied. For definiteness, we assume that for  $L > N$  the power distribution control system minimizes the quadratic norm of the control vector. Then, for the general case  $L \geq N$ ,

Translated from *Atomnaya Énergiya*, Vol. 59, No. 3, pp. 183-187, September, 1985. Original article submitted May 7, 1984.

$$\mathbf{p} = (CS^*)^+ \{\Delta - CDE_u\}, \quad (6)$$

In channel reactors fast feedbacks alone ensure a stable radial distribution of power, whereas a positive graphite temperature coefficient of reactivity produces an unstable distribution. To first approximation, we may ignore the variation of poisoning as a much slower effect than the deviation of graphite temperature [4]. In this case, considering the aperiodic growth of the inertial harmonic components, we find that the stabilizing action of the control system on the neutron field is characterized by the expression

$$\mathbf{F}_n = \{\text{diag}(1/T_i)\} \{Z_u(CS^*)^* \Delta + [I - Z_u(CS^*)^* CD] \mathbf{F}_u\}, \quad (7)$$

$$\omega_i < 0 \quad \text{for } i = 1, 2, \dots, N, \quad (8)$$

A basic requirement for control systems is the existence of steady-state coordinate values after the reference setting vector  $\Delta$  has been determined. In the steady state we have for an astatic controller

$$\Delta = (CS^* - CDZ_u) \rho. \quad (9)$$

This relationship makes it possible to estimate the controls when determining the reference settings and also the sensitivity of the power distribution control system to sensor signal errors  $\delta$ . A necessary condition for nondegeneracy of the structure of the slow-movement control system is

$$\text{rank}(CS^* - CDZ_w) = N. \quad (10)$$

Thus, using (3) and assuming that (10) is satisfied, we write the control vector of the power distribution control system in the form

$$\mathbf{p} = \{CS + CD(Z_s - Z_w)\}^+ \{\Delta - C\delta\}. \quad (11)$$

In order to determine the conditioning and the rank of the matrices in (2), (5), (6), (10), (11) for purposes of analysis of control system efficiency and noise-tolerance, we successfully applied the procedure of singular decomposition [8] with respect to fast movements

$$\|\rho\|_{\Delta}^F \sim \text{cond}\{(CS^*)^+\} \quad (12)$$

and slow movements

$$\|\rho\|_{\Delta}^S \sim \text{cond} \{CS + CD(Z_s - Z_{\eta})\}^+, \quad (13)$$

where  $\{\dots\} = \sigma_{\max}/\sigma_{\min}$  is the conditioning of a matrix with maximum and minimum eigenvalues  $\sigma_{\max}$  and  $\sigma_{\min}$  respectively;  $\|\dots\|$  is the quadratic norm.

The estimates (12) and (13) provide a quantitative characteristic of the spatial noise-tolerance of the systems being compared. The limiting value of the estimates is determined individually for each concrete structure of the power distribution control system and it depends, in particular, on the number of control rods. However, numerous calculations have

TABLE 1. The Reference-Changing Control as a Function of the Distance between the Sensors and the Control Rod in the Spatial Stability Region

$\ell$ , number of cells	$k$ , %/cent	$\rho/\Delta$ , cent/%	
		fast reaction	statics
5	2,0	0,5	$\infty$
6	1,9	0,53	-10,0
8	1,5	0,67	-2,0
12	1,0	1,0	-1,0
20	0,7	1,43	-0,77

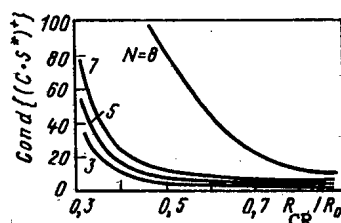


Fig. 2

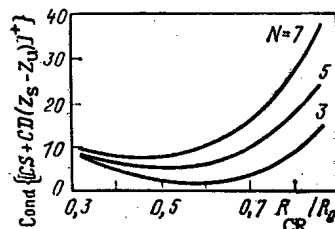


Fig. 3

Fig. 2. The fast-movement sensitivity functional of the HAC-LIC system as a function of the distance between the control rods and the core center for various  $N$  ( $R_0$  is the geometical radius of the core).

Fig. 3. The stabilization functional of the controlled harmonics (in the steady state) for the HAC-LIC system as a function of the distance between the control rods and the core center.

shown that for large values of the estimates (12) and (13) ( $\text{cond}\{\dots\} > 10$ ), the power distribution control system may be classified as unstable (ineffective) with respect to either fast or slow movements, which is manifested in poor spatial noise-tolerance. This leads to substantial travel of the control rods from the nominal position due to small errors in the reference setting or in the sensor signals, resulting in substantial local nonuniformities of the neutron field, which are poorly controlled by the proposed power distribution control system.

Let us demonstrate the proposed procedure for the case of a total-power control system in a reactor with "fast" power coefficient of reactivity  $k_p = +\beta/\Phi$  using a single control rod at the core center. The sensors are several in-core inertialess detectors placed along a circular perimeter at a distance  $\ell$  from the control rod. According to the results of [4], the fundamental harmonic transfer function for the given  $k_p$  has the form

$$W_0(p) = 1 + 2/(T_0 p - 1),$$

where  $T_0 \approx 12$  sec.

The influence function  $S$  is determined using the results of [6].

Thus, with the sensors placed in a smoothed zone,

$$S = k - f(l); Z_s = 0; Z_u = 2; C = D = 1.$$

The system is stable with respect to fast movements for all  $\ell$ , since

$$\det(CS) = k > 0; \rho = 1/k \leq 2 \text{ [cent / \%]}.$$

Stability analysis gives

$$I - Z_u(CS^*)^* CD = (k - 2)/k.$$

Declassified and Approved For Release 2013/02/20 : CIA-RDP10-02196R000300070003-2  
 Therefore,  $k < 2$  is a necessary condition which defines the region of operation of the system parameters. In this case, the sensors should be placed not closer than five cells from the control rod. (The same result can be obtained, say, using the Nyquist criterion.)

Slow-movement noise resistance is given by the expression

$$\rho = \{CS^* + CD(Z_s - Z_u)\}^+ \Delta = \Delta / (k - 2).$$

Table 1 lists the reference-changing controls for various distances between the sensors and the control rod. The sensors clearly should be moved away from the control rod. This minimizes the magnitude of the controls and also the local nonuniformity of the neutron field caused by the movement of the control rod in response to the change in reference setting.

The proposed analytical procedure using matrix criteria was implemented by a package of FORTRAN programs. It proved to be an efficient instrument for studying various structures of harmonic control systems of power distribution in a reactor. The HAC systems assume direct estimation of the amplitudes of a specified number of dominant reactor harmonics from the signals of discrete sensors and movement of the control rods so as to bring these amplitudes in line with the reference settings (which are usually zero) [5]. For HAC systems

$$C = (D')^+; U = (Z')^+,$$

where  $D'$ ,  $Z'$  are submatrices of the matrices  $D$  and  $Z$ , respectively, consisting of columns (rows) corresponding to the controlled harmonics.

As an example, let us consider the results of a comparative analysis of the HAC system using signals from lateral ionization chambers (LIC); eight control rods are placed uniformly over a circle of radius  $R_{CR}$  facing the LIC. The control criteria were taken in the form

$$I_1 = \text{cond} \{ (CS^*)^+ \}; \quad (14)$$

$$I_2 = \text{cond} \{ [CS + CD(Z_s - Z_u)]^+ \}. \quad (15)$$

The results of analysis as a function of the distance between the control rods and the core center for different numbers of controlled azimuthal harmonics are plotted in Figs. 2 and 3. In what follows the HAC-LIC system will be denoted by HAC-N, where  $N$  is the number of controlled "lower" dominant azimuthal harmonics, which determine the spatial-temporal behavior of the neutron field (they have been selected in the order of increasing eigenvalues). Note that in the particular case corresponding to the configuration HAC-8, this system is equivalent to the LAC-LIC system [3], since the product of the matrices  $U$  and  $C$  is a unit diagonal matrix, i.e., structural transformations reduce HAC-8 to the LAC-LIC system.

Our results lead to the following conclusions.

1. The stabilizing action of the HAC system increases as the control rods are moved farther from the sensors, and the stabilizing effect for each of the controlled azimuthal harmonics is independent of the number of these harmonics, being entirely determined by the relative location of the control rods and LICs.
2. As the control rods are moved farther from the LICs, the influence matrix of the control rods on the sensors becomes less conditioned, which leads to deterioration of the noise tolerance of the fast-movement control system.
3. As the control rods are moved closer to the LICs, the control system becomes more sensitive to sensor errors and to changes in the slow-movement reference vector, which causes the control rods to drift as unstable harmonics grow.
4. Noise-tolerance of the power-distribution control system is improved as the number of controlled harmonics is reduced.

Some of the conclusions are consistent with the results of [2, 3, 9, 10], which were obtained using a different methodology with LAC systems. These studies also revealed a conflict between the need to ensure high efficiency and high quality of fast-process control in the neutron field and the attempt to maximize the stabilizing action of the control rods on the power generating field. To corroborate these conclusions, we carried out a numerical comparison of our HAC system using a digital model of the RBMK reactor which incorporates instantaneous control rod influence functions and the dynamic behavior of the "first" 20 dominant harmonics [5, 6]. The limiting estimate of the relative simulation error in accordance with the findings of [6] was 0.8%  $\phi_0$ . The systems were compared using the following performance functionals:

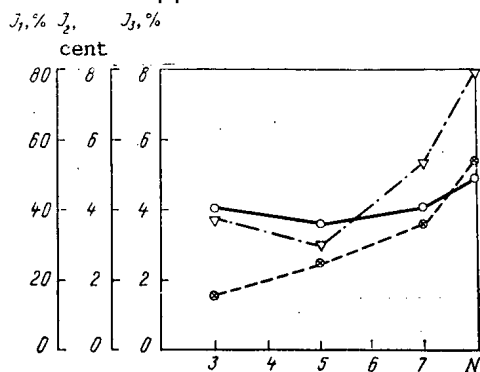


Fig. 4

Fig. 4. The performance functionals of HAC systems as a function of  $N$  for a +1 cent disturbance near LIC ( $R_{CR} = 2/3R_0$ ): O)  $I_1$ ; •)  $I_2$ ; V)  $I_3$ .

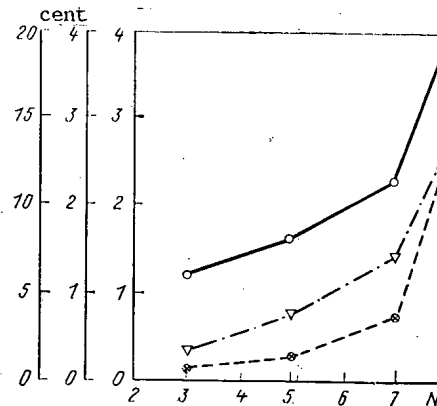


Fig. 5

Fig. 5. The sensitivity functionals of HAC systems as a function of  $N$  for an error of +1%  $\phi_0$  in one of the LICs ( $R_{CR} = 2/3R_0$ ): O)  $I_1$ ; •)  $I_2$ ; V)  $I_3$ .

$$I_1(t) = \left\{ \int_V \varphi^2(r, t) dr \right\}^{1/2}; \quad (16)$$

$$I_2(t) = \sum_{i=1}^L \text{abs}[\rho_i(t)]; \quad (17)$$

$$I_3(t) = \max_{r \in V} \{\text{abs}[\varphi(r, t)]\}, \quad (18)$$

where  $V$  is the core volume.

We estimated the efficiency of suppression of fast deformations ( $t = 50$  sec) by the HAC- $N$  system for various values of  $N$ . The disturbance was represented by a spatial delta-function  $\delta(r - r_j)$ . The calculations show that the systems ensure close performance under disturbances in the smoothed zone, but the HAC-LIC system controlling a small number of the least stable harmonics gives better performance under disturbances at the periphery of the core (near the sensors). Figure 4 plots the functionals (16)-(18) as a function of  $N$  in HAC systems with disturbances near LIC. Analysis of our results shows that small control forces are required in order to suppress the least stable harmonics (the fundamental harmonic and the first azimuthal harmonic), and the main increment of the control performance functional  $I_2$  is attributable to the formation of the neutron field profile due to the higher harmonics in the spatial spectrum. In case of disturbances at the periphery, the neutron field is particularly strongly saturated with the "higher" azimuthal harmonics. This increases the control forces developed by the HAC-8 system stabilizing eight azimuthal harmonics. The growth of the functional (16)-(18) with increasing  $N$  (see Fig. 4) becomes more pronounced as the control rods are placed closer to the center of the reactor (see Fig. 2).

A study of the noise-tolerance of HAC systems by simulation of the control processes corroborated the results of the analytical investigation. A test disturbance simulating an imperfection in the control loop was represented by a +1%  $\phi_0$  error in one of the LIC signals in a stationary neutron field. Figure 5 plots the functionals (16)-(18) versus  $N$ , as a characteristic of noise-tolerance of the control system. We recall that the HAC-8 system is equivalent to the LAC-LIC system. Simulation results also show that in order to increase the noise-tolerance of the power distribution control system,  $N$  must be reduced to the smallest possible value consistent with the practical need of harmonic stabilization and the actual harmonic dynamics. A fast-response control system should not be expected to shape the neutron field profile by regulating the higher harmonics. The purpose of the power distribution control system is to stabilize the least stable harmonics and to regulate the overall reactor power.

We have thus established that in time-domain synthesis of control systems, noise tolerance can be improved by filtering out the high-frequency harmonics of the time-domain spec-

trum, ~~methods in the synthesis of spatial noise~~ harmonics of the spatial spectrum, representing "spatial noise." An appropriate filter is provided by harmonic control systems which make it possible to achieve the required filtering characteristics for each spatial harmonic selectively. The implementation of the space-time filter in reactor control systems utilizing the harmonic control principle with the number of control rods and sensors exceeding the number of controlled harmonics opens certain new control possibilities and in some cases increases control effectiveness.

#### LITERATURE CITED

1. I. Ya. Emel'yanov, A. P. Eperin, A. N. Aleksakov, et al., "An automatic control system of power distribution in a power reactor," *At. Energ.*, 49, No. 6, 357-364 (1980).
2. I. Ya. Emel'yanov, L. N. Podlazov, A. N. Aleksakov, et al., "Synthesis of local automatic control systems for power reactors," *At. Energ.*, 53, No. 5, 301-305 (1982).
3. I. Ya. Emel'yanov, L. N. Podlazov, A. N. Aleksakov, et al., "Synthesis of a power distribution stabilization and power control system for a reactor using lateral ionization chambers," *At. Energ.*, 56, No. 1, 11-15 (1984).
4. E. V. Filipchuk, P. T. Potapenko, and V. V. Postnikov, *Regulation of the Neutron Field in a Nuclear Reactor* [in Russian], Énergoizdat, Moscow (1981).
5. P. T. Potapenko, "Harmonic power control for a power reactor," *At. Energ.*, 50, No. 1, 8-12 (1981).
6. P. T. Potapenko, "Harmonic simulation of a power reactor," *At. Energ.*, 53, No. 3, 151-152 (1982).
7. O. L. Bozhenkov, "A digital harmonic model of the neutron field in a nuclear reactor," in: *Control of Nuclear Power Installations* [in Russian], No. 5, Énergoizdat, Moscow (1981), p. 85.
8. G. E. Forsythe, M. Malcolm, and C. Moler, *Computer Methods for Mathematical Computations*, Prentice-Hall (1977).
9. V. N. Konev and B. Z. Torlin, "A procedure for two-dimensional stability analysis of neutron distribution in a reactor," *At. Energ.*, 53, No. 1, 25-29 (1982).
10. V. N. Konev and B. Z. Torlin, "A well-posed control problem for neutron distribution in a reactor," *At. Energ.*, 54, No. 6, 390-394 (1983).

#### USING TIME POWER SERIES TO TAKE ACCOUNT OF NONUNIFORM FUEL BURNUP IN REACTORS

I. S. Akimov and F. T. Tukhvetov

UDC 621.039.51

The choice of various schemes of partial reloading of fuel assemblies, the sequence of movements of the compensating elements (CE) ensuring the required power distribution in the between-loading period, and a series of other problems associated with determining the power profile varying in the course of fuel burnup in reactors are usually solved as follows.

the reactor is calculated for the beginning of the given time interval with the CE position ensuring both critical conditions and the required power contour;

under the assumption of invariability of the power distribution in the given interval, the energy liberation of each fuel assembly is determined together with the varying (on account of fuel burnup) neutron-physical characteristics of the reactor cells;

calculation is performed for the beginning of the next time interval, with selection of the new CE position, and so on.

Certain changes in this scheme are possible, but the assumption of constancy of the neutron-flux distribution in the course of the time step is usually retained. This imposes definite constraints on the length of the given time intervals. In addition, such calculation schemes are difficult to automate.

---

Translated from *Atomnaya Énergiya*, Vol. 59, No. 3, pp. 187-190, September, 1985. Original article submitted October 30, 1984.

Another method is possible, associated with the representation of the neutron-flux distribution in the form of a time power series. It was formulated in [1] and subsequently developed and realized in computer programs for one-dimensional multigroup diffusion equations of the reactor in [2].

In the present work, the problem of applying this approach to operational calculations of the reactors of the Bilibinskii Atomic Central-Heating and Power Plants (BACHPP) is formulated and solved. In formulating and solving the problem, the following considerations are taken into account.

1. The model of the reactor must correspond to the model used in two-dimensional physical calculations of such reactors (this predetermines the use of a two-group diffusional approximation, two-dimensional  $x, y$  geometry, the need to take account of cylindrical absorbers, fuel burnup in each fuel assembly, equilibrium xenon contamination, etc. [3]).

2. As shown by the practice of reactor use at the BACHPP, compensation of the decrease in reactivity margin is by means of withdrawing groups of rods from a small number of CE ( $\sim 4$ ). Series expansion is valid in the time interval during which extraction of the rods is undertaken. The interval is sufficiently short to permit the retention of only the linear terms of the power-series expansion.

#### Formulation of the Problem and Scheme of Solution

It is assumed that the dependence of the group neutron-physical characteristics associated with fuel burnup is known. So as not to burden the exposition with details that do not relate directly to the method of solving the problem, the group equations of the reactor are written in matrix-vector form, without specifying the form of the matrices

$$\hat{L}\varphi + \hat{M}\varphi - \frac{1}{k_{\text{eff}}} \hat{Q}\varphi = 0. \quad (1)$$

Here the matrix  $\hat{L}$  describes the absorption, leakage, and retardation of neutrons;  $\hat{M}$  describes the absorption of neutrons in the CE;  $\hat{Q}$  describes the neutron breeding as a result of nuclear fission of the fuel. It is also assumed that the time dependence of  $\hat{L}$  and  $\hat{Q}$  is known, and the group of CE removed from the reactor in the given time interval is specified.

Following [1, 2],  $\hat{L}(r, t)$ ,  $\hat{Q}(r, t)$ , and  $\hat{M}(r, t)$  and the desired distribution  $\varphi(r, t)$  are written as series in terms of the time  $t$ , retaining only the linear terms of the expansion

$$\begin{aligned} \hat{L}(r, t) &\simeq \hat{L}_0(r) + \hat{L}_1(r) t; \\ \hat{Q}(r, t) &\simeq \hat{Q}_0(r) + \hat{Q}_1(r) t; \\ \varphi(r, t) &\simeq \varphi_0(r) + \varphi_1(r) t; \\ \hat{M}(r, t) &\simeq \hat{M}_0(r) [\hat{I} - \hat{m}(r) wt], \end{aligned} \quad (2)$$

where  $\hat{I}$  is the unit matrix;  $\hat{m}(r) = \hat{I}$  if the CE at point  $r$  is withdrawn,  $\hat{m}(r) = 0$  if the CE at point  $r$  is not withdrawn;  $w$  is the rate of withdrawal of the CE.

Substituting Eq. (2) into Eq. (1) and grouping terms with the same power of  $t$ , it is found that

$$\begin{aligned} \hat{L}_0\varphi_0 + \hat{M}_0\varphi_0 - \frac{1}{k_{\text{eff}}} \hat{Q}_0\varphi_0 &= 0; \\ \hat{L}_0\varphi_1 + \hat{M}_0\varphi_1 - \frac{1}{k_{\text{eff}}} \hat{Q}_0\varphi_1 &= q, \end{aligned} \quad (3)$$

where

$$q(r) = -\hat{L}_1\varphi_0 - \frac{1}{k_{\text{eff}}} \hat{Q}_1\varphi_0 - \hat{M}_0\hat{m}\varphi_0 w.$$

The first relation in Eq. (3) is the usual steady equation of the reactor. The left-hand side of the second relation in Eq. (3) coincides completely with the left-hand side of the first equation, but the right-hand side includes the nonzero neutron source  $q$ , which is a function of the solution of the first equation. This equation may have a steady solution if the value of the source is zero

$$\int_V (q, \varphi^+) dr = 0. \quad (4)$$

Declassified and Approved For Release 2013/02/20 : CIA-RDP10-02196R000300070003-2  
 here the integration extends over the entire volume of the reactor and  $\varphi$  is the value vector function of the neutrons, which is a solution of the equation conjugate with the first relation in Eq. (3)

$$\hat{L}_0^* \varphi^* + \hat{M}_0^* \varphi^* - \frac{1}{k_{ef}} \hat{Q}_0^* \varphi^* = 0. \quad (5)$$

Using Eq. (4), the unknown rate of withdrawal of the absorber  $w$  appearing in the expression for  $q$  may be determined

$$w = \frac{\int_V \left[ \left( -\hat{L}_1 \varphi_0 + \frac{1}{k_{ef}} \hat{Q}_1 \varphi_0 \right), \varphi^* \right] dr}{\int_V (\hat{M}_0 \hat{m} \varphi_0, \varphi^*) dr}. \quad (6)$$

Methods of solving Eq. (5) and the first relation of Eq. (3) are well known. The method of solving the second relation in Eq. (3), proposed in [4] and also used in [2], reduces to summing all the neutron generations stemming from the source  $q$ . The use of this approach for numerical solution of two-dimensional problems leads to a series of difficulties: it does not correspond to a developed scheme of accelerated convergence, requires high precision of the internal iterations in each external iteration (the errors are summed), and in practice does not allow some nonlinear effects, for example, xenon contamination, to be taken into account. The iterative method of [5] is preferable; in this case

$$\varphi_1^{(n+1)} = (\hat{L}_0 + \hat{M}_0)^{-1} \left( q + \frac{1}{k_{ef}} \hat{Q}_0 \varphi_1^{(n)} \right); \quad n=0, 1, \dots \quad (7)$$

In this approach, it is simple to obtain the ordinary scheme of accelerated convergence, high accuracy of the internal iterations is only necessary when performing subsequent external iterations, and it is possible to take account of nonlinear effects. The solution of the equation is not only the vector  $\varphi_1$  obtained from Eq. (7) but also the vector

$$\varphi_1 + A \varphi_0, \quad (8)$$

where  $A$  is a constant determined from the normalization condition.

In the course of solution by the scheme in Eq. (7),  $\varphi_1$  must not contain the component  $\varphi_0$ , since this disrupts convergence. In connection with the possibility of generating this component on account of rounding errors, the use of a solution with some correction was proposed in [6]

$$\varphi_1 - \frac{(\varphi_1, \hat{Q}^* \varphi^*)}{(\varphi_0, \hat{Q}^* \varphi^*)} \varphi_0. \quad (9)$$

#### Description of the Reactor Model and Representation of Group Constants

As already noted, the model and method of solving the descriptive equations for calculating the BACHPP basically correspond to those outlined in [3]: a two-dimensional model in  $x, y$  geometry, a two-group diffusion approximation, a coarse quadratic calculation grid with one point in each cell of the reactor. The reactor fuel assemblies not only differ in the initial enrichment of the fuel but also each one has a different energy liberation, in the general case, and therefore the two-group characteristics of practically all the reactor cells are different. Additional differences are introduced by the deviations in the fuel loading and its enrichment (within the limits of technological tolerances), which are also taken into account in the model (the rating data for all the fuel assemblies are stored in the computer archive of fuel data).

The cylindrical absorbers are also taken into account in accordance with the recommendations of [3]; partially immersed CE are replaced by completely immersed CE with the corresponding reduction in efficiency, which is determined by means of empirical data taking account of the individual burnup of each CE. It is also possible to take account of the equilibrium xenon contamination.

This model completely corresponds to the model of the two-dimensional MTK program developed by the station personnel and used at the BACHPP basically for planning the partial fuel reloadings, determining the reactivity margin of the reactors (using measurements), and predicting the CE movements [7].

$$a(E) = a_0 + a_1 E + a_2 E^2 + a_3 E^3, \quad (10)$$

where  $a_n$  are coefficients. The acceptability of this model of "independent cells" (the properties of the cell depend on the properties of the corresponding fuel assembly) has been confirmed by many years of practical experience in using programs of MKT type at various atomic power plants.

In reactor operation in conditions of partial reloading, fuel assemblies with different energy liberation are present. Suppose that, at the beginning of the time interval in which series expansion with respect to time is employed, the fuel assembly has an energy liberation  $E_0(r)$ . Then any characteristics of the cell represented by Eq. (10) may be rewritten in the following form

$$a(E) = \sum_{n=0}^3 a_n E^n = \sum_{n=0}^3 a_n (E_0 + \varepsilon)^n = \sum_{n=0}^3 a_n^*(E_0) \varepsilon^n, \quad (11)$$

where  $\varepsilon$  is the increment in energy liberation; and

$$\begin{aligned} a_0^*(E_0) &= \sum_{n=0}^3 a_n E_0^n; \\ a_1^*(E_0) &= \sum_{n=1}^3 n a_n E_0^{n-1}; \\ a_2^*(E_0) &= a_2 + 3 a_3 E_0; \\ a_3^*(E_0) &= a_3. \end{aligned}$$

The relation between  $\varepsilon$  and the time  $t$  is

$$\varepsilon(r, t) = \int_0^t P(r, t) dt, \quad (12)$$

where  $P(r, t)$  is the power distribution in the reactor.

Writing  $P(r, t)$  in the form of an expansion

$$P(r, t) = P_0(r) + P_1(r) t, \quad (13)$$

it is found that

$$\varepsilon(r, t) \simeq \left[ P_0(r) + \frac{1}{2} P_1(r) t \right] t. \quad (14)$$

On the other hand, taking into account that

$$P(r, t) = (\Sigma_f, \varphi) \quad (15)$$

( $\Sigma_f$  is the vector of macroscopic fission cross section of the reactor cells) and that  $\Sigma_f$ , like any other group characteristic of the cell, is written in the form of the expansion in Eq. (11), and  $\varphi$  in the form of the expansion in Eq. (2), it is found that

$$P(r, t) = (\Sigma_{f0}, \varphi) + [(\Sigma_{f1}, \varphi_0) P_0 + (\Sigma_{f0}, \varphi_1)] t. \quad (16)$$

Comparing Eqs. (13) and (16), it is found that

$$\begin{aligned} P_0(r) &= (\Sigma_{f0}, \varphi_0); \\ P_1(r) &= (\Sigma_{f0}, \varphi_1) + (\Sigma_{f1}, \varphi_0) P_0. \end{aligned} \quad (17)$$

In calculating  $P_0$  and  $P_1$ , account is also taken of the constancy of the total reactor power

$$\int_V P(r, t) dr = N = \text{const}$$

or

$$\int_V P_0(r) dr = N; \quad \int_V P_1(r) dr = 0. \quad (18)$$

To ensure that the last relation in Eq. (18) is satisfied, Eq. (8) is used, and  $P_1$  and  $\varphi_1$  are corrected

$$\varphi_1^*(r) = \varphi_1(r) - A\varphi_0(r),$$

where

$$A = \frac{\int_V P_1(r) dr}{\int_V P_0(r) dr}.$$

Since all the two-group characteristics of the reactor cells are written in the form in Eqs. (10) and (11) in the given model, the coefficients of the matrices  $\hat{L}$  and  $\hat{Q}$  in Eq. (3) may be simply determined

$$\begin{aligned}\hat{L}_1(r) &= \frac{\partial \hat{L}}{\partial E} \frac{dE}{dt} = \frac{\partial \hat{L}}{\partial E} P_0(r); \\ \hat{Q}_1(r) &= \frac{\partial \hat{Q}}{\partial E} \frac{dE}{dt} = \frac{\partial \hat{Q}}{\partial E} P_0(r).\end{aligned}\quad (20)$$

In Eq. (20), the derivatives  $\partial/\partial E$  and  $d/dt$  are taken at the points  $E = E_0$  and  $t = 0$ , respectively.

As in ordinary two-dimensional calculations, the equilibrium xenon contamination is taken into account using an additional iterative cycle. The contribution of xenon to the macroscopic cross section of thermal-neutron absorption  $\Delta\Sigma(r, t)$  is written in the form of an expansion

$$\Delta\Sigma(r, t) = \Delta\Sigma_0(r) + \Delta\Sigma_1(r) t, \quad (21)$$

where  $\Delta\Sigma_0(r)$  and  $\Delta\Sigma_1(r)$  depend on the distribution of the thermal-neutron flux and power - on  $\varphi_0^{(2)}$ ,  $P_0$  and  $\varphi_1^{(2)}$ ,  $P_1$ , respectively.

#### Some Results of the Calculation

On the basis of the method outlined above, the PDP (power-distribution prediction) program has been developed at the BACHPP for the plant CM-4 computer. The algorithm is written in Fortran-4; the RAFOS operational system is used. The program is formulated as a radical phase and seven overlaps of different levels. The minimum information necessary for the operation of the program is introduced from a video terminal: the number of the reactor, characteristics of its state and power, the number of CE and their assignment to particular groups of removable rods. The remainder of the necessary information is derived from files on magnetic computer disks. In comparison with the two-dimensional MTK program, the only additional information relates to the assignment of CE to different groups.

In the calculation,  $\varphi_0$ ,  $\varphi^+$ ,  $\varphi_1$  are first systematically determined for the stage of withdrawal of the first group of CE. Taking account of the time of CE-group withdrawal  $T$  and the power distributions  $P_0(r)$  and  $P_1(r)$  obtained as a result of the calculation, the fuel-assembly energy liberation is recalculated according to Eq. (13) for the end of the time interval or, equivalently, for the beginning of the next interval. Then the calculation cycle is repeated, but for the stage of withdrawal of the second group of CE, and so on. The initial approximation for calculating the next stage is the solution obtained for the end of the preceding stage ( $\varphi = \varphi_0 + \varphi_1 T$ ). For each time interval, the dependence of the nonuniformity coefficient of the power distribution over time is output on a printer, with notation of the number of the reactor cell in which the fuel-assembly power is a maximum.

Turning to Eq. (6), its numerator is proportional to the change in reactivity on account of the fuel burnup and the denominator is proportional to the reactivity introduced by the CE group withdrawn. These contributions to the reactivity are calculated from the formula of small-perturbation theory, when the neutron-flux distribution  $\varphi_0(r)$  and the value distribution  $\varphi^+(r)$  are taken for the same (initial) state of the reactor. Hence, there follows the unambiguous conclusion that the rate of withdrawal of the absorber is overestimated, since no account is taken of the change in external block effect of the control rods. The use of the following terms of the expansion over time ( $\nu t^2$ ,  $\nu t^3$ , ...) would automatically take account of this effect. However, if the calculation is required to lead to satisfactory results even when only terms of the expansion that depend linearly on the time are taken into account, a correction must be introduced in determining the rate of withdrawal of the absorber. This is simply accomplished, by introducing the corresponding correction (for the

An additional correction to the time interval is introduced at the beginning of the calculation at the stage of withdrawing the next CE group (after the first external iterations in determining  $\varphi_0$ ). It is calculated from the condition of invariability of  $k_{ef}$  of the reactor in the course of withdrawing the CE groups. The corresponding correction for the fuel-assembly energy liberation is introduced simultaneously.

The error of the calculation may be estimated by comparing the power distribution at the end of the time interval  $-[P(r, T) \simeq P_0(r) + P_1(r) T]$  - and at the beginning of the next interval (direct calculation). The mean square deviation of such distributions is  $\sim 0.5\%$ .

The program here developed allows the change in power distribution - in particular, the nonuniformity coefficient of the energy distribution - in the course of fuel burnup with various schemes of CE withdrawal from the reactor to be predicted. The method employed may be useful in developing optimization algorithms for fuel reloading in reactors.

#### LITERATURE CITED

1. I. S. Akimov and E. I. Grishanin, "Analytical method of calculating fuel burnup in nuclear reactors," *At. Energ.*, 16, No. 6, 500-504 (1964).
2. K. Naguib, I. Akimov, O. Sallam, and I. Hamouda, *Atomkernenergie*, 41, 40-44 (1982).
3. I. S. Akimov, M. E. Minashin, and V. N. Sharapov, "Development of methods of physical calculation of nuclear reactors from the world's first atomic power station to the present," *At. Energ.*, 36, No. 6, 427-431 (1974).
4. L. N. Usachev, "Perturbation theory for the conversion ratio and other number ratios of various processes in a reactor," *At. Energ.*, 15, No. 6, 472-476 (1963).
5. V. V. Khromov, A. M. Kuz'min, and V. V. Orlov, *Method of Successive Linearization in Optimization Problems for Fast-Neutron Reactors* [in Russian], Atomizdat, Moscow (1978).
6. S. M. Zaritskii, "Some possible perturbation-theory formulas," in: *Physics of Nuclear Reactors* [in Russian], No. 1, Atomizdat, Moscow (1968), pp. 39-54.
7. N. S. Akimov, V. G. Rybakov, and F. T. Tukhvetov, "Program for reactor calculation and its use at the Bilibinskii atomic power plant for determining the reactivity margin," in: *Energetics and Electrification: Express Information on Power, Series on the Use and Maintenance of Equipment at Atomic Power Plants* [in Russian], No. 7 (1984), pp. 8-10.

# TEMPERATURE CONDITIONS OF THE IRRADIATION OF FUEL ELEMENTS OF THE BOR-60 REACTOR

V. D. Grachev and R. R. Mel'der

UDC 621.039.55:621.039.534.63

At present, information about the radiation resistance of various fuel arrangements and structural materials, and as a result, that of fuel assemblies (FA) and other structural elements of fast reactor cores can be obtained only by way of in-reactor studies. An extensive program of testing fuel and structural materials for industrial fast reactors is carried out on the BOR-60 reactor. The improvement of these tests and the possibility to derive useful information from them greatly depend on detailed studies of thermal and hydraulic conditions of the irradiation of materials. The level of temperature and its distribution in an irradiation unit (IU) depend not only on the energy release and hydraulic parameters of the considered FA itself; they also depend greatly on the heat exchange at the FA boundaries which is determined by the following factors: heat-transfer coefficient in liquid metals; leak of the coolant through the gaps between FA (it was experimentally observed that a leak due to a throttling of sodium from the feed chamber through the spring packings of the FA tail pieces amounts to 3-4% of the sodium flow rate through FA); flows of the relatively cold coolant through the sleeves of safety and control rods, screening assemblies and materialogical assemblies (MA).

An intensive heat exchange between FA and adjacent "cold" assemblies can substantially distort the temperature field of a FA. The core of the BOR-60 reactor contains a considerable amount of MA and experimental FA with parameters different from those of standard FA. Temperature conditions of testing these assemblies are greatly determined by their heat exchange with adjacent standard FA. Therefore, the methodology of the irradiation of fuel and structural materials under specified thermal conditions is closely connected with processes affecting the FA temperature field.

## Mathematical Model

A channel method [1] is used for analyzing the heat-exchange system, namely an FA surrounded by six different assemblies (FA or MA). In this method, a bundle of fuel elements cooled by the coolant flowing along it is subdivided into a number of channels with parallel interacting flows between fuel elements. Planes connecting the axes of adjacent fuel elements serve as channel boundaries. At the periphery of FA, channel boundaries are determined by planes passing through axes of fuel elements along the normal to the shell lateral faces. Gaps between FA as well as sectors of the adjacent assemblies (Fig. 1), are singled out into separate channels. The following assumptions are characteristic of the channel method:

within each channel, properties of the coolant, its velocity and temperature are assumed to be constant over a cross section at any height mark; at channel boundaries, they are assumed to undergo a discontinuous change;

there is an exchange of mass, heat, and pulse between adjacent channels within a FA, due to convective flowing over of the coolant and to turbulent mixing;

heat exchange between channels separated by FA shells is taken into account.

The set of balance equations for a channel analysis of FA is obtained by the integration of initial differential equations of hydrodynamics and the integration of energy-conservation equations over the volumes of typical FA channels. With some simplifying assumptions, the terms of the equations describe the integral processes for the channels, including interactions between adjacent channels. These terms can be expressed through the experimentally obtained coefficients.

---

Translated from Atomnaya Énergiya, Vol. 59, No. 3, pp. 191-194, September, 1985. Original article submitted July 25, 1984.

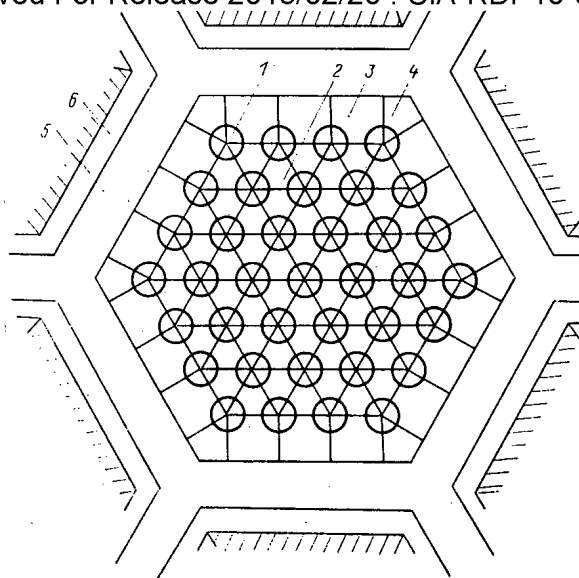


Fig. 1. An analysis scheme of the heat-exchange system: 1) a fuel element; 2) a standard FA channel; 3) a side channel of a FA; 4) a corner channel of a FA; 5) a gap between FA; 6) an adjacent FA or MA.

At a specified coolant-flow rate through a FA, its distribution over the FA channels can be found with the use of simultaneous equations of the conservation of the lengthwise momentum in channels, and with the use of the mass-balance equation. The coolant flow is assumed to be stabilized. The radial pressure gradient is equal to zero. The equation of the conservation of the lengthwise momentum in an  $i$ -th channel of the FA for a stabilized coolant flow can be written as [2]:

$$\frac{dp}{dz} = \frac{1}{f_i} \left( \tau_i \Pi_i + \sum_j \tau_{ij} S_{ij} \right); \quad i = 1, \dots, M, \quad (1)$$

where  $dp/dz$  is the axial pressure gradient in the FA;  $\tau_i$ , tangential stress at the wetted surface of the  $i$ -th channel;  $\tau_{ij}$ , tangential stress at a conventional boundary between the  $i$ -th and  $j$ -th channels;  $f_i$ , cross-sectional area of the channel;  $\Pi_i$ , wetted channel perimeter;  $z$ , axial coordinate;  $M$ , number of FA channels;  $S_{ij}$ , width of the gap between fuel elements.

The tangential stresses can be calculated from

$$\tau_i = -\lambda_i \frac{\rho w_i^2}{8}; \quad \tau_{ij} = \frac{\mu \bar{G}}{S_{ij}} (w_j - w_i),$$

where  $\lambda_i$  is the coefficient of the friction resistance of the  $i$ -th channel;  $\rho$ , coolant density;  $w_i$ ,  $w_j$ , coolant velocities in adjacent channels  $i$  and  $j$ ;  $\bar{G}$ , average mass-flow rate in adjacent channels  $i$  and  $j$ ;  $\mu$ , mixing coefficient.

The mixing coefficient was calculated with the use of relationships [3]

$$\begin{aligned} \mu &= a^{\max}/\pi; \\ a^{\max} &= 1.5\varphi(x)\psi(\text{Re})/h; \\ \varphi(x) &= 1.8x - 2.5e^{-119(x-1)^{2.12}} + 0.7; \\ \psi(\text{Re}) &= 1.085 - 0.754e^{-0.132 \cdot 10^{-3} \text{Re}}, \end{aligned} \quad (2)$$

where  $x$  is the relative fuel element spacing;  $\text{Re}$ , Reynolds number;  $h$ , winding pitch.

The mass-balance equation for a stabilized coolant flow takes the form

$$\sum_{i=1}^M G_i = G_{\text{FA}}, \quad (3)$$

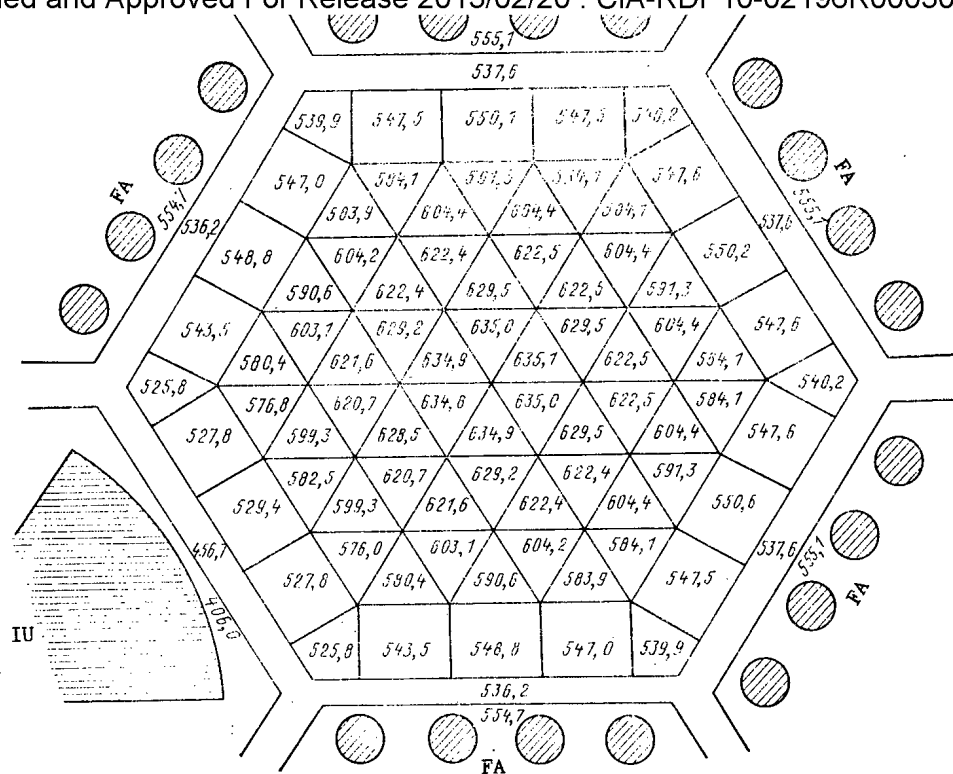


Fig. 2. Temperature cartogram of the heat-exchange system.

where  $G_{FA}$  is the mass-flow rate of coolant through a FA;  $G_i$  is the mass-flow rate of coolant in the  $i$ -th channel.

The set of equations (1) and (3) unequivocally determines  $G_i$  and the axial pressure gradient in the bundle  $dp/dz$ . This system of equations is solved with the use of the following computational techniques.

Mass-flow rates  $G_i$  are determined from Eqs. (1) by means of the quickest descent technique [4] for a given initial estimate of the derivative  $dp/dz$ . The adjustment of the derivative  $dp/dz$  is carried out in the outer iterative loop using the unbalance of Eq. (3) and the relationship

$$\left(\frac{dp}{dz}\right)^{(n+1)} = \left(\frac{dp}{dz}\right)^{(n)} + \tau \left(G_{FA} - \sum_{i=1}^M G_i^{(n)}\right),$$

where  $n$  is the iteration number, and  $\tau$  is the iterative parameter.

The energy-conservation equation for the  $i$ -th channel of the heat-exchange system can be written as:

$$\frac{dt_i(z)}{dz} = - \sum_{j=1}^N a_{ij} [t_i(z) - t_j(z)] + c_i q_i(z); \quad (4)$$

$i = 1, \dots, M$

with a common boundary condition

$$t_i|_{z=z_0} = t_{in}, \quad (5)$$

where  $i$  is the serial number of the channel considered (channels of the FA, a gap between the FA, adjacent assemblies);  $j$ , serial number of the channel adjacent to the  $i$ -th channel;  $M$ , number of channels in the analysis scheme;  $N$ , number of channels adjacent to the  $i$ -th channel;  $t_i(z)$  and  $t_j(z)$ , functions of the average coolant-temperature distribution with height in channels  $i$  and  $j$ ;  $q_i(z)$ , function of the energy-release distribution with height in the  $i$ -th channel;  $t_{in}$ , coolant temperature at the inlet of the reactor; and  $a_{ij}$  and  $c_i$ , equation coefficients.

$$a_{ij} = \frac{m_{ij} \mu (G_i + G_j)}{2G_i} + \frac{\lambda_e (1 + q_t)}{G_i C_p} \quad (6)$$

The effective coefficient of the interchannel exchange allows for the convective (due to the effect of the fuel-element ribs) and for the turbulent energy transport between channels. It also takes into account the interaction of adjacent channels due to the thermal conductivity of the coolant and of the fuel-element can. The heat transfer between channels due to the thermal conductivity of the fuel-element core is neglected as the thermal conductivity of the fuel (uranium dioxide) is small.

For channels separated by the assembly shell

$$a_{ij} = \frac{k_{ij} p_{ij}}{G_i C_p} \quad (7)$$

Free term coefficients are given by

$$C_i = \frac{1}{G_i C_p} \quad (8)$$

Coefficient  $m_{ij}$  in relationships (6)-(8) allows for the effectiveness of the coolant mixing between different FA channels:  $m_{ij} = 1$  for standard (triangular) channels, and  $m_{ij} = 0.75$  for the case when at least one of the adjacent channels is nonstandard (rectangular or corner-situated);  $C_p$ , specific heat of the coolant;  $\mu$ , calculated by relationship (2) with due regard for the coefficient of limited similitude between the heat and mass transport, which is equal approximately to 0.7 [3] for a rod bundle;  $\lambda_e$ , effective thermal conductivity of the ligament between fuel elements [5];  $q_t$ , correction which allows for the turbulent energy transport from one channel into another [5];  $K_{ij}$  and  $P_{ij}$ , heat-transfer coefficient and the perimeter of heat exchange between channels  $i$  and  $j$ .

The effect of the mixing coefficient on the temperature field in an assembly has been analyzed in [6] with due regard for some arbitrariness in the values of coefficients  $m_{ij}$  used for the description of the heat exchange between different-type FA channels. It has been found that a variation of  $\mu$  by 25% has only a slight effect on the temperature distribution in the lattice.

The heat-transfer coefficient between channels  $i$  and  $j$  separated by an assembly shell is determined by the formula

$$K_{ij} = 1 / (1/\alpha_i + \delta/\lambda + 1/\alpha_j),$$

where  $\alpha_i$  and  $\alpha_j$  stand for the heat-transfer coefficients between the shell surface and the coolant of channels  $i$  and  $j$ , respectively;  $\delta$  is the shell thickness, and  $\lambda$  is the thermal conductivity of the shell.

Let us assume the fluid-velocity profile in the gap between the FA to be turbulent ( $Re = 6 \cdot 10^3$  [6]). The heat-transfer coefficient between the external surface of the FA shell and the coolant in the gap between the FA is calculated by means of the relationship recommended by N. I. Buleev for the heat exchange in a flat slit:

$$Nu = 5.4 + 0.02 Pe^{0.8}.$$

The dependence of thermal parameters of the coolant (sodium) on the temperature is neglected. The set of equations (4) with the boundary conditions (5) is solved by the Runge-Kutta method.

The computational techniques considered are realized in a computer program GERAT. Results of machine computations agree well with the experimental data obtained by in-reactor experiments on thermometrically monitored FA and MA [6].

### Results of the Calculations

Calculations have been carried out for real core parameters in order to investigate the heat exchange between the IU and FA. Figure 2 shows a coolant-temperature distribution in the outlet cross section of the core in the channels of the heat-exchange system: in a FA surrounded by five similar FA and an IU. Maximum linear load on fuel elements was assumed to be 45,000 W/m, the coolant-flow rate through a FA was 2.083 kg/sec, the coolant-flow rate

An analysis of the results obtained shows that the temperature field of an FA is substantially distorted by an adjacent cold assembly. There is a marked increase in azimuthal nonuniformity of temperatures of peripheral fuel-element cans in the sector facing the cold materialogical assembly. The difference of shell-face temperatures can be as high as 80°C. Heat losses from the FA side facing the IU amount to 7900 W, i.e., 22% of the energy release in the peripheral channels of the FA. Heat onflow to the coolant of the IU from one face of the FA through the gap between two FA is 4774 W, i.e., almost 2.4 times the energy release in the IU sector facing the FA. Heat transfer to the coolant in the gap between two FA from the FA side facing the FA amounts to 2590 W, i.e., 7.3% of the energy release in the peripheral layer of the FA.

A temperature cartogram has been also obtained for a heat-transfer system consisting of a FA surrounded by five FA and one IU with energy release of 11,940 W as in the preceding case, but with cooling by the coolant of the gap between two FA. In the latter case, the materialogical assembly practically does not distort the temperature field of the adjacent FA. The cooling of the IU by the coolant of the gap between two FA is also preferable due to the extension of the IU experimental volume and to a higher technological effectiveness of its manufacturing.

The temperature nonuniformity within the FA  $\Delta t^{\max}/\Delta t$  amounts to 1.19 even when the given FA is symmetrically surrounded by similar FA. This is due to a nonoptimal coolant-flow rate distribution in the channels of standard FA of the BOR-60 reactor. The coolant flow rate in a side channel of the FA is 1.7 times the coolant flow rate in an internal standard channel. The interchannel heat exchange within a FA contributes markedly to the energy balance of peripheral channels (23-29% of the energy release into these channels, depending on the surroundings), but is partly compensated by the heat sink into the gap between two FA, and cannot provide for complete flattening of the temperature over the FA cross section.

Thus, while determining the temperature conditions of fuel-element irradiation in the experimental FA, the operating conditions of the standard FA fuel elements of the BOR-60 reactor, and the irradiation conditions of the materialogical assemblies, one has to take into account the real surroundings of the assembly under study and the coolant leaks in the gaps between assemblies.

#### LITERATURE CITED

1. A. V. Zhukov, A. P. Sorokin, P. A. Ushakov, and Yu. S. Yur'ev, "A channel method of the thermohydraulic design of nuclear-reactor fuel-element assemblies," *At. Energ.*, 51, No. 5, 307-311 (1981).
2. Yu. V. Mironov and S. V. Shpanskii, "The distribution of the two-phase-flow parameters over the cross-section of a channel with a fuel-element bundle," *At. Energ.*, 39, No. 6, 403-408 (1975).
3. A. V. Zhukov, E. Ya. Sviridenko, N. M. Matyukhin, et al., Preprint FÉI-799, Obninsk (1977).
4. B. P. Demidovich and I. A. Maron, *Elements of Calculus Mathematics* [in Russian], Nauka, Moscow (1980).
5. V. I. Subbotin, M. Kh. Ibragimov, P. A. Ushakov, et al., *Hydrodynamics and Heat Exchange in Nuclear Power Plants* [in Russian], Atomizdat, Moscow (1975).
6. N. A. Aseev, V. M. Gryazev, V. D. Grachev, and R. R. Mel'der, Preprint NIIAR-27 (435), Dimitrovgrad (1980).

## IRRADIATION STRENGTHENING OF METALS

I. V. Gorynin, S. I. Aleksandrov,  
and V. D. Yaroshevich

UDC 621.039.531

At the present time, it is generally accepted [1-3] that the increase in the yield stress (strength)  $\tau_{0.2}$  of metals and alloys irradiated with neutrons at  $T \geq 0.2T_{mp}$  and tested at  $T \leq 0.2T_{mp}$  is only due to the change in its athermal component  $\tau_{\mu}$ . This fact indicates that the radiation-induced defects causing a change in the yield stress at a temperature below  $0.2T_{mp}$  and a moderate strain rate are not thermally activated.

In the general case, the initial yield stress of an unexposed specimen can be expressed by the following equation [4]

$$\tau_{0.2ini} = \tau_{\mu ini} + \tau^*, \quad (1)$$

where  $\tau_{\mu ini} = \alpha G b \sqrt{\rho}$  is the athermal component of the yield stress;  $\rho$ , number of athermal barriers to dislocation movement per unit slipped area;  $G$ , shear modulus;  $b$ , Burgers vector;  $\alpha$ , a constant close to unity; and  $\tau^*$ , thermally activated component of the yield stress.

Similarly, the yield stress of an irradiated specimen is given by

$$\tau_{0.2irr} = \tau_{\mu irr} + \tau^*. \quad (2)$$

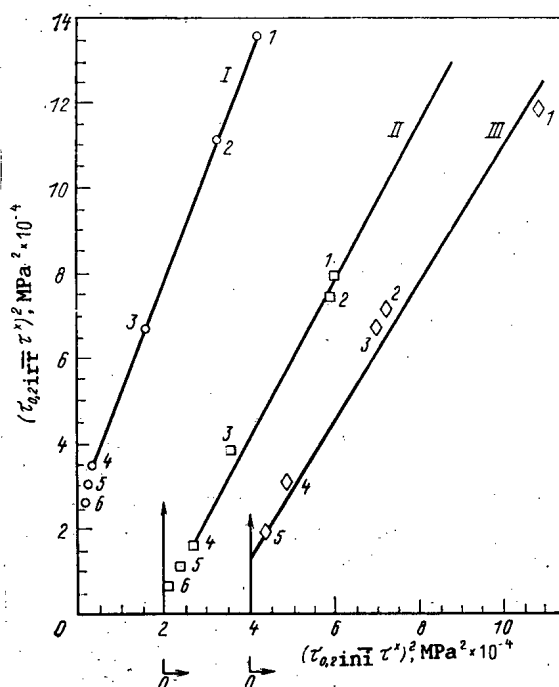


Fig. 1. Variation of the athermal component of the yield stress of the neutron irradiated molybdenum and niobium alloys: I, II) niobium alloys ( $\Phi_n = 1 \cdot 10^{24} \text{ m}^{-2}$ ;  $T_{irr} = 373$  and  $873^\circ\text{K}$ ); III) molybdenum alloys; the numbers near the points are the serial numbers of the alloys given in Table 1.

Translated from Atomnaya Energiya, Vol. 59, No. 3, pp. 194-197, September, 1985. Original article submitted June 15, 1984.

TABLE 1. Basic Composition, Heat Treatment Regimes, and the Yield Strength of the Alloys Based on Niobium and Molybdenum

Alloy number	Alloys	Heat treatment (temp., °C; time, h)	$\sigma_{0.2}$ , MPa
Niobium alloys			
1	Nb-0,01 Y	1573; 1	100
2	Nb-0,04 La	1573; 1	120
3	Nb-1 Zr-0,02 La	1573; 1	190
4	Nb-1 Zr-0,01 Y	1473; 1	325
5	Nb-5 Mo-1 Zr	1673; 1	420
6	Nb-16 W-0,2 Zr	1673; 1	470
Molybdenum alloys			
1	Mo-0,02 C-0,005 Ce	1173; 2	570
2	Mo, powder metallurgical	1473; 1	470
3	Mo-0,02 C	1173; 2	580
4	Mo-0,08 Zr-0,02 C	1773; 1	425
5	Mo-0,5 Ti	1173; 2	680

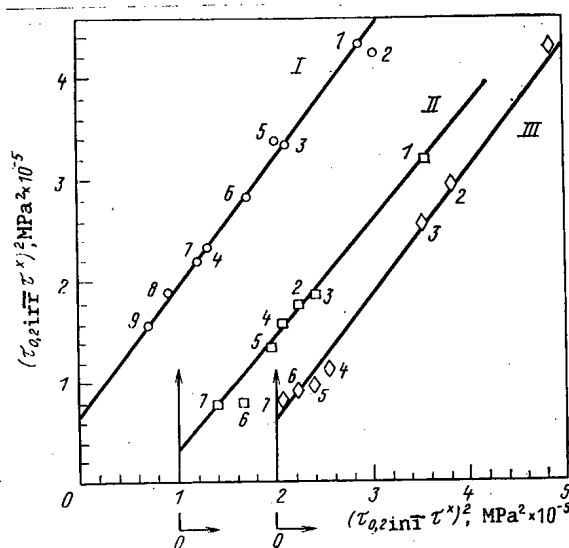


Fig. 2. Variation of the athermal component of the yield stress of the neutron irradiated steels ( $T_{\text{test}} = 293^\circ\text{K}$ ): I) steel 15Kh3MFA ( $\Phi_n = 1.3 \cdot 10^{24} \text{ m}^{-2}$ ,  $E \geq 0.5 \text{ MeV}$ ,  $T_{\text{irr}} = 323\text{--}353^\circ\text{K}$  [10]): 1) quenching (from)  $1253^\circ\text{K}$ ; 2, 3, 4) quenching  $1253^\circ\text{K}$  + tempering 10 h at 873, 903,  $933^\circ\text{K}$ ; 5, 6, 7, 8, 9) quenching  $1253^\circ\text{K}$  + tempering  $933^\circ\text{K}$  for a period of 1, 3, 10, 20, 50 h; II) ferritoparlitic steels ( $\Phi_n = (0.8\text{--}1.0) \cdot 10^{24} \text{ m}^{-2}$ ,  $E \geq 1 \text{ MeV}$ ,  $T_{\text{irr}} = 493\text{--}513^\circ\text{K}$  [11]): 1) 2KhMS, quenching  $1323^\circ\text{K}$  + tempering  $923^\circ\text{K}$ ; 2) 2KhMS, annealing  $1373^\circ\text{K}$ ; 3) 2Kh6MST, quenching  $1273^\circ\text{K}$  + tempering  $923^\circ\text{K}$ ; 4) 2Kh6MST, annealing  $1173^\circ\text{K}$ ; 5) 1Kh12MS, quenching  $1273^\circ\text{K}$  + tempering  $923^\circ\text{K}$ ; 6) 1Kh12MS, annealing  $1173^\circ\text{K}$ ; 7) 1Kh16MSB, annealing  $1173^\circ\text{K}$ ; III) austenitic stainless steels ( $\Phi_n = (1\text{--}1.2) \cdot 10^{24} \text{ m}^{-2}$ ,  $E \geq 1 \text{ MeV}$ ,  $T_{\text{irr}} = 373^\circ\text{K}$  [12]): 1, 2) 1Kh18N9B, annealing + cold working 55 and 17%; 3, 4, 6, 7) 1Kh18N9T (3) quenching  $1373^\circ\text{K}$  + cold working 25%; 4) austenitizing + cold working 25%; 6) quenching  $1373^\circ\text{K}$ ; 7) austenitizing; 5) Kh20N14S2, quenching  $1323^\circ\text{K}$ .

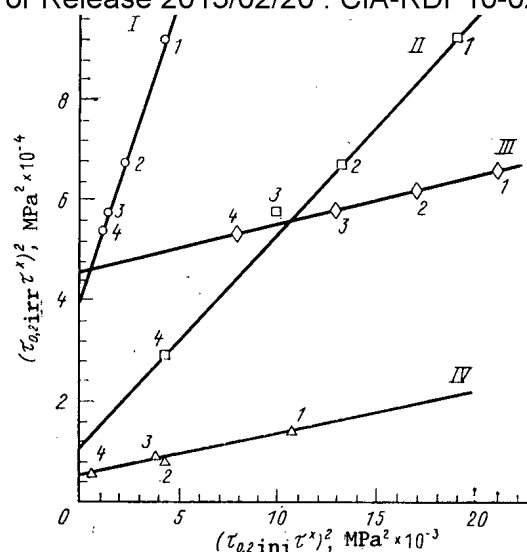


Fig. 3. Variation of the athermal component of the yield stress of the neutron irradiated materials ( $T_{\text{test}} = 293^\circ\text{K}$ ); I) nickel ( $\Phi_n = 3 \cdot 10^{23} \text{ m}^{-2}$ ,  $E \geq 1 \text{ MeV}$ ,  $T_{\text{irr}} = 493-523^\circ\text{K}$  [13]): 1, 2, 3, 4) annealing 923, 1223, 1323,  $1473^\circ\text{K}$ ; II) zirconium alloys ( $\Phi_n = 1.1 \cdot 10^{24} \text{ m}^{-2}$ ,  $E \geq 1 \text{ MeV}$ ,  $T_{\text{irr}} = 353^\circ\text{K}$  [12]): 1) Zr-2.5 Nb; 2) Zr-1 Nb; 3) Zr-0.5 Ta; 4) Zr, iodide grade; III) iron ( $\Phi_n = 3 \cdot 10^{23} \text{ m}^{-2}$ ,  $E \geq 1 \text{ MeV}$ ,  $T_{\text{irr}} = 493-523^\circ\text{K}$  [14]): 1, 2, 3, 4) annealing at 1033; 1303; 1373;  $1423^\circ\text{K}$ ; IV) aluminum alloys ( $\Phi_n = (1-1.3) \cdot 10^{26} \text{ m}^{-2}$ ,  $E \geq 1 \text{ MeV}$ ,  $T_{\text{irr}} = 385-390^\circ\text{K}$  [14]): 1) 6063 Al (DRN-83); 2) 1100 Al (DRN-52); 3) 6063 Al (DRN-63); 4) 1100 Al (DRN-27).

In view of the fact that irradiation leads not only to the formation of new radiation defects, but also to a change in the density of the old defects existing in the original material [5, 6], the equation for the athermal component of the yield stress of an irradiated specimen may be presented in the following form:

$$\tau_{u \text{ irr}} = \alpha G b \sqrt{k\rho + n}, \quad (3)$$

where  $k$  is a coefficient that takes into account the transformation of the initially existing athermal barriers during irradiation; and  $n$  is the density of new radiation-induced athermal barriers.

From Eqs. (1)-(3) it follows that the magnitude of the yield stress of the irradiated specimen must be a function of the initial yield stress

$$(\tau_{0,2 \text{ irr}} - \tau^*)^2 = (\tau_{0,2 \text{ ini}} - \tau^*)^2 k + (\alpha G b)^2 n. \quad (4)$$

An analysis of Eq. (4) shows that in the general case where  $k$  and  $n$  vary from specimen to specimen, i.e., depend on  $\rho$  (of the initial structure), the relationship between the athermal components of the yield stress of the original and the irradiated specimens is determined by a complex function. Furthermore, Eq. (4) shows that if  $k$  and  $n$  are independent of  $\rho$ , or if  $n$  is a linear function of  $\rho$  ( $k$  remaining independent of  $\rho$ ) through the constant factors  $A$  and  $C$

$$n = A(1 + C\rho), \quad (5)$$

then there must be a linear relationship between the squares of the athermal components of the yield stresses of the original and the irradiated specimens. The existence of such a relationship permits one to suggest, based on Eq. (4), a new method of evaluating the effect of the initial structure and the chemical composition of the material on the degree of its irradiation strengthening (hardening). For conducting experimental studies, we made molybdenum and niobium based alloys that were strengthened up to different levels by introducing trace and alloying elements into them (see Table 1).

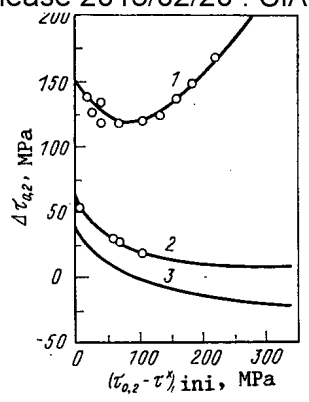


Fig. 4. Dependence of irradiation strengthening of the alloys on the initial athermal component of the yield stress: 1) niobium alloys,  $k = 1.92$ ,  $(\alpha Gb)^2 n = 4000 \text{ MPa}^2$ ; 2) aluminum alloys,  $k = 1.02$ ,  $(\alpha Gb)^2 n = 4300 \text{ MPa}^2$ ; 3) theoretical curve for an alloy with  $k = 0.84$  and  $(\alpha Gb)^2 n = 1600 \text{ MPa}^2$ ;  $\circ$ ) experimental values; —) curves calculated for a material with  $k < 1$  according to Eq. (4).

The tensile specimens of niobium alloys were irradiated at 373 and 873°K up to a neutron fluence  $\Phi_n = 1 \cdot 10^{24} \text{ m}^{-2}$ , and those of molybdenum alloys were irradiated at 1073°K up to a fluence  $\Phi_n = 1.5 \cdot 10^{24} \text{ m}^{-2}$  ( $E \geq 1 \text{ MeV}$ ). The irradiated specimens were tested until fracture at 293°K. The magnitude of the athermal component of the yield stress  $\tau_{0.2}$  of the initial and the irradiated specimens was determined according to the available methods [7].

Figure 1 shows the results of processing the obtained experimental data, and Figs. 2 and 3 give the results of processing the published data. In the latter case, we assumed that  $\tau_{0.2} \gg \tau^*$  at 273°K (the test temperature).

An analysis of the data obtained on the properties of numerous metals, steels, and alloys (30 designations) having different types of crystal lattices permits one to conclude that the linear relationship between the squares of the athermal components of the yield stresses of the irradiated and the original specimens is a general distinguishing feature of irradiation strengthening of metals and alloys. The existence of the aforementioned relationship makes it possible to reveal important details of the irradiation strengthening process. In the first place, it is found that for a given class of materials, the contribution (to the yield stress) related to the formation of new radiation defects  $n$  in the structure is either independent of the density of athermal barriers that are structure sensitive, or such a relationship obeys Eq. (5). Besides this, the contribution to irradiation strengthening by changing the initial density of athermal barriers that determine the yield stress of the unexposed material is not only proportional to the density of such barriers, but also a function of the degree of their resistance to neutron radiation, a fact which is extremely important. This contribution is equal to zero in the materials having the most stable structure under the given irradiation conditions (for example, Al alloys); it is proportional to the initial density of athermal barriers in the metals and alloys with  $k > 1$  (the alloys of Mo, Nb, Zr, etc.); and it may become negative in the case of the alloys having  $k < 1$  in which the density of the athermal barriers decreases during the irradiation process. Apparently, it is precisely this situation that causes the observed [8, 9] irradiation softening of materials.

Figure 4 shows that the degree of stability of the initial structure can radically affect the nature of dependence of irradiation strengthening of the alloys on the athermal component of the yield stress. For example, in the alloys having  $k > 1$ , this relationship is described by a curve exhibiting a minimum, whereas in the alloys with  $k \leq 1$  the curves gradually fall off with increasing athermal component of the yield stress.

stability, the alloys having  $k \sim 1$  are the most attractive ones, in particular, those having  $k < 1$ . In such alloys the increased density of the radiation-induced athermal barriers may be compensated by decreasing the existing density of athermal barriers under the action of radiation (dissolution or coagulation of the crystalline (phase) precipitates, reducing the dislocation and dipole density, etc.).

It is natural to assume that the total effect determined by the intensity of occurrence of these two processes that are directed in opposite directions, in turn, determines the degree of change in the strength characteristics and, consequently, the deformation characteristics of an irradiated material. This fact must be taken into account for developing the alloys that either retain their mechanical properties or exhibit minimum changes during irradiation. In this context, the decisive factor in such alloys is to ensure occurrence of the processes of coagulation and dissolution of the dispersed precipitates which, in the temperature range up to  $\sim 0.3T_{mp}$ , act as athermal barriers to dislocation movement.

#### LITERATURE CITED

1. N. Milasin, Rad. Effects, 15, Nos. 3/4, 153-165 (1972).
2. S. I. Aleksandrov, E. N. Soboleva, and V. D. Yaroshevich, "Thermal activation analysis of the plastic deformation in neutron irradiated molybdenum," Fiz. Met. Metalloved., 54, No. 2, 366-369 (1982).
3. V. A. Kazakov, A. S. Pokrovskii, A. V. Smirnov, and L. I. Smirnova, "Radiation strengthening of dilute molybdenum alloys," ibid., 42, 357-363 (1976).
4. A. Jaeger, Dislocations and Mechanical Properties of Crystals [Russian translation], IL, Moscow (1960).
5. I. Silicock, Research Rept. of Fulmer Research Inst., R10/56 (1957).
6. K. Liu, O. Kawano, I. Murakami, and H. Yoshida, Rad. Effects, 15, 37 (1972).
7. V. D. Yaroshevich and D. T. Ryvkina, "Thermal activation character of plastic deformation of metals," Fiz. Tverd. Tela, 12, No. 1, 464-477 (1970).
8. A. V. Efimov, O. A. Kozhevnikov, V. A. Nikolaev, et al., "Effect of neutron irradiation on the mechanical properties of the austenitic steels having different strength levels," in: Effect of Nuclear Radiations on Materials [in Russian], Izd. Akad. Nauk SSSR, Moscow (1962).
9. E. A. Markovskii, M. M. Krasnoshchekov, V. I. Tikhonovich, and V. G. Chernyi, Effect of Nuclear Radiations on the Structure and Properties of Metals and Alloys [in Russian], Naukova Dumka, Kiev (1968).
10. A. M. Morozov, V. A. Nikolaev, and V. V. Rybin, "Effect of the initial structure on the radiational embrittlement of the quenched and tempered steel 15Kh3MFA," Probl. Prochn., No. 3, 62-68 (1982).
11. Sh. Sh. Ibragimov, I. M. Voronin, and A. S. Kruglov, "Effect of neutron radiation on the structure and the mechanical properties of alloy steels," At. Energ., 15, No. 1, 30-35 (1963).
12. N. F. Pravdyuk, A. D. Amaev, P. A. Platonov, et al., "Effect of neutron radiation on the properties of structural materials," in: Effect of Nuclear Radiations on Materials [in Russian], Izd. Akad. Nauk SSSR, Moscow (1962).
13. Sh. Sh. Ibragimov and I. M. Voronin, "Strengthening of iron and nickel during neutron irradiation," Fiz. Met. Metalloved., 15, No. 6, 895-899 (1963).
14. E. Sturcken, Nucl. Mater., 2, No. 1, 39-53 (1979).

## GAS EVOLUTION FROM ABSORBING MATERIALS

I. G. Gverdtseteli, Sh. P. Abramidze,  
A. G. Kalandarishvili, G. S. Karumidze,  
and V. A. Kuchukhidze

UDC 621.039.565

The investigation of gas evolution is an important problem on the way to the production of radiation-resistant absorbing materials. Among the known methods of studying gas evolution from absorbing materials [1-4] the most effective are those in [3, 4] based on a determination of gas evolution directly during irradiation. The emitted gases are recorded by using sensitive elements (pressure indicators) whose disposition in the immediate vicinity of sampling points is impossible [5] because of the rigid requirements imposed on these systems. In addition, the use of conduits decreases the operativeness, introduces a lag into the measuring process, and decreases the radiation safety of the experiment.

We consider a method for investigating gas evolution from absorbing materials by using the principle of a gas controlled heat pipe (GCHP). We studied the dependence of gas evolution from crystalline boron on the thermal neutron fluence and the irradiation temperature.

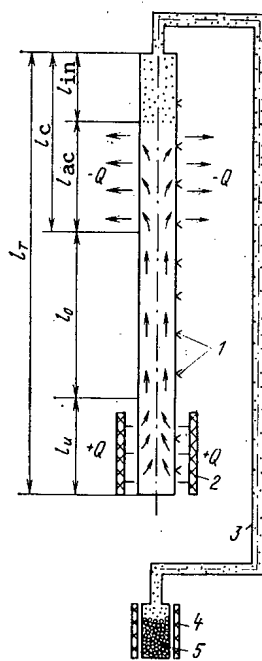


Fig. 1. Schematic diagram of arrangement for investigating gas evolution from absorbing materials: 1) thermocouples;  $l_u$ , evaporation zone;  $l_a$ , adiabatic zone;  $l_{ac}$ , active part of condensation zone;  $l_{in}$ , inactive part of condensation zone;  $l_c$ , condensation zone;  $l_T$ , total length of pipe;  $Q$ , power input; 2) evaporation zone heater; 3) gas pipe; 4) sample heater; 5) sample under study.

Translated from *Atomnaya Energiya*, Vol. 59, No. 3, pp. 197-200, September, 1985. Original articles submitted July 24, 1984.

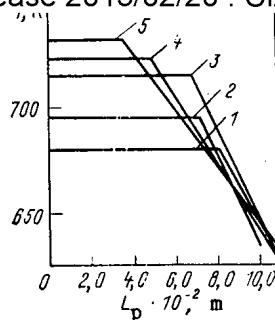


Fig. 2. Variation of the temperature distribution over the length of the adiabatic zone of the GCHP for a constant input heat power of 30 W to the evaporation zone and an irradiation temperature of the boron powder of  $800 \pm 25^\circ\text{K}$ ; the thermal neutron fluences were:  
 1)  $7.1 \cdot 10^{16}$ ; 2)  $7.5 \cdot 10^{17}$ ;  
 3)  $1.9 \cdot 10^{18}$ ; 4)  $2.4 \cdot 10^{18}$ ;  
 5)  $3.0 \cdot 10^{18} \text{ cm}^{-2}$ .

Figure 1 shows a schematic diagram of the arrangement for measuring gas evolution by this method. The vessel with the sample under study is connected through a gas pipe with the reservoir of uncondensed gas, the adiabatic zone with the temperature indicators, and the evaporation zone with an electric heater.

In the operating GCHP the following relation holds [6]:

$$p_{v,a} = p_g \quad (1)$$

where  $p_{v,a}$  is the saturated vapor pressure of the coolant in the adiabatic part of the GCHP, and  $p_g$  is the pressure of the uncondensed gas in the pipe.

It was shown in [6, 7] that a GCHP can be used to study the temperature dependence of the saturated vapor pressure of various elements in the range  $(6.5-550) \cdot 10^3 \text{ Pa}$ . Thus, by measuring the temperature in the adiabatic part of the GCHP, it is possible to determine the pressure of the gas from Eq. (1).

This method enables one to determine the amount  $\Delta m$  of gaseous products of a nuclear reaction which enters the volume occupied by the uncondensed gas. The main condition for the use of this method is the assurance of steady operation of the pipe under definite chosen conditions with a constant temperature distribution in the adiabatic zone. The evolution of gas from an absorbing material leads to its accumulation in the gas reservoir, which is accompanied by an increase in pressure, and consequently by an increase in  $p_{v,a}$  with a corresponding change of the temperature of the adiabatic zone of the GCHP. This change  $\Delta T$  recorded by the temperature indicators enables us to calculate the amount of gas  $\Delta m$  evolved from the absorbing material as a result of irradiation.

In considering the physical bases of the proposed method, it was assumed that the gaseous products of a nuclear reaction obey the ideal gas law, that there is no intermixing of vapor and gas at the interface, and that the following conditions are satisfied:

$$T_g = \text{const}; Q = \text{const}; p_{v,in} \ll p_g \quad (2)$$

where  $T_g$  is the absolute temperature of the gas,  $^\circ\text{K}$ ;  $Q$  is the heat power input to the GCHP evaporator, W;  $p_{v,in}$  is the saturated vapor pressure of the coolant in the inactive part of the condensation zone, Pa.

With an increase in the irradiation of the absorbing material there is an increase in the amount of gaseous products of a nuclear reaction which diffuse through the sample and enter the gas reservoir of the GCHP, resulting in a pressure increase  $dp_g$ , which leads to a

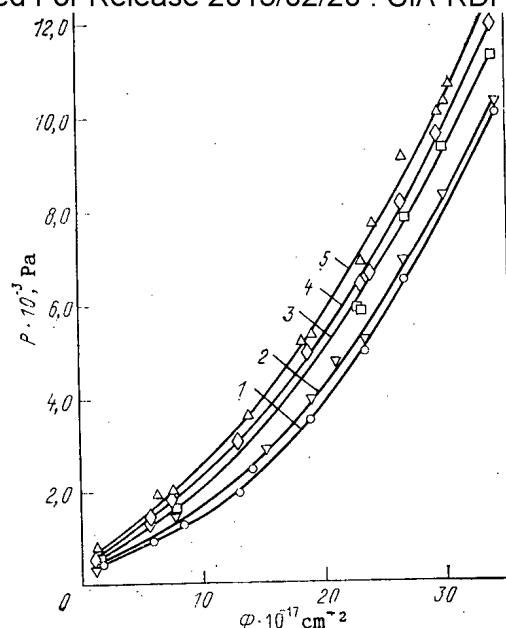


Fig. 3. Helium pressure as a function of the thermal neutron fluence for various irradiation temperatures: 1) 300; 2) 370; 3) 515; 4) 650; 5) 800°K.

displacement of the vapor-gas interface before equilibrium is established in accordance with Eq. (1). Using Eqs. (1) and (2), the temperature change of the vapor in the adiabatic part of the GCHP,  $dT_v/T_v$ , according to the equation of state of an ideal gas and the Clapeyron-Clausius equation, is

$$\frac{dT_v}{T_v} = \frac{RT_v}{\mu_v \lambda_v} \left[ \frac{dm_g}{m_g} - \frac{dV_g}{V_g} \right], \quad (3)$$

where  $R$  is the universal gas constant, J/mole·deg K;  $\lambda_v$ , latent heat of vaporization, J/kg;  $\mu_v$ , molecular mass of the vapor, kg/mole;  $dV_g/V_g$ ,  $dm_g/m_g$ , respectively, changes in volume and mass of the gas as a result of the accumulation of gaseous products of a nuclear reaction. Equation (3) shows that the sensitivity of the method can be increased by increasing the volume  $V_g$  and decreasing the mass  $m_g$  of the uncondensed gas, i.e., by decreasing the initial pressure of the uncondensed gas in the system. A second way of increasing the sensitivity is based on the use of a coolant with a low temperature variation of the saturated vapor pressure, i.e., a coolant with a small value of  $d(\ln p_v)/dT_v$ . Using the Clapeyron-Clausius equation and assuming that the vapor is ideal, we obtain

$$\frac{d(\ln p_v)}{dT_v} = \frac{\lambda_v \mu_v}{RT_v^2}. \quad (4)$$

Thus, it follows from Eqs. (3) and (4) that the sensitivity of the determination of the pressure of the gaseous products by measuring the temperature of the coolant can be increased by decreasing the factor  $\lambda_v \mu_v$ , which is a convenient parameter for the choice of coolant. Of the coolants used at the present time in heat pipes, the most acceptable for investigating gas evolution under the rigorous conditions of reactor irradiation are the alkali metals (except lithium) and also lead and silver.

When the GCHP operates under steady conditions and Eq. (2) is satisfied, the mass of the gaseous products of nuclear reactions is given by

$$m_g = \frac{\mu_g p_{v,a}}{RT_g} (V_r + S_p l_{in}), \quad (5)$$

where  $\mu_g$  is the molecular mass of the gaseous products of nuclear reactions, kg/mole;  $V_r$ , volume of the gas reservoir, m³;  $S_p$ , cross section of the pipe, m²;  $l_{in}$ , length of the inactive zone of the condenser, m.

The method described was used to study the gas evolution from a finely dispersed powder of crystalline boron containing 86%  $^{10}\text{B}$ . The experimental ampoule shown in Fig. 1 consisted

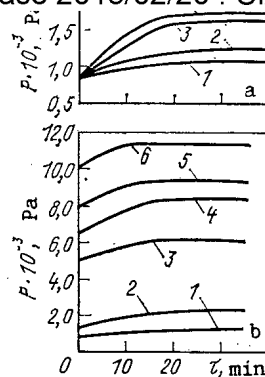


Fig. 4. Increase of helium pressure: a) for a constant thermal neutron fluence of  $5.73 \cdot 10^{17} \text{ cm}^{-2}$  at temperatures of 1) 300; 2) 370; 3) 650; 4) 800°K; b) at a constant irradiation temperature of 515°K for neutron fluences of 1)  $5.73 \cdot 10^{17}$ ; 2)  $7.53 \cdot 10^{17}$ ; 3)  $2.30 \cdot 10^{18}$ ; 4)  $2.65 \cdot 10^{18}$ ; 5)  $2.98 \cdot 10^{18}$ ; 6)  $3.41 \cdot 10^{18} \text{ cm}^{-2}$ .

of two independent subassemblies of similar construction. The gas pipe and the condensation zone of the GCHP were at the coolant temperature. The powders studied were of various compactness, and were heated to 300-800°K by an electric heater; the temperature was monitored with calibrated chromel-alumel thermocouples. The free volume over the powder under study, which is needed for the calculation of the gas evolution from boron, was determined before the assembly of the experimental ampoule. All the components of the experimental equipment were degassed on a heat stand at a temperature of  $\sim 1200^\circ\text{K}$  and a static vacuum  $\leq 10^{-3} \text{ Pa}$ , after which the pipes were filled with coolant - 99.99% pure cesium, especially pure lithium - and sealed. The parameters of the heat pipes and the irradiated samples are listed below:

	Pipe	
	1	2
Height of zone, m:		
evaporation	0.05	0.05
condensation	0.035	0.035
Total length of pipe, m	0.235	0.235
Cross section of pipe, $10^{-4} \text{ m}^2$	0.50	0.50
Mass of coolant, g	2.004	1.909
Volume of gas reservoir, $\text{cm}^3$	28.5	23.4
Initial gas pressure, Pa	410	1340
Volume occupied by powder, $\text{cm}^3$	6.724	6.378
Density of filling of boron powder, $\text{kg/m}^3$	0.867	0.860
Perturbed thermal neutron flux density at 1 MW (thermal), $10^{12}/\text{cm}^2 \cdot \text{sec}$	2.34	1.84

The tests were performed in a low temperature vertical loop of the IRT-M apparatus at the Institute of Physics of the Academy of Sciences of the Georgian SSR at zero power of the apparatus to decrease the measurement errors from radiation heating of the temperature indicators.

During the experiment the change of volume of uncondensed gas ( $\Delta V_g$ ) was determined from the variation of the temperature distribution over the height of the GCHP (Fig. 2), and  $\Delta T_v$  was found from the temperature of the adiabatic zone. Using the data obtained, the dependence of the helium pressure  $p_g$  on the thermal neutron fluence (Fig. 3) was calculated. As a result the kinetic dependences of the helium pressure on the irradiation temperature for the same thermal neutron fluence (Fig. 4a) and on the thermal neutron fluence at a constant irradiation temperature (Fig. 4b) were obtained.

The relations obtained (Figs. 3 and 4) show that the helium yield from boron powder of a given dispersion occurs more rapidly the higher the irradiation temperature and the thermal neutron fluence. With an increase in temperature the diffusion of gas bubbles to the surface of the powder particles increases, and the boron crystals are fractured as a result of irradiation.

Estimates show that the error in measuring the helium pressure by this method is ~10%.

#### LITERATURE CITED

1. Ya. Chudars, I. Taure, I. Mednis, and O. Veveris, "Determination of the boron concentration in gaseous mixtures by using neutron beams," *Izv. Akad. Nauk Latvian SSR*, 3, 57-64 (1960).
2. Patent No. 1252592 (Great Britain).
3. V. D. Klimov, V. I. Matveev, B. T. Arabei, et al., "Test of samples of absorbing elements of fast power reactors in the BR-5 reactor," in: *Status and Prospects of Work on the Construction of a Fast Reactor Plant* [in Russian], Obninsk (1975), pp. 713-735.
4. B. V. Samsonov et al., "A device for the remote measurement of the amount of gases," *Inventor's Certificate No. 402069*, *Byull. Izobret.*, No. 41, 183 (1973).
5. N. A. Trofimov and V. V. Lappo, *Measurement of Parameters of Thermophysical Processes in Nuclear Power Engineering* [in Russian], Atomizdat, Moscow (1979), p. 99.
6. Y. Bohdanský and H. Schins, *J. Appl. Phys.*, 36, 3683 (1965).
7. Y. Bohdanský and H. Schins, *J. Phys. Chem.*, 71, 227 (1965).

#### EFFECT OF COMPOSITION AND STRUCTURAL STATE ON THE RADIATION-INDUCED SWELLING OF HIGH-NICKEL ALLOYS

V. A. Nikolaev, I. P. Kursevich,  
O. N. Zhukov, and A. N. Lapin

UDC 621.039.531:669.245

One of the possible reasons for the increased resistance of the high-nickel alloys to radiation swelling as observed in simulation experiments [1, 2] is their ability to form an ordered structure [3]. The existence of such type of transformations (formation of the so-called K-state) in these alloys is indicated by the abnormal increase in the electrical resistivity during annealing and its decrease during cold deformation or irradiation.

To reduce swelling of the ordered alloys, due to their inherent low vacancy-diffusion rate, the alloys need not contain elastically deformed microregions which are considered [4] to cause accelerated recombination (reunion) of the point defects.

Besides this, suppression of the swelling tendency of the complex high-nickel alloys is most probably not due to the operation of a single mechanism. In this process the importance of solute (dissolved) atoms is beyond doubt [5-7].

The purpose of the present work is to study the radiation-induced swelling of certain high-nickel alloys during neutron irradiation up to high fluences, to establish the relationship between the observed effects and the structural transformations in these materials, and to explore the possibility of evaluating the contribution of various mechanisms under consideration in suppressing the swelling process.

#### EXPERIMENTAL MATERIALS AND THE IRRADIATION AND TEST PROCEDURES

In order to evaluate the actual contribution of different mechanisms in suppressing the swelling tendency of high-nickel alloys, we undertook comparative studies on the ternary as well as the commercial Fe-Cr-Ni alloys that differ in the type of alloying additions (Table 1).

The main experimental material is the alloy 03Kh20N45M4BRTs that contains 45% nickel and, consequently, with respect to the nature of variation of electrical resistance during the

Translated from *Atomnaya Énergiya*, Vol. 59, No. 3, pp. 200-204, September, 1985. Original article submitted May 10, 1984.

TABLE 1. Chemical Composition of the Experimental Materials

Material	Weight content of elements, %											
	C	Si	Mn	Cr	Ni	Mo	Nb	Ti	Al	B	other elements	Fe
Kh20N45	0,08	0,7	1,0	19,2	44,8	---	---	---	---	---	---	Remainder »
03Kh20N45M4BRTs	0,02	0,29	0,55	19,56	45,4	3,79	0,82	0,03	0,14	0,005 (calc.)	0,035 (calc.)	
Kh14N35	0,05	0,28	1,2	14,6	37,3	---	---	---	---	---	---	Base »
Kh15N35M2BTYuR	0,05	0,28	1,2	14,6	37,3	---	1,25	1,1	1,0	0,002	0,01	

TABLE 2. Phase Composition and the Structural Features of the Experimental Materials

Material	Heat treatment regime	Phase composition	Weight content (B), size (d), and concentration (N) of the main secondary phases	$\sigma_{0.2}$ at 20°C MPa
Kh20N45, Kh15N35	Austenitizing (1050°C, 1 h), air cooling	Austenite	Absent	300
03Kh20N45M4BRTs	Austenitizing (1050°C, 1 h), water quench	Austenite + Nb (C, N) type primary carbonitrides	Absent	300
	Austenitizing (1200°C, 5 h), water quench	Austenite + Nb (C, N) type primary carbonitrides	Absent	300
	Austenitizing (1050°C, 1 h), water quench + aging (500°C, 10 h), air cooling	Austenite + Nb (C, N) type primary carbonitrides	Absent	300
	Austenitizing (1050°C, 1 h), water quench + aging (700°C, 5000 h), air cooling	Austenite + Nb (C, N) type primary carbonitrides + $Cr_{23}C_6$ and $Me_6C$ type carbides + $Fe_2Mo$	B = 2.7%; d $\approx$ 500 nm (carbides), d $\approx$ 500-2500 nm (Laves phase) $N_{tot} \approx 5 \cdot 10^{10} cm^{-3}$	300
Kh15N35M2BTYuR	Austenitizing (1100°C, 1 h), air cooling	Austenite + (Ti, Nb) (C, N) type primary carbonitrides	Absent	300
	Austenitizing + aging (550°C, 10 h), air cooling	Same	Absent	300
	Austenitizing + aging (750°C, 24 h), air cooling	Austenite + (Ti, Nb) (C, N) type primary carbonitrides + $\gamma'$ -phase	$\gamma'$ -phase: B $\approx$ 5%; d $\approx$ 10 nm; N $\approx 3 \cdot 10^{16} cm^{-3}$	600
	Austenitizing + aging (750°C, 10,000 h), air cooling	Austenite + primary carbonitrides + $\gamma'$ -phase $Ni_3(Ti, Al)$ + Laves phase $Fe_2Mo$	$\gamma'$ -phase: B $\approx$ 10%; d $\approx$ 10 nm; N $\approx 10^{14} cm^{-3}$	450

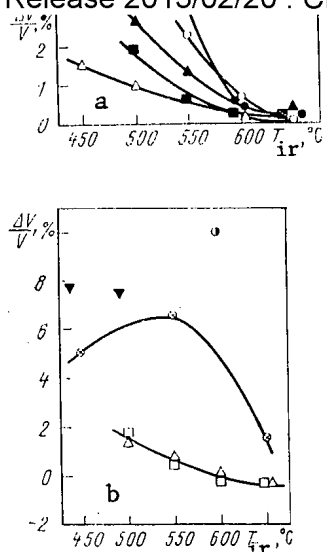


Fig. 1. Dependence of radiation-induced swelling of the alloys of the base compositions Kh20N45 (a) and Kh15N35 (b) under different structural states on the irradiation temperature:  $\circ$ ) Kh20N45;  $\Delta$ ) 03Kh20N45M4BRTs (1200 $^\circ\text{C}$ , 1 h, water);  $\blacksquare$ ) 03Kh20N45M4BRTs (1050 $^\circ\text{C}$ , 1 h, water);  $\blacktriangle$ ) 03Kh20N45M4BRTs (1050 $^\circ\text{C}$ , 1 h, water + 550 $^\circ\text{C}$ , 10 h);  $\bullet$ ) 03Kh20N45M4BRTs (1050 $^\circ\text{C}$ , 1 h, water + 700 $^\circ\text{C}$ , 5000 h);  $\odot$ ) Kh15N35;  $\square$ ) Kh15N35M2BTYuR (1080 $^\circ\text{C}$ , 1 h, air);  $\Delta$ ) Kh15N35M2BTYuR (1080 $^\circ\text{C}$ , 1 h, air + 550 $^\circ\text{C}$ , 10 h);  $\blacktriangledown$ ) Kh15N35M2BTYuR (1080 $^\circ\text{C}$ , 1 h, air + 750 $^\circ\text{C}$ , 24 h);  $\odot$ ) Kh15N35M2BTYuR (1080 $^\circ\text{C}$ , 1 h, air + 750 $^\circ\text{C}$ , 10,000 h).

processes of annealing, cold deformation, it is virtually identical to the typical ordered binary alloys in which one of the components is a transition element with an unfilled d-shell [8]

The age (dispersion) hardening alloy Kh15N35M2BTYuR was used as a model material for verifying the hypothesis regarding the accelerated recombination of defects at the coherent interfaces (interphase boundaries) in view of the formation of the precipitates of  $\gamma'$ -phase in its structure at certain stage of aging and the possibility of reliably recording the coherence of these precipitates with the matrix from the strain contrast. The structural state and the concentration of the alloying elements in the solid solution were changed by incorporating variations in the prior heat treatment regimes of the materials (Table 2). For the purpose of comparison, we studied the alloys of the base composition of both the steels (type Kh15N35 and Kh20N45) in the main structural state after austenitizing. The phase composition of the alloys was determined using physicochemical and x-ray methods, and the microstructural features were studied using optical and electron microscopes.

The swelling phenomenon was investigated by recording the linear dimensions of the specimens (measuring 26-27 mm in length) before and after irradiation. The errors in the measurements carried out using an IZV-3 vertical length measuring machine and a special attachment fitted with a micron-indicator amounted to 1 and 2  $\mu\text{m}$ , respectively.

All the specimens were irradiated in a BOR-60 reactor up to a neutron fluence of  $1 \cdot 10^{23} \text{ cm}^{-2}$  ( $E > 0.1 \text{ MeV}$ ) at different temperatures in the 400-650 $^\circ\text{C}$  range. For this purpose, specific clearances were incorporated between the internal surface of the argon-filled ampul

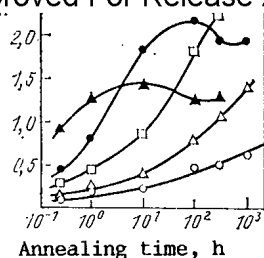


Fig. 2

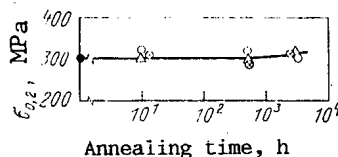


Fig. 3

Fig. 2. Kinetics of increase in the electrical resistivity of the alloy 03Kh20N45M4BRTs during annealing:  $\circ$ ,  $\Delta$ ,  $\square$ ,  $\bullet$ ,  $\blacktriangle$ ) annealing temperature 350, 450, 500, 550°C.

Fig. 3. Dependence of the yield strength of the alloy 03Kh20N45M4BRTs on the annealing temperature and time:  $\circ$ ,  $\Delta$ ,  $\bullet$ ) annealing temperature 450, 500, 550°C.

and the specimen cassettes. The calculated error in determining the irradiation temperature did not exceed 30°C.

### EXPERIMENTAL RESULTS

Figure 1a shows the data on the specific volumetric expansion of the Kh20N45 type alloys due to neutron irradiation. The experimental materials of this type exhibit a high resistance to swelling ( $\Delta V/V \leq 3\%$ ) independent of alloying and the heat treatment regime. This result agrees well with the simulation experimental data obtained after irradiating the alloys under consideration with heavy ions up to a fluence corresponding to 150 displacements per atom [2]. In the given series of low-swelling alloys, the minimum tendency to swelling (over a wide temperature range) was shown by the commercial alloy 03Kh20N45M4BRTs after high-temperature (1200°C) austenitization (solution treatment) that takes maximum amount of alloying elements into the solid solution. Another extreme is shown by the same alloy in the overaged condition (700°C, 5000 h) leading to maximum depletion of the alloying elements from the solution and their precipitation as secondary phases.

The results obtained on the alloys of the Kh15N35 composition are shown in Fig. 1b. They indicate quite a significant swelling of the ternary alloy of the base composition ( $\Delta V/V_{\max} = 6.3\%$ ) that considerably exceeds the effect at a fluence corresponding to  $\sim 150$  displacements per atom [1] predicted on the basis of the simulation studies conducted in an accelerator.

Swelling of the age hardening alloy Kh15N35M2BTYuR significantly depends on the regime of prior heat treatment. Thus, swelling of the alloys does not exceed 2% after austenization treatment that makes the solid solution supersaturated (to the maximum extent) with the alloying elements, and after additional aging at 500°C for a period of 10 h. Furthermore, at an irradiation temperature of 600°C the density of these alloys increases owing to the exit of titanium and aluminum atoms from the solid solution during the precipitation of the  $\gamma'$ -phase  $\text{Ni}_3(\text{Ti}; \text{Al})$ .

After aging at 750°C for a period of 24 h (typical heat-treatment regime) and, in particular, for 1000 h (undue overaging), the alloy shows a high swelling tendency ( $\Delta V/V = 8-10\%$ ) due mainly to the separation of the alloying elements (Ni, Ti, Al) from the solution to constitute the intermetallic compound.

### DISCUSSION OF RESULTS

The experimental data on the swelling phenomenon of the neutron irradiated materials under consideration confirm the low pore forming tendency of the commercial Fe-Cr-Ni alloys having a (Fe, Cr)/Ni ratio close to unity and indicate that the properties of the ternary base composition are responsible for this. These assertions are in complete agreement with the hypothesis [3] regarding the relationship between the stability of such alloys against swelling and their tendency to form the K-state in which the vacancy-migration rate decreases and the growth of pores slows down correspondingly.

In general, the K-state is interpreted in two ways [5, 9]. It is either a homogeneous short-range ordered state under thermodynamic equilibrium or a type of structure with its matrix showing a distribution of ordered domains whose size (d) and number (N) may change during the aging process according to the same laws that govern the growth of the second-phase particles. In the first case, the increase in electrical resistance must come down (decay) with time as the equilibrium state is approached at the given aging temperature. In the second case, the curves of electrical resistance must exhibit maxima corresponding to the attainment of certain (specific) values of d and N. The results of investigations on the temperature-time dependence of electrical resistivity (Fig. 2) of the alloy 03Kh20N45M4-BRTs during isothermal anneals up to 1000 h rather confirm the latter standpoint because at the temperatures 500 and 550°C we observe the presence of maxima that are shifted towards longer durations of holding with decreasing temperature. Nevertheless, the complex chemical composition of the alloy does not exclude the possibility of simultaneous occurrence of phase transformations during the aging process with the formation of the K-state. As a consequence of such transformations, one would expect an analogous reduction in the electrical resistance at sufficiently high temperatures and long periods of holding.

The reduced tendency of the experimental alloy to swelling and the substantial interaction of the defects with the coherent interfaces lead to the question whether the mechanism of accelerated recombination of defects at the interface between the ordered domains and the matrix operates in the given case as was postulated [4, 6] to operate in the case of age hardening alloys. However, this concept must be rejected because of a number of reasons. In the first place, heat treatment of the alloy 03Kh20N45M4BRTs according to the regimes causing an intense increase of its electrical resistance do not lead to the appearance of the regions of strain contrast under an electron microscope. Secondly, no significant changes in the yield stress are observed (Fig. 3) although generation of internal stresses at the boundaries of the secondary-phases (or domains) is expected to strengthen the material. These two facts indicate quite convincingly that the nature of the temperature-time dependence of the electrical resistance of the experimental alloy is not determined by the transformations leading to the development of such stresses as, for example, in the aged alloy Kh15N35M2BTYuR.

However, in the latter case also, depending on the form of stress state, the existing deformation zones must possess the property of selective capture of either vacancies or the interstitial atoms, because of which there would be an inevitable radiation-induced stress-relaxation effect perceptible even at a neutron fluence of  $10^{20} \text{ cm}^{-2}$  [10]. In view of this, even before the beginning of intense pore formation, i.e., at a neutron fluence  $< 1 \cdot 10^{22} \text{ cm}^{-2}$ , the deformation zones existing at the boundaries would lose their ability to serve as the traps (sinks) of point defects, because of which their presence does not significantly affect the kinetics of swelling even at this fluence.

Based on the proposed mechanism of the effect of the deformation (distorted) zones on the recombination of the Frenkel' pairs, we expect that the reduction in the number of the surviving defects must simultaneously suppress the processes of swelling as well as radiation hardening. The existing experimental data do not support this. For example, the yield stress of the low-swelling alloy 03Kh20N45M4BRTsCh after irradiation at 450-470°C up to a fluence of  $2.2 \cdot 10^{22} \text{ cm}^{-2}$  increases from 290 up to 700 MPa which is quite comparable to the strengthening observed in the high-swelling steel Kh18N10T [7]. At the same time, the hypothesis regarding the low swelling tendency of the ordered alloys is not associated with the requirement of reduced radiation hardening.

The data presented in Figs. 1a and b indicate the extremely important role of the solute (dissolved) atoms in decreasing the swelling tendency. Thus, the experimental alloys exhibit minimum swelling tendency when the solid solution is enriched to the maximum degree with the atoms of the alloying elements. The maximum swelling tendency develops either in the absence of additional alloying (for example, in the alloys of the base compositions Kh20N45 or Kh15N35) or when the solid solution is depleted from these atoms to the maximum extent, for example, under prolonged high-temperature dwells (700°C for a period of 5000 h and 750°C for a period of 10,000 h). In comparison with the coherent precipitates of the type  $\text{Ni}_3$  (Ti, Al), the dissolved Ti and Al atoms, owing to their high concentration, can play a particularly significant role as traps of radiation-induced defects in the alloy Kh15N35M2BTYuR.

The relative effectiveness of such type of structural traps may be evaluated on the basis of the flux intensity parameter  $J \propto N_t r$  (where  $N_t$  is the volumetric density of spherical traps;

traps in the alloy Kh15N35M2BTYuR transformed into the solid solution state, we assume that their capture radius of vacancies is equal to the shortest interatomic distance, i.e.,  $r \approx 0.25 \text{ nm}$  and  $N_t \approx 8 \cdot 10^{22} \text{ cm}^{-3}$ .

In the aged condition  $r \approx 5 \text{ nm}$  and  $N_t \approx 3 \cdot 10^{16} \text{ cm}^{-3}$  and, consequently,  $J$  is approximately  $10^5$  times less than that observed in the material possessing a homogenized structure.

The atoms of the alloying elements may affect the nucleation and growth kinetics of pores due mainly to the formation of the vacancy-solute-atom complexes. Such complexes must be stable, i.e., they must possess a sufficiently high bond energy and a low diffusional mobility, i.e., their migration must be slower than that of the individual vacancies. Then a question arises: what are the selection criteria for the elements satisfying these requirements? Apparently, the differences in the atomic volumes form the basis for the bond energy characteristics. From this standpoint, the atoms of Al, Ti, and Nb whose atomic radii (sizes) are greater than those of the atoms of the matrix (Fe, Cr, Ni) by 13-17% must facilitate a reduction in the swelling tendency.

According to Nikolaev [11], the bond strength and the diffusional mobility of the vacancy-solute-atom complexes may be predicted on the basis of the general thermodynamic considerations, in particular, based on the values of the enthalpy of dissolution of the alloying component and the enthalpy of additional (extra) phase separation, and also, on the concentration dependence of the solidus temperatures. A detailed examination of this aspect is beyond the scope of this paper. For the practical purposes, we underline again the basic fact that the atoms of the alloying elements existing in the solid solution exert a significantly greater influence on the pore formation process than the segregates or the nuclei of the coherent phases.

### CONCLUSIONS

1. The age hardening alloy Kh15N35M2BTYuR shows the maximum resistance to swelling in the austenitized condition in which the solid solution is enriched to the maximum extent with the alloying elements that differ from the main elements of the matrix with respect to the atomic radii. The presence of the coherent precipitates of  $\gamma'$ -phase does not ensure sufficient reduction in the swelling tendency of this alloy.

2. The increased resistance to swelling observed in the alloy 03Kh20N45M4BRTs is attributed not only to the effect of the atoms of the alloying elements, but possibly, to the ordering tendency of the ternary base composition at a ratio  $(\text{Fe, Cr})/\text{Ni} \approx 1$ .

### LITERATURE CITED

1. W. Johnston, J. Rosolowski, A. Turkalo, and P. Lauritzen, "An experimental survey of swelling in commercial Fe-Cr-Ni alloys bombarded with 5-MeV Ni ions," *J. Nucl. Mater.*, 54, No. 1, 24-40 (1974).
2. V. F. Zelenskii, A. M. Parshin, I. M. Neklyudov, et al., "Vacancy-related swelling of a high-nickel alloy in different structural states during bombardment with heavy ions," *Vopr. At. Nauki Tekh., Ser. Fiz. Rad. Povrezhd. Rad. Mater.*, Iss. 2 (13), 18-22 (1980).
3. I. P. Kursevich, V. A. Nikolaev, O. N. Zhukov, and A. A. Kuznetsov, "Structural changes and radiation damage in high-nickel steels and alloys," *ibid.*, Iss. 4 (32), 57-64 (1984).
4. A. M. Parshin, *Structure and Radiation Swelling of Steels and Alloys* [in Russian], Énergoatomizdat, Moscow (1983).
5. C. Dimitrov, M. Tenti, and O. Dimitrov, "Resistivity recovery in austenitic Fe-Cr-Ni alloys neutron irradiated at 23°K," *J. Phys. F: Metal Phys.*, 11, 753-765 (1981).
6. K. Bagley, L. Bramman, and C. Cawthorne, "Fast neutron induced voidage in nonfissile metals and alloys," in: *Proc. BNES European Conf.*, March (1971).
7. V. V. Andreev, O. N. Zhukov, I. P. Kursevich, et al., "Effect of irradiation with fast neutrons on the mechanical properties and swelling of austenitic steels in different structural states," *Vopr. Sudostr., Ser. Metalloved.*, Iss. 22, 39-41 (1975).
8. Yu. L. Rodionov, G. G. Isfandiyarov, and V. S. Sarsenbi, "Strengthening of iron-nickel alloys," *Fiz. Met. Metalloved.*, 48, No. 5, 979-985 (1979).
9. B. Sharma, K. Sonnenberg, G. Antesberger, and W. Kesternich, "Electrical resistivity of electron-irradiated concentrated Fe-Cr-Ni alloys during isochronal annealing," *Philos. Mag.*, A, 37, No. 6, 777-788 (1978).

- Declassified and Approved For Release 2013/02/20 : CIA-RDP10-02196R000300070003-2
10. P. A. Piatonov, "Stress relaxation in neutron irradiated metals, recovery, and annealing of radiational defects," in: Effect of Nuclear Radiations on Materials [in Russian], Moscow (1962), pp. 106-120.
  11. V. A. Nikolaev, "Mechanisms of the effect of solute atoms on the radiational embrittlement and strengthening (hardening) of the iron-base alloys," Vopr. At. Nauki Tekh., Ser., Fiz. Rad. Povrezh. Rad. Mater., Iss. 2 (13), 47-60 (1980).

#### RADIOLYSIS OF AQUEOUS SOLUTIONS OF GADOLINIUM NITRATE

V. D. Ganzha, K. A. Konoplev,  
V. P. Mashchetov, S. P. Orlov,  
and V. D. Trenin

UDC 541.15:621.039.56

The use of gadolinium nitrate for liquid regulation of the reactivity of nuclear reactors is attractive because this substance has a large neutron-absorption cross section and is highly soluble in coolants. However, a usable absorber must also have sufficiently high chemical and physical resistance to reactor radiation under all regimes of liquid regulation.

Under the conditions of power reactors, gadolinium nitrate decomposes and forms a precipitate, and it is therefore unsuitable for liquid regulation at temperatures above 135°C [1, 2]. The literature contains no reports of any practical use of gadolinium nitrate in research reactors.

Important questions in the technology of liquid regulation are those relating to the radiolysis of solutions, the radiochemical reactions of the volume-compensator gas, gas generation, and the radiochemical resistance of the absorber. The present study is devoted to the investigation of these questions.

The radiolysis of pure water and aqueous solutions after sufficiently long irradiation is characterized by the establishment of a stationary state if the reaction products are not removed from the system (closed systems) or the establishment of an equilibrium state in which the removed reaction products are continuously replaced as a result of direct reactions (open systems). In closed systems the quantitative values of the stationary concentrations of the molecular products of radiolysis constitute the main characteristic of the radiolysis process.

For pure water the stationary concentrations of the molecular products (hydrogen, hydrogen peroxide, and oxygen) are very low, ranging approximately from  $10^{-5}$  to  $10^{-6}$  moles/liter [3]. However, in solutions of salts the level of stationary concentrations of water-radiolysis products may become much higher, since the dissolved substances facilitate the process of the reactions with radical products of the decomposition of the water under the action of the radiation. Even very small quantities of a substance that is introduced into the water and interacts with the radicals can protect the molecular products from recombination reactions. Raising the temperature of the solution has an opposite effect, i.e., it initiates the recombination reactions and leads to a lowering of the stationary concentrations of the molecular products of water radiolysis.

It is known that in solutions of boric acid placed in sealed ampules and irradiated in a reactor, there has been observed a linear increase in the pressure of the gaseous water-radiolysis products from 0.1 MPa at the beginning of the experiment to 0.4 MPa at the end. Raising the temperature to 200°C sharply reduced the pressure. Singh and Leblanc [5] described similar experiments on the irradiation of a solution of gadolinium nitrate in ampules, where the pressure of the gaseous products of water radiolysis reached a value of 1.46 MPa.

Another important factor is the resistance of the compound itself to the action of reactor irradiation. As the characteristic of the radiochemical resistance of gadolinium nitrate in our case, we may take the amount of hydroxide compounds of gadolinium that are formed and precipitated out. The formation of gadolinium hydroxide may be the result of the direct action of irradiation on the gadolinium nitrate or a consequence of its chemical reaction with

---

Translated from Atomnaya Energiya, Vol. 59, No. 3, pp. 204-209, September, 1985. Original article submitted January 16, 1984.

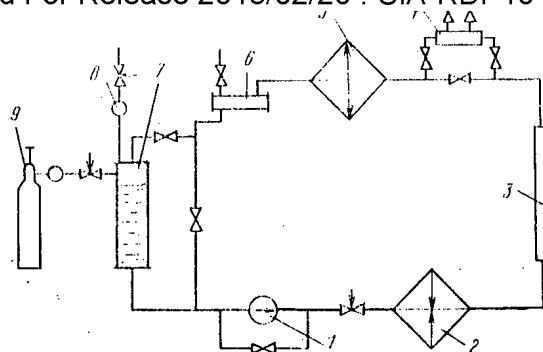


Fig. 1. Schematic diagram of the loop of the VVR-M reactor: 1) circulating pump; 2) heater; 3) irradiated volume in the reactor core; 4) device for introducing the solution of  $Gd(NO_3)_3$ ; 5) heat exchanger; 6) transparency indicator; 7) volume compensator; 8) throttle device for blowing out the nitrogen; 9) compressed-nitrogen tank.

the ammonia formed in the process of radiochemical interaction of the nitrogen dissolved in the water (the volume-compensator gas) with the products of water radiolysis.

In the case of purely chemical interaction the precipitation of gadolinium hydroxide from nitrate solutions takes place at a pH of 6.83 and a concentration relation  $[OH^-] = 0.3[Gd]$  [6].

Equally important are the questions related to the generation of gas from the solution of absorbent. The gaseous products may enter the solution of absorbent from the gaseous cushion of the volume compensator and are formed according to radiolysis reactions. Obviously the generation of a gaseous phase in the solution of the liquid-regulation system is unacceptable, since this could cause fluctuations in reactivity. We can evaluate the conditions under which the solution of absorbent remains homogeneous. At moderate pressure in the system, the solubility of the gases is governed by Henry's law:

$$p_i = C_i / K_i, \quad (1)$$

where  $p_i$  is the partial pressure of the  $i$ -th gas above the solution;  $C_i$ , concentration of the  $i$ -th gas in the solution;  $K_i$ , proportionality constant characterizing the solubility of the  $i$ -th gas at a given temperature. For a mixture of gases

$$\sum p_i = \sum \frac{C_i}{K_i}. \quad (2)$$

If the solution is saturated with the mixture of gases to the point of establishing equilibrium at a pressure  $p_{tot}$  in the system, then obviously  $\sum p_i = p_{tot}$ . The sum of the values of the partial pressures of the dissolved gases, calculated according to Eq. (2), is a suitable criterion of the degree of saturation of the solutions with the gases. If  $\sum p_i \leq p_{tot}$ , the solution is single-phase, whereas if  $\sum p_i > p_{tot}$ , the solution is supersaturated with the gases and the formation of a gaseous phase is possible.

Experimental investigations were carried out on a special loop of the VVR-M reactor (Fig.

1). The principal parameters of the reactor are given below:

Volume of solution in the system, liters	15-30
Irradiated volume in the core, $cm^3$	12-500
Flow rate of solutions in the loop during circulation, liters/h	150-380
Concn. of gadolinium nitrate, moles/liter	0.027
Temp. in the irradiation zone, $^{\circ}C$	50
Temp. of the solution in the volume compensator during degassing, $^{\circ}C$	70
Pressure in the loop, MPa	0.1-1.6
Volume compensator gas	Nitrogen, compressed air

Nitrogen flow rate in the blowout system

during degassing of the solutions,

normal  $\text{dm}^3/\text{h}$ 

170

Dose rate of reactor radiation absorbed

by the water in the core [7],

 $\text{eV}/(\text{g} \cdot \text{sec})$  $(0.16-5.2) \cdot 10^{19}$ 

The preparation of the loop for operation was carried out before the VVR-M reactor went to full power. The filling and the presence of the gaseous phase in the loop were monitored visually by means of a transparency indicator. After the solution had become saturated with the gases to a given concentration, the volume compensator was switched to a dead-end regime. During the process of operation of the loop, we periodically analyzed the circulating solution to determine the amount of dissolved nitrogen, hydrogen, and oxygen and the amount of hydrogen peroxide,  $\text{NH}_4^+$  ions, and  $\text{Gd}^{3+}$  ions, and we also measured the pH values. The duration of one cycle of operation of the loop was determined by the graph of reactor operation at full power (1-2 weeks). The variation of the molecular-product concentration as a function of the duration of loop operation in one of the experiments is shown in Fig. 2, from which it can be seen that the concentration of molecular products of the radiolysis of pure water reaches a stationary level about 20 h after reactor startup, and the concentration of radiolysis products (hydrogen, oxygen, and hydrogen peroxide) is no more than about  $10^{-4}$  moles/liter. The concentration of nitrogen - the volume-compensator gas - is determined by its solubility at saturation pressure (0.5 MPa) and remains constant during the entire period of irradiation, when the water does not yet contain any gadolinium nitrate. The sum of the values of the partial pressures of the dissolved gases, calculated from their stationary concentrations, was 0.58 MPa and did not exceed the total pressure in the system (0.6 MPa). No generation of any gaseous phase was observed in the loop.

After the introduction of gadolinium nitrate into the water (in Fig. 2 this time is indicated by the first dashed line) to a concentration of  $10^{-3}$  moles/liter, we observed a significant increase in the concentration of radiolysis products. About 5 h after the absorbent was introduced, the hydrogen concentration increased eighteenfold and reached a value of  $1.6 \cdot 10^{-3}$  moles/liter, the oxygen concentration increased sevenfold (to  $4 \cdot 10^{-4}$  moles/liter), and the hydrogen peroxide concentration increased fifteenfold (to  $9 \cdot 10^{-4}$  moles/liter). From this moment on, we noted the appearance of the gaseous phase in the transparency indicator of the loop and the decrease of the nitrogen concentration in the circulating solution. The sum of the values of the partial pressures of the dissolved gases amounted to 0.8 MPa and exceeded the total pressure in the loop (0.6 MPa). The continuous formation of hydrogen and oxygen in the radiolysis process led to a supersaturation of the solution with gases and to the displacement of nitrogen from the solution.

A further increase of the gadolinium nitrate concentration (the second dashed line in Fig. 2) resulted in a new increase in the concentration of the molecular products of radiolysis. The process of forcing out the nitrogen from the solution continued. The gas so generated was discharged through the air-hole of the transparency indicator into the ventilation system, which resulted in the establishment of an equilibrium state.

As can be seen from Fig. 2, the pH of the gadolinium nitrate solutions is independent of the duration of the loop operation and of the variation of the concentrations of nitrogen, oxygen, and hydrogen. The ammonia concentration, according to the data of chemical analyses, did not exceed  $3 \cdot 10^{-5}$  moles/liter. This suggests that the dissolved nitrogen does not enter into radiochemical reactions with the water radiolysis products which significantly change the chemical composition of the solution. The products of the radiolysis of aqueous solutions of gadolinium nitrate are hydrogen, oxygen, and hydrogen peroxide. However, if the irradiation lasts long enough, the formation of hydrogen peroxide slows down and the hydrogen and oxygen removed from the reaction zone are constantly replenished. An extensive series of experiments was conducted on the loop of the VVR-M reactor. The concentration of gadolinium nitrate was varied from  $10^{-3}$  to 0.27 moles/liter, the initial concentrations of the gases in the solution from  $2.4 \cdot 10^{-4}$  to  $1.1 \cdot 10^{-2}$  moles/liter in the case of nitrogen and from  $3.1 \cdot 10^{-5}$  to  $3.2 \cdot 10^{-3}$  moles/liter in the case of oxygen, and the working pressure in the loop from 0.35 to 1.6 MPa. In all cases the nature of the curves was similar to those of Fig. 2.

The concentration of the gaseous radiolysis products reached the limit of solubility at a given pressure, and we observed a continuous generation of the discharge of the gaseous phase in the loop contour. The hydrogen peroxide concentration reached a stationary level

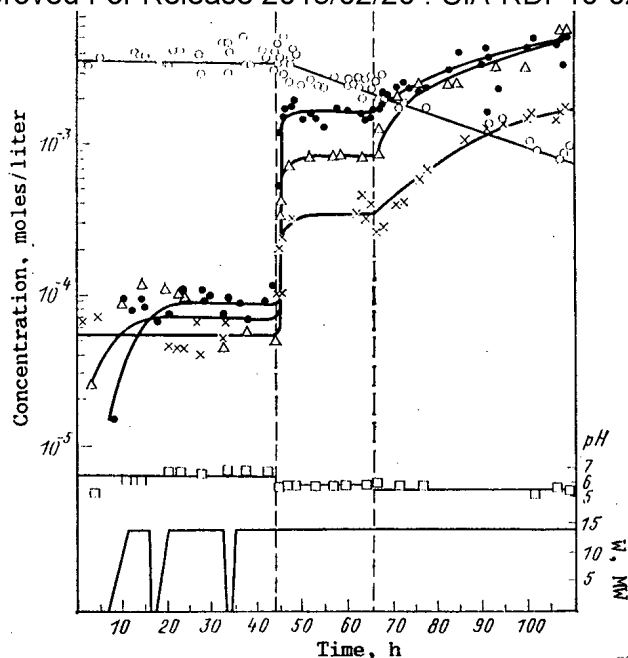


Fig. 2. Concentration of hydrogen ( $\bullet$ ), oxygen ( $\times$ ), hydrogen peroxide ( $\Delta$ ), nitrogen ( $\circ$ ), pH ( $\square$ ) in the circulating solution as functions of the time of operation of the loop, shown together with a diagram of reactor operation. The dashed lines indicate the instants of time at which the gadolinium nitrate solution is introduced into the loop: the left-hand portion, up to the first dashed line, indicates pure water, the portion between the dashed lines indicates the time when the gadolinium nitrate concentration is  $10^{-3}$  moles/liter, and in the right-hand portion, after the second dashed line, the gadolinium nitrate concentration is  $4.7 \cdot 10^{-3}$  moles/liter.

of  $2 \cdot 10^{-2}$  moles/liter. Thus, as can be seen from the results obtained, when we use liquid regulation with the aid of gadolinium, the circulating solution of gadolinium nitrate must be continuously degassed. The radiolysis of water in closed-cycle systems with degassing is determined by the radiochemical yield of gaseous products and the absorbed dose of radiation. Since the water decomposes into hydrogen and oxygen, it follows from the law of conservation of material balance that in order to find the amount of gases formed, it is sufficient to determine the amount of any one product, for example the hydrogen.

The rate of formation of hydrogen in the system,  $\Pi_{H_2}$ , can be found from the relation (moles/h):

$$\Pi_{H_2} = \frac{G_{H_2} I m 3600}{400 A}, \quad (3)$$

where  $G_{H_2}$  is the radiochemical yield of  $H_2$ , in molecules/100 eV;  $I$  is the absorbed radiation dose rate, eV/(g·sec);  $m$  is the mass of the water in the irradiation zone, in grams;  $A$  is Avogadro's number.

The rate of removal of the hydrogen in the degasser,  $J_{H_2}$ , is determined by the relation (moles/h):

$$J_{H_2} = Q \xi C, \quad (4)$$

where  $Q$  is the flow rate of the solution through the degasser, liters/h;  $\xi$ , efficiency of removal of the  $H_2$ ;  $C$ , concentration of  $H_2$  in the solution at the degasser inlet, moles/liter.

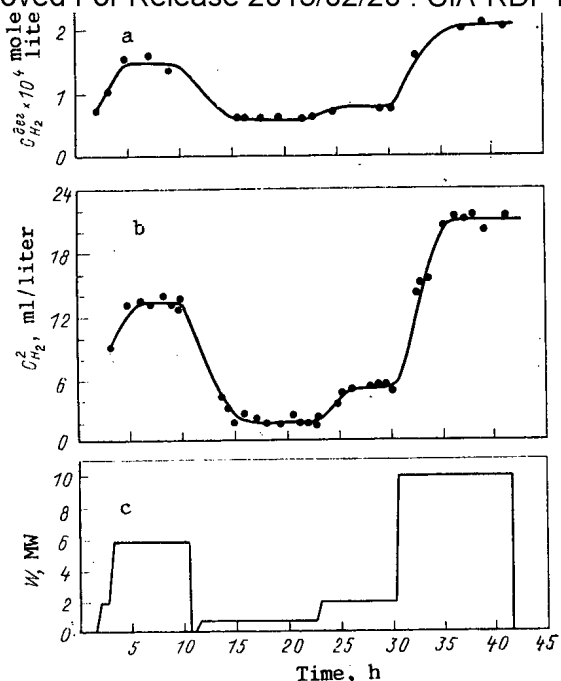


Fig. 3. Concentration of hydrogen in the liquid phase of the degasser (a), concentration of hydrogen in the gaseous phase of the nitrogen-venting system (b), and reactor power (c) as functions of the time of reactor operation. The  $Gd(NO_3)_3$  concentration was  $1.4 \cdot 10^{-3}$  moles/liter; the pressure in the volume compensator was 1.1 MPa; the nitrogen flow rate in the venting system was 170 normal  $dm^3/h$ .

In the equilibrium state  $J_{H_2} = \Pi_{H_2}$ ,  $C = C_p$ , where  $C_p$  is the equilibrium concentration of the hydrogen in the solution. From the equality of the expressions in Eqs. (3) and (4) we find that

$$Q_{\Sigma}^{\text{ex}} = \frac{G_{H_2} \cdot I m 3600}{400 A C_p}. \quad (5)$$

As can be seen from the relations (3) and (5), in order to determine the parameters of the degassing system, we must have data on the radiochemical yield of hydrogen. The absorbed radiation dose rate is given by the parameters of the reactor and the liquid-regulation system. The allowable equilibrium concentration of hydrogen must be given from the condition that the solution remains homogeneous, and we calculate it from Eq. (2), taking account of the pressure in the system and the concentration of other gases. The radiochemical yield of hydrogen and its variation with the irradiation intensity, the hydrogen concentration, and the gadolinium nitrate concentration were determined experimentally on the loop of the VVR-M reactor, partially altered for these experiments. The solution was kept circulating by means of a volume compensator, in which it was degassed. The nitrogen was admitted through the gas space of the compensator at a constant flow rate without reducing the total pressure in the system, and it was blown into the special ventilation system by means of a throttling device.

In order to reduce the equilibrium concentration of nitrogen in the circulation solution, and also in order to make sure that it was possible to dissolve the hydrogen and oxygen formed during the radiolysis in the zone of action of the radiation, the heater was set up in front of the compensator-degasser, while the cooler was set up at the inlet to the irradiated volume. Using the fact that the solubility of the gases varies with the temperature, we found a more effective method of removing the hydrogen and oxygen and precluded the generation of a gaseous phase in the solution in the irradiation zone. The method used in the experiments was the following. After starting up the loop, we raised the reactor power and

m, g	Q, liters/h	$C_{H_2}^{deg}$ , moles/liter	$\Pi_{H_2}$ , liters/h	Gd(NO <sub>3</sub> ) <sub>3</sub> concn., moles/liter	W, MW	CH <sub>2</sub> , moles/liter	GH <sub>2</sub> , molecules per 100 eV
100	360	$0,1 \cdot 10^{-4}$	0,3	$1,4 \cdot 10^{-3}$	0,8	$0,47 \cdot 10^{-4}$	0,86
100	360	$0,5 \cdot 10^{-4}$	0,8	$1,4 \cdot 10^{-3}$	2,0	$1,49 \cdot 10^{-4}$	0,92
100	360	$1,5 \cdot 10^{-4}$	2,25	$1,4 \cdot 10^{-3}$	6,0	$4,29 \cdot 10^{-4}$	0,86
100	360	$2 \cdot 10^{-4}$	3,5	$1,4 \cdot 10^{-3}$	10,0	$6,34 \cdot 10^{-4}$	0,81
100	360	—	4,66	$2,8 \cdot 10^{-3}$	16,0	—	0,67
100	360	—	4,16	$4,1 \cdot 10^{-2}$	16,0	—	0,60
500	380	—	2,99	0,2	14,0	—	0,10
500	150	—	3,05	0,2	14,0	—	0,10

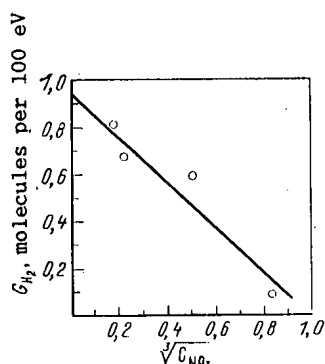


Fig. 4. Radiochemical yield of hydrogen as a function of the cube root of the NO<sub>3</sub><sup>-</sup> ion concentration in the radiolysis of aqueous solutions of Gd(NO<sub>3</sub>)<sub>3</sub> when subjected to reactor radiation.

measured the concentration of hydrogen in the gaseous phase in the nitrogen-venting system, and in the liquid phase at the outlet of the degasser, depending on the duration of the reactor operation at constant power. When equilibrium had been established — indicated by constant values of the measured hydrogen concentrations in the gaseous and liquid phases — we varied the reactor power stepwise and continued the experiment until a new equilibrium was reached. The absence of any gaseous phase in the transparency indicator was monitored continuously. The relationships found are shown in Fig. 3.

The rate of formation of hydrogen in the loop was calculated from the equation (liters/h):

$$\Pi_{H_2} = 10^{-3} C_{H_2}^g Q_{N_2}, \quad (6)$$

where  $C_{H_2}^g$  is the equilibrium concentration of hydrogen in the nitrogen-venting system, ml H<sub>2</sub>/liter N<sub>2</sub>;  $Q_{N_2}$  is the nitrogen flow rate in the venting system, liters N<sub>2</sub>/h.

The concentration of hydrogen in the irradiated volume was determined from the equation (moles/liter)

$$C_{H_2} = C_{H_2}^{deg} + \frac{\Pi_{H_2}}{Q_{22,4}}, \quad (7)$$

where  $C_{H_2}^{deg}$  is the equilibrium concentration of hydrogen in the liquid phase at the degasser outlet, moles/liter.

The radiochemical yield of hydrogen was found from the expression (molecules/100 eV)

$$G_{H_2} = \frac{\Pi_{H_2} 400 A}{0,33 \cdot 10^{19} W m 3600 \cdot 22,4}, \quad (8)$$

We conducted experiments with different concentrations of gadolinium nitrate as the reactor power was varied from 0.8 to 16 MW.

The variation of the radiochemical yield of hydrogen as a function of the gadolinium nitrate concentration, reactor power, and hydrogen concentration in the irradiated volume is shown in Table 1. The radiochemical yield of hydrogen for a gadolinium nitrate concentration of  $1.4 \cdot 10^{-3}$  moles/liter is equal to  $0.86 \pm 0.03$  molecules per 100 eV. Within the limits of measurement error, it remains constant over a considerable range of variation (by a factor of more than 10) of the intensity of reactor radiation and the hydrogen concentration in the irradiated volume; as the gadolinium nitrate concentration increases, this yield decreases. The transparency indicator did not reveal any generation of gaseous phase during the degassing of the circulating solution. It is known that some substances dissolved in the water reduce the radiochemical yield of molecular products of radiolysis. The  $\text{NO}_3^-$  ion is a known acceptor of hydrogen atoms. In general form, the yield of molecular products of radiolysis is a linear function of the cube root of the acceptor concentration for moderate concentrations. Such a functional relation, obtained from experimental data, is shown in Fig. 4. The values of the radiochemical yield of hydrogen lie fairly satisfactorily along a straight line. Extrapolation of the results to  $[\text{NO}_3^-]^{1/3} = 0$  yield  $G_{\text{H}_2}^0 = 0.97 \pm 0.11$  (the so-called molecular-product yield at zero acceptor concentration).

For aqueous solutions of calcium nitrate irradiated with a mixed flux of neutrons and gamma-emitting nuclides, a similar extrapolation yielded a value of  $G_{\text{H}_2}^0 = 0.82$  [8]. For a  $10^{-2}$  mole/liter solution of KBr irradiated in the reactor, the value found was also  $G_{\text{H}_2}^0 = 0.82$  [3]. Analysis of a large amount of experimental data, given in [3], shows that  $G_{\text{R}_2}^0$  - the yield of molecular product at zero acceptor concentration - is independent of the nature of the dissolved substance but depends on the type of radiation and the pH of the medium. It may be assumed that in our case as well, the decisive influence on the radiolysis is that of the  $\text{NO}_3^-$  ions present in the solution. A higher value of  $G_{\text{H}_2}^0$  may be attributed to the reduction of the pH of the aqueous solutions of gadolinium nitrate owing to its hydrolysis; it may also be due to the increase in the contribution made by the radiation dose from secondary radiation which arises during the capture of thermal neutrons by gadolinium nuclei. This radiation was not taken into consideration in calculating the absorbed dose.

During each experiment, we measured the gadolinium nitrate concentration in the circulating solution of the loop, since we had to make sure that there was no deposition of gadolinium in the form of the hydroxide together with the corrosion products. The gadolinium nitrate concentration remained constant to within the 10% measurement error. We found no deposition of gadolinium on the loop equipment surfaces, nor any formation of hydroxide compounds or sorption of the gadolinium on the corrosion products.

Thus, our investigations have established that gadolinium nitrate in aqueous solutions is a radiation-stable chemical compound and can be used as a neutron absorber in the liquid regulation of the reactivity of low-temperature nuclear reactors. Nitrogen or air may be used as the gaseous "cushion" of the volume compensator. The radiolysis of water in the presence of gadolinium nitrate in a closed system leads to the generation of a gaseous phase containing a detonating mixture of  $\text{H}_2$  and  $\text{O}_2$ . In an open system with degassing no generation of a gaseous phase is observed. The results of the investigations have been used in designing the liquid reactivity regulation system of the PIK reactor.

The authors express their deep gratitude to R. G. Pikulik for his assistance in conducting the experiments on the VVR-M reactor, to A. N. Borisov and Yu. P. Grigor'ev for their practical help, and also A. I. Egorov for his part in the evaluation of the results.

#### LITERATURE CITED

1. P. Cohen, Water Technology of Power Reactors [Russian translation], Atomizdat, Moscow (1973), p. 161.
2. L. Koenig, "Thermal stability of gadolinium nitrate solution at high temperature," IDO-16674. Phillips Petroleum Co., Atomic Energy Division, May, 1961.
3. I. V. Vereshchinskii and A. K. Pikaev, Introduction to Radiochemistry [in Russian], Izd. Akad. Nauk SSSR, Moscow (1963).

4. F. I. Dolin and B. V. Emsler, "Radiolysis of water in the presence of  $H_2$  and  $O_2$  when subjected to reactor radiation, fission fragments, and x rays," in: Materials of the International Conference on the Peaceful Uses of Atomic Energy, Geneva, 1955, Vol. 7 [in Russian], Goskhimizdat, Moscow (1958), p. 687.
5. A. Singh and G. Leblanc, Use of Gadolinium as a Neutron Absorber in Nuclear Reactors: Radiolysis of Gadolinium Nitrate Solutions, Whiteshell Nuclear Research Establishment, Pinawa, Manitoba, ROE-110, November, 1976.
6. T. Moller and H. Kremers, "Observations on the rare earths," J. Phys. Chem., 48, 39 (1944).
7. V. D. Trenin, "Investigation of the radiolysis of water in the VVR-M reactor," Author's Abstract of Candidate's Dissertation, Technical Sciences, Leningrad (1975), p. 31.
8. R. Sowden, J. Am. Chem. Soc., 79, 1263 (1957).

#### SELECTION OF THE MATERIAL AND THE TEMPERATURE CONDITIONS OF THE PICKUP PLATE OF A FAST-ION INJECTOR

V. G. Tel'kovskii, A. A. Pisarev,  
V. N. Tsyplakov, and A. N. Igritskii

UDC 533.924

In plasma units with injection of fast particles there arises the problem of absorbing that part of the injected beam which was not captured by the plasma. When a pickup plate accumulates the hydrogen introduced in the form of fast ions or atoms, the material of the pickup plate of the injector must be characterized by low reverse gas liberation while a large amount of introduced hydrogen is being accumulated.

Depending upon their interaction with hydrogen, all metals can be divided into two groups. There exist metals which dissolve hydrogen endothermically, i.e., with absorption of heat (Al, Mo, Ni, Cu, stainless steel), whereas other metals dissolve the hydrogen exothermically, i.e., under liberation of heat (Nb, Zr, Ta, V, Ti, and Pd). Accordingly, on the diagram of the potential energy of a hydrogen-metal system (Fig. 1), the energy level of the hydrogen in the metal is either higher or lower than in the free molecule. In the first case, from the energy viewpoint the hydrogen atom is more advantageously released into the vacuum chamber, whereas the hydrogen remains in the metal in the second case. The diagrams of Fig. 1 are extremely simplified and do not show adsorption states on the surface or details in the change of the potential near the surface. Such diagrams exemplify the interaction of hydrogen gas with metals under equilibrium conditions and are not always correct for the introduction of ions. However, such diagrams are occasionally used for describing the penetration [1] or the accumulation and liberation [2] of hydrogen in the introduction of hydrogen ions; the use of these diagrams in computational models renders results which are in good agreement with the experimental results. It follows from the diagram of Fig. 1 that the pickup plates must be made from a metal with a negative heat of solution of hydrogen.

The material of the plate must provide for a fast removal of the hydrogen from the slowing-down area into the bulk of the material without release through the surface into the vacuum chamber so that the accumulation cannot take place in a thin-layer metal surface but in the entire thickness of the sample. As a result, the "capacity" of the pickup plate increases enormously, and the concentration of the hydrogen near the surface decreases at the same time and, accordingly, the rate of gas liberation through the surface decreases too. Thus, for assessing the capability of a material to capture hydrogen, first of all two parameters must be analyzed: the mobility of hydrogen by diffusion and the penetration of the surface. The mobility by diffusion is characterized by the activation energy  $Q_d$  and the penetration by the barrier  $Q_s$  which must be overcome in the transition of a hydrogen atom from the metal into vacuum. For metals which are active with respect to hydrogen (see Fig. 1) we have  $Q_s = 1/2(|E_{SH_2}| + E_a)$ , where  $1/2|E_{SH_2}|$  denotes the absolute value of the heat of solution or absorption;  $1/2E_a$  denotes the additional surface barrier which is equal to the activation energy of dissociative chemisorption and which depends upon the state of the surface [1].

Translated from Atomnaya Energiya, Vol. 59, No. 3, pp. 209-213, September, 1985. Original article submitted October 22, 1984.

Constant	Ti	Id	Nb	Zr	Ta	V
$1/2  E_{sH_2} $ , kJ/mole	39,3—47,3	8,4	36,0	60,7	36,0	31,8
$Q_d$ , kJ/mole	51,9	22,2	10,0	24,7—29,3	13,4	4,2
$D_0^*$ , cm <sup>2</sup> /sec	$1,8 \cdot 10^{-2}$	$2,9 \cdot 10^{-3}$	$5 \cdot 10^{-4}$	$(4,7-6,6) \cdot 10^{-4}$	$1,4 \cdot 10^{-4}$	$3,1 \cdot 10^{-4}$

\* $D_0$  denotes the factor before the exponential.

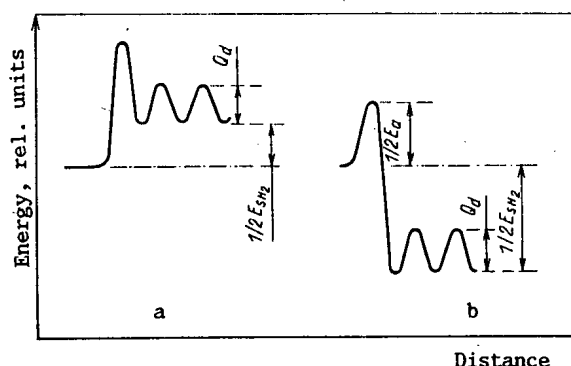


Fig. 1. Simplified diagram of the potential energy of a hydrogen atom in a) endothermic and b) exothermic solution in a metal:  $1/2 E_{sH_2}$  denotes the heat of solution referred to an atom; and  $Q_d$  denotes the additional surface barrier.

For preparing the pickup plate of an injector, one most conveniently uses a metal with a very large ratio of surface barrier to diffusion barrier and also with a high coefficient of diffusion of hydrogen. Vanadium meets these requirements better than all the other elements and is followed by niobium and tantalum, which is similar in regard to the basic characteristics (Table 1). Experimental investigations have shown a high capture efficiency of hydrogen ions and niobium at high fluxes and temperatures (see Fig. 2). It is therefore possible to use niobium as the material of the pickup plate of an ion injector of hydrogen atoms or ions. If intense heating of the plate at high ion-beam powers takes place, zirconium can be employed.

In assessing the liberation of hydrogen from a metal, thermal and radiation-stimulated desorption must be taken into account. The rate of gas liberation by radiation-stimulated processes is usually given by the formula

$$J_i = I\sigma N, \quad (1)$$

where  $J_i$  denotes the flux of the gas liberated;  $I$ , flux of the ions onto the surface;  $\sigma$ , cross section of ion-stimulated desorption; and  $N$ , number of captured particles per unit area (in the case of a low diffusion mobility, when the entire hydrogen introduced is contained in the area in which the ions are slowed down) or the number of hydrogen atoms per unit area in the layer near the surface, where an interaction of the ion beam takes place (in the case of a high diffusion mobility of the hydrogen). When we assume that hydrogen is knocked off by radiation in the entire area of thickness  $\ell$  in which the ions are slowed down, we have  $N = C_0 \ell$ , where  $C_0$  denotes the average volume concentration of the hydrogen in the region near the surface. Equation (1) then assumes the form

$$J_i \simeq I\sigma \ell C_0. \quad (2)$$

For the majority of metals the  $\sigma$  value at a hydrogen ion energy of  $\sim 10$  keV amounts to  $10^{-18}$  cm<sup>2</sup> and increases when this energy decreases. The rate of reverse gas liberation from metals by thermal processes can be determined with a formula of [5]:

$$J_i = K(T) C_0,$$

where

$$K(T) = AT^{-1/2} \exp(-2Q_s/RT). \quad (4)$$

The notation is interpreted as follows:  $K(T)$ , coefficient of recombination of atoms on the surface under formation of molecular hydrogen;  $T$ , temperature; and  $A$ , an experimental constant which depends upon the type of the metal and the hydrogen isotope. The height  $Q_s$  of the barrier is the most important parameter for determining  $K$ . For pure surfaces, for example, for surfaces under the conditions of thermal evaporation of a metal [6] or of an intense ion bombardment [7], we have  $Q_s = 1/2|E_{SH_2}|$ . But the surface of metals is in many cases passivated (e.g., oxidized), and therefore there exists an additional potential barrier for the liberation of the absorbed hydrogen, this barrier being equal to  $1/2E_a$  (see Fig. 1b). Thus, oxidation of the surface is a positive effect in regard to increasing the efficiency of hydrogen-ion capture. The thickness of the oxide layer must not be greater than several atomic layers because otherwise a considerable part of the ion beam will be slowed down in a thick oxide layer and this implies inadmissibly high hydrogen concentrations in the layer as a consequence of the low diffusion mobility. This means that a thin natural oxide layer fully suffices for efficiently reducing the penetration of the surface. Such an oxide layer is extremely stable but under intense ion irradiation the layer may be removed by cathodic sputtering through fast ions. This deteriorates the conditions of operation of the pickup plate. Besides that, deoxidation of the surface of the pickup plate and, accordingly, a reduction of the surface barriers can take place under the influence of the hydrogen atmosphere and a high temperature ( $\sim 800^\circ\text{K}$  in the case of Nb).

Equations (2) and (3) show that the liberation of gas increases in the introduction of ions in proportion to the increase in the hydrogen concentration in the region near the surface. When the temperature of the metal is low, a large quantity of hydrogen accumulates in the region of its introduction. Thermal liberation of gas is irrelevant at low temperatures but radiation-stimulated processes can sharply increase the reverse liberation of gas. The temperature of the metal must be raised for reducing  $C_0$  and  $J_i$  because in this way an outflow of hydrogen by diffusion from the zone of hydrogen introduction into deep layers of the metal is secured. Nevertheless, the temperature must not be too high because then the thermal liberation of the gas can be inadmissibly intense even at low  $C_0$  values. Thus, the operational temperature  $T$  of the pickup plate must be within a certain interval  $T_l - T_h$ , as confirmed by experimental measurements [8] and calculations [9] of the efficiency of the capture in the introduction of hydrogen ions into metals with activity with respect to the hydrogen. In a certain temperature interval the efficiency of capture is almost 100% even with an extremely high ion flux. At a lower temperature, the efficiency decreases rapidly with increasing flux because of the radiation-stimulated liberation of gas; at higher temperatures, the efficiency also decreases as a result of the thermal liberation of the gas.

In order to estimate the lower ( $T_l$ ) and upper ( $T_h$ ) limit of the interval, one can use the solution of the diffusion equation for a source in the form of an ion beam under the conditions of thermal and radiation-stimulated liberation of gas in accordance with the model proposed by the authors of [10]. The hydrogen concentration can be increased in the zone of hydrogen introduction by radiation-induced defects, which are taken into account in the cited model. Therefore, the temperature of the metal must be high enough so that the hydrogen concentration in the defects is reduced and, hence, the influence of the defects upon the capture of ions in the area near the surface is less pronounced.

Let us determine as an example the conditions of operation of the pickup plate of the injector of the OGRA-4 unit. The parameters of the  $H^+$  beam are as follows: energy 10 keV, current 20 A in the pulse, pulse length 20 msec, interval between pulses 2 min, and area of the irradiated surface 600  $\text{cm}^2$ . Two hundred and fifty pulses are generated during an operational period. With these parameters, the ion current intensity in a pulse is  $I = 2 \cdot 10^{17} \text{ cm}^{-2} \cdot \text{sec}^{-1}$ , the ion flux during a pulse is  $4 \cdot 10^{15} \text{ cm}^{-2}$ , the range of the ions is  $l \approx 10^{-5} \text{ cm}$ , and the cross section of radiation stimulated desorption is  $\sigma \approx 10^{-18} \text{ cm}^2$ . We assume that the admissible current of reverse liberation of gas is  $J_{adm} = 10^{-2} I$ , i.e., comparable with the flux of the kinetically reflected ions. A niobium plate with a thickness  $L = 1 \text{ mm}$  is considered.

The admissible concentration  $C_{adm}$  of the hydrogen ions in the area of slowing down is  $10^{21} \text{ cm}^{-3}$  according to the condition of ion-stimulated desorption (Eq. (2)). When the ion

TABLE 2. Pickup Plate Temperature Development during a Pulse under Stationary Cyclic Thermal Conditions

Surface blackness	Temp. (°K) of the surrounding surface	
	273	300
0,9	354/319 *	374/339
0,7	365/330	381/346
0,5	382/347	395/360
0,3	417/382	427/392
0,1	521/486	526/491

\*The first value denotes the temperature at the end of the pulse (K); the second value denotes the temperature (K) before the beginning of the next pulse.

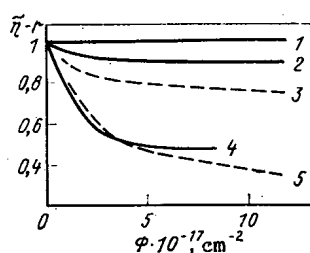


Fig. 2. Dependence of the difference between the coefficient ( $\eta$ ) of introduction and the coefficient ( $r$ ) of reflection of  $D^+$  ions upon the flux  $\Phi$  of the bombarding ions in the case of niobium: —) refers to the results of our work for an ion current density of  $3 \cdot 10^{14} \text{ cm}^{-2} \cdot \text{sec}^{-1}$  and  $E_{D_2^+} = 15 \text{ keV}$ ; ---) refers to the results of [2] for the ion current density  $4 \cdot 10^{15} \text{ cm}^{-2} \cdot \text{sec}^{-1}$  and  $E_{D_2^+} = 18 \text{ keV}$ ; curves 1-5 refer to the temperatures 280-670, 880, 450, 1070, and 560°K, respectively.

energy decreases,  $\lambda$  becomes shorter [11] but the cross section  $\sigma$  increases [12] while the  $C_{\text{adm}}$  value depends slightly upon the energy. When the diffusion of hydrogen is low,  $C_0 = 10^{21} \text{ cm}^{-3}$  is obtained with an ion flux of  $10^{16} \text{ cm}^{-2}$ . This value of the admissible flux must be considered too low because the admissible flux was  $\sim 10^{17} \text{ cm}^{-2}$  in the experiments of [6] with 18 keV  $D^+$  ions at 77 K. One can therefore assume that  $C_{\text{adm}} \approx 10^{22} \text{ cm}^{-2}$ . Accordingly, at a low temperature the flux limit will be reached already after a few dozen pulses and a significant fraction of bombarding ions will return into the vacuum chamber as a consequence of ion-stimulated desorption; i.e., low operating temperatures of the pickup plate and materials with a low mobility of hydrogen (e.g., titanium) are necessarily unsuitable.

This means that the hydrogen introduced must have the possibility to migrate into the inner regions of the metal for reducing  $C_0$ . Thus, at a temperature of 300-700°K, the shift of the diffusion front ( $\chi \approx \sqrt{Dt}$ ) in niobium is  $4 \cdot 10^{-4} - 1.3 \cdot 10^{-3} \text{ cm}$  during a single pulse. These values exceed many times the dimensions of the zone of slowing down. We have in this case  $C_0 = 10^{19} - 10^{18} \text{ cm}^{-3}$ . During approximately 2 min (time interval between pulses), the shift  $\chi$  increases to  $3 \cdot 10^{-2} - 4 \cdot 10^{-1} \text{ cm}$  and becomes comparable with the thickness of the plate, whereas  $C_0$  decreases to  $1.3 \cdot 10^{17} - 1 \cdot 10^{16} \text{ cm}^{-3}$ . During a single operational period, the average concentration of the hydrogen atom reaches  $\sim 10^{19} \text{ cm}^{-3}$ .

At an operational temperature above 300°K the concentration of the hydrogen atoms in the layer near the surface of a niobium plate (during the time of a pulse as well as on the average during an operational period) is below the limit value at which radiation-stimulated liberation of gas must be taken into account. In this case a concentration of  $10^{21}$  cm<sup>-3</sup> will be reached in 100 operational periods (the concentration is the lowest critical value at which radiation-stimulated desorption takes place). Thus, the safe life of a plate with guaranteed low radiation-stimulated liberation of gas at  $T > 300^\circ\text{K}$  is not less than 100 operational periods. During this entire time, the radiation-stimulated liberation of gas will not exceed 1% of the current of incident ions.

As indicated above the thermal liberation of gas depends upon the state of the surface. It has been shown that at high current densities and fluxes, when the surface is continuously purified by sputtering of material, the experimental results are in good agreement with the assumption  $Q_s = 1/2|E_s| = 36$  kJ/mole [2]. In this case the efficiency of capture begins to decrease already at  $T \approx 400^\circ\text{K}$ . In experiments on thermal desorption and liberation of gas during the time of irradiation at a lower current density, the value  $Q_s \approx 105$  kJ/mole was obtained, i.e., this value is much greater than that of [2]. The efficiency of capture is kept at high values even at 800°K under these conditions (see Fig. 2).

Calculations made with Eq. (4) have shown that in the case of a passivated surface ( $Q_s = 105$  kJ/mole), the flux of thermal gas liberation from niobium reaches 1% of the flux of the incident ions only at  $\sim 800^\circ\text{K}$  for  $C_{\text{adm}} = 10^{21}$  cm<sup>-3</sup>. This means that the thermal liberation of gas is slight at a lower temperature.

When the niobium surface is clean, the admissible temperature is 480, 390, and 350°K for the condition  $J < 10^{-2}$  I to be fulfilled in one, ten, and one hundred operational periods, respectively. Thus, the upper temperature limit is more rigidly fixed.

At 800°K the surface in a medium of hydrogen can be cleaned by deoxidation and therefore the plate must not be heated above 800°K. Cleaning also may occur as a consequence of sputtering of the material by bombarding ions. But the coefficient of cathodic sputtering of niobium oxide by 10 keV hydrogen ions does not exceed  $10^{-2}$ - $10^{-3}$  atoms per ion. This means that at most 1-10% of a monolayer will be sputtered within one pulse. In principle, several monolayers can be sputtered within an operational period but the high rate of niobium oxidation leads us to the conclusion that new oxide layers can develop between pulses, provided that the partial pressure of oxygen is high enough.

According to calculations, defects of the crystal structure only slightly affect the absorption of hydrogen ions at temperatures of 450-500°K. Thus, the measurements of the concentration profiles [11] have shown that at an ion flux of  $\sim 10^{18}$  cm<sup>-2</sup>, the concentration of the hydrogen ions in the surface layer of zirconium is less than 10% at 475°K, whereas the concentration reaches 90% at 335°K.

Thus, the operational temperature of a plate with an oxidized surface is within the interval 300-800°K; the optimal value is 450-500°K because in this case a sufficiently high diffusion mobility, a stable oxide layer, and a low accumulation of hydrogen in defects are obtained. In the case of a clean surface, the admissible operational temperature is 300-350°K.

When the operational temperature of the pickup plate is analyzed, there arises the problem of temperature changes in the surface layer due to absorption of ion-beam energy. Approximating calculations on the basis of the thermal balance show that during a single pulse of  $\sim 0.02$  sec (the thermal front propagates in this time about 0.07 cm and one can therefore assume that the temperature is approximately the same in the entire depth of a  $\sim 0.1$  cm thick plate), the target is heated by about 40°K with a power transfer of 200 kVA and an insignificant emission from the surface. In the time interval between pulses, the surface emits thermal energy and therefore the temperature in stationary operation is 220°K. A detailed calculation on the basis of the solution of the equation of heat conduction shows that at the end of a pulse, the temperature at the entry and reverse surfaces has increased by about 50°K and 20°K, respectively; thereafter, an average temperature, which exceeds the initial temperature by 35°K, is rapidly established in the entire thickness of the plate. In the time interval between pulses, the temperature decreases by emission of radiation. The calculations show that after 10-20 pulses, stationary conditions have been reached and the temperature increases during a pulse and drops again toward the beginning of the subsequent pulse (see Table 2).

After prolonged operation (~100 operational periods), the plate must be replaced or degassed either by heating with simultaneous cleaning of the surface layer (e.g., by a gas discharge) or by tempering in vacuum. When during a few seconds the concentration of the hydrogen atoms is to be reduced to  $10^{18} \text{ cm}^{-3}$ , one needs a temperature of 700 and 1200°K in the two cases, respectively.

Let us note in conclusion that in the selection of the material of injector pickup plates for fast ions, metals with a high negative thermal dissolution of hydrogen, a surface-activation barrier, and a large coefficient of hydrogen diffusion must be tried. Niobium is the most suitable material as far as the coincidence of these parameters is concerned. The niobium surface is covered with a thin natural oxide film. The temperature of the pickup plate is chosen on the basis of a compromise between attempts to increase the temperature for obtaining rapid diffusion over the entire thickness of the plate (reducing radiation-stimulated desorption, increasing the capacity of the plate for hydrogen, reducing the deuterium concentration in radiation defects, and decreasing the probability of hydride formation) and the need for reducing the temperature to avoid thermal liberation of gas and decomposition of the oxide film. Experiments have shown that a high efficiency of deuterium-ion capture in niobium can be maintained up to high fluxes and high irradiation temperatures. The optimal temperatures of the niobium pickup plate for the injector of the OGRA-4 unit are 450-500°K in the case of an oxidized surface and 300-350°K in the case of a self-cleaning surface. Calculations of the heating which results from injected ions have shown that the temperature remains within admissible limits in stationary operation.

#### LITERATURE CITED

1. A. I. Livshits et al., Absorption and Transmission of Hydrogen by Metals Under Non-equilibrium Conditions [in Russian], Vol. 1, Preprint IAE-3516/18.
2. E. Hotston and G. Mc Cracken, J. Nucl. Mater., 68, NO. 2, 227 (1977).
3. Metal Hydrides [in Russian], Atomizdat, Moscow (1973).
4. G. Ahlefeld and I. Völkl, Hydrogen in Metals [Russian translation], Vol. 1, Mir, Moscoow (1982).
5. M. Baskes, J. Nucl. Mater., 92, 318 (1980).
6. A. I. Livshits et al., The Interaction of Thermal Hydrogen Atoms and Molecules with Metal Membranes [in Russian], Vol. II, Preprint IAE-3517/8.
7. S. Myers and W. Wampler, J. Nucl. Mater., 111-112, 579 (1982).
8. G. Mc Cracken, D. Jefferies, and P. Goldsmith, in: Proc. of the 4th Int. Vacuum Congress, 5/1, 149 (1968).
9. A. A. Pisarev and V. M. Smirnov, "Accumulation of gas in metals in the case of ion introduction," Poverkhnost'. Fiz., Khim., Mekh., No. 7, 138 (1984).
10. A. A. Pisarev and V. M. Smirnov, "Calculation of the coefficient of hydrogen-ion capture by metals," Poverkhnost'. Fiz., Khim., Mekh., No. 3, 112 (1985).
11. A. F. Burenkov, F. F. Komarov, M. A. Umakhov, and M. M. Temkin, Tables of the Parameters of the Spatial Distribution of Ion-Implanted Impurities [in Russian], Belorussian State Univ., Minsk (1980).
12. C. Braganza et al., J. Nucl. Mater., 76-77, 298 (1978).
13. W. Möller, J. Böttiger, and P. Børgesen, J. Nucl. Mater., 76-77, 287 (1978).

# USING THE CONCEPT OF RADIATION CAPACITY IN CALCULATIONS OF THE GREATEST ADMISSIBLE WASTE RELEASE

A. L. Kononovich, N. A. Verkhovetskii,  
V. I. Peshkov, and S. V. Bezmenov

UDC 621.039

When water reservoirs are to be protected from radioactive contamination, the calculation of the greatest admissible waste release (AWR) is one of the important measures. The problem of calculating the AWR can be divided into two parts which can be individually treated by calculating monitored concentrations and the ratio of the arrival rate of radioactive materials in the water system to the concentration of the radioactive materials in the observed (monitored) objects; this ratio is termed the radiation capacity [1]. The concept of radiation capacity is used in the present work in calculating the greatest admissible waste release even when only a few independent monitored concentrations are available.

For the sake of a convenient exposition, we will term any object which is characterized by a certain monitored concentration in a water system an object of monitoring. If owing to peculiar local features various monitored concentrations (e.g., various sections of the bottom) correspond to various parts of an object, the object will be considered a set of several objects. The objects are numbered by a subscript  $k$ ; there is a total of  $m$  objects. Radioactive contamination can arrive at each object over  $n$  mutually independent "paths"  $i$  ( $1 \leq i \leq n$ ).

That fraction of the released radioactive material which arrives on the  $i$ -th path is termed  $\eta_i$  and the totality of these fractions is represented in the form of an  $n$ -dimensional vector (single-column matrix). The concentration in each of the monitored objects is considered a component of an  $m$ -dimensional vector. The development of the contamination in the  $k$ -th object over the  $i$ -th path is characterized by a certain partial radiation capacity  $R_{ki}$ . The set of quantities which are the inverse of the partial radiation capacities is also written in the form of a matrix with  $m$  lines and  $n$  columns. Then the vector of the specific activities of the monitored objects at the most exposed points is defined by a relation the validity of which can be easily verified for each component:

$$(q_k) = Q(Z_{ki})(\eta_i), \quad (1)$$

where  $Q$  denotes the rate at which radioactive materials arrive in the water system;  $(Z_{ki})$ , matrix of quantities which are the inverse of the radiation capacities;  $(q_k)$ , matrix vector of the radionuclide concentrations in the objects monitored; and  $(\eta_i)$ , matrix vector of quantities which define the released radionuclide fraction transported over the  $i$ -th path.

It follows from an analysis of the published data and of the recommendations of [2, 3] that in computational formulas, the dose of the internal and external irradiation of man is proportional to the radionuclide concentration in the monitored object. The proportionality coefficient depends upon the criteria assumed or the principle of normalization. Accordingly, the dose which results from several objects contaminated by the same nuclide is equal to the sum of doses resulting from each of the objects per se:

$$D = (\alpha_k)^+ (q_k), \quad (2)$$

where  $D$  denotes the dose absorbed by some crucial organ;  $(\alpha_k)$ , matrix vector of the coefficients of the proportionality between the radionuclide concentration in the  $k$ -th object and the dose absorbed by the crucial organ; and  $+$ , matrix transposition.

The set  $\alpha_k$  satisfies the self-evident equation

$$D_{adm} = \alpha_k q_{0k}, \quad (3)$$

where  $D_{adm}$  denotes the irradiation dose limit of a limited part of a population by liquid waste; and  $q_{0k}$ , monitored concentration of the radionuclide.

Translated from *Atomnaya Énergiya*, Vol. 59, No. 3, pp. 213-216, September, 1985. Original article submitted April 16, 1984; revision submitted April 29, 1985.

$Q$  is equal to the greatest admissible waste release AWR), we obtain  $1/Q_{AWR} = (1/q_{ok})^+ \times (Z_{ki})(\eta_i)$ , where  $Q_{AWR}$  denotes the AWR value; and  $(1/q_{ok})$ , matrix vector of quantities which are the inverse of the monitored concentrations.

We consider as an example the AWR calculation for some model system which resembles the cooling water reservoir of an atomic power station.

It was assumed in the calculations that the cooling water reservoir is a pond with an area of  $9.5 \text{ km}^2$  and a volume of  $5 \cdot 10^7 \text{ m}^3$ . The cooling water is taken up (at a rate of  $100 \text{ m}^3/\text{sec}$ ) and released at opposite banks of the pond which has smooth coastlines so that no stagnant zones exist. It is assumed that the water intake is on the bottom and therefore pond regions situated above and below a thermal ridge necessarily exchange their waters. Water losses are replenished by water from some other superficial water reservoir (which is to be considered external in regard to the coolant reservoir), i.e., a reservoir with a volume many times greater than the volume of the coolant water reservoir. The water reservoirs are divided by enclosing ground dams. The water level in the pond is  $2.5 \text{ m}$  above the water level in the larger reservoir. In order to maintain the quality of the water in the coolant water reservoir, a circulation with the waste into the external reservoir is effected (at a rate of  $0.27 \text{ m}^3/\text{sec}$ ). Since the water levels differ, the water is filtered across the dam and through the bottom (at a total rate of  $1.1 \text{ m}^3/\text{sec}$ ) with an average time of 10 days of water movement from the pond to the large reservoir. In the region of the atomic power station, the average flow rate in the water reservoir is  $0.07 \text{ m/sec}$ ; the average wind speed is assumed to amount to  $3.9 \text{ m/sec}$ . It was assumed in the calculations that in the coolant water reservoir, fishing and bathing are prohibited and that no water is to be taken for farming; in the water reservoir all forms of water utilization are permitted; part of the radioactive material which is in the undissolved state forms a radioactive suspension by sorption at the particles of the natural suspended materials. The granulometric composition of the suspended material corresponds to fine sands [4] (six particle fractions with diameters of  $0.5\text{-}0.005 \text{ mm}$  were considered).

In the case under consideration, the monitored objects are: the water of the coolant water reservoir ( $k = 1$ ), the water of the external water reservoir ( $k = 2$ ), and the ground of the external water reservoir ( $k = 3$ ). The arrival paths are: redistribution of dissolvable compounds in the water of the coolant water reservoir ( $i = 1$ ), filtering of the water through the bottom and enclosing dam ( $i = 2$ ), release of dissolved compounds through the circulation unit ( $i = 3$ ), and transfer of undissolvable particles over six paths ( $i = 4\text{-}9$ ) corresponding to six particle fractions.

The matrix elements of the radiation capacity were calculated with a mathematical model which is the result of the compilation of several known models of hydrodynamic mixing processes and the propagation of suspended material [5-8]. These models hold for the temperate region in areas of alluvial and alluvoglacial deposits, provided that the Frude number is  $< 1$ .

The following assumptions were made:

1. In the coolant water reservoir, flow of water takes place under the influence of the circulating discharge from the atomic power station and of wind. The wind speed was estimated with the equation  $w = Kw_B\sqrt{3 + 10h}$  of [7], where  $w$  denotes the speed (m/sec) of the water flow in the surface layer or in the countercurrent at the bottom;  $w_B$ , wind speed (m/sec);  $h$ , height (m) of the waves; and  $K$ , an empirical coefficient assuming various values in calculations of the speed of the surface flow or the bottom countercurrent.

2. Radioactive impurities in the water are mixed according to the laws of turbulent diffusion [6] for which the diffusion coefficient is [7]:

$$D = \frac{g}{100} H^{2/3} d_r^{1/3} \sqrt{w_{av}^2 + (\theta h / \pi H)^2},$$

where  $g$  denotes the acceleration ( $\text{m/sec}^2$ ) by the force of gravity;  $H$ , depth (m);  $d_r$ , grain diameter (mm) of the rock material forming the ground with a 10% coverage;  $\theta$ , phase velocity (m/sec) of wave propagation; and  $w_{av}$ , average transit velocity (m/sec) of the flow.

3. The arrival of radioactive material in the environment by evaporation and the quantity of radioactive material contained in the biomass are negligible.

Object	$i = 1$	$i = 2$	$i = 3$	$i = 8$	$i = 9$
$k = 1$	$6,25 \cdot 10^{-9}$	0	0	$3,57 \cdot 10^{-10}$	$7,44 \cdot 10^{-10}$
$k = 2$	0	$4,4 \cdot 10^{-9}$	$6,25 \cdot 10^{-9}$	$3,4 \cdot 10^{-10}$	$6,6 \cdot 10^{-10}$
$k = 3$	0	$3,5 \cdot 10^{-9}$	$5,1 \cdot 10^{-9}$	$1,92 \cdot 10^{-6}$	$9,34 \cdot 10^{-7}$

Remark. The unit of the measurement of the elements listed in lines 1 and 2 is  $\text{yr/m}^3$ , that of the elements of line 3 is  $\text{yr/kg}$ .

4. The bottom sediments are contaminated in two ways: diffusion of dissolved material into the upper layer and reverse sorption of the material by the particles of the bottom sediments, and precipitation of undissolvable particles from the water volume onto the bottom.

It was assumed that the dissolved materials in their sorption by bottom sediments form a uniformly contaminated, 0.05-m-thick layer, that the ratio of the specific activity of the bottom to the average specific activity of the bottom is constant and depends only upon the radionuclide, and that the suspended radioactive particles are transported by a water current and distributed along a flow line according to an exponential law [7]:

$$q(x) = q(0) G \exp \left[ -\frac{xu}{Hv^*(1-\Gamma)} \right], \quad (4)$$

where  $q(0)$  and  $q(x)$  denote the concentration of the suspended particles in the initial section line and in the section line spaced by the distance  $x$  from the initial section line;  $H$ , depth;  $u$ , hydraulic fineness;  $v^*$ , speed of the water flow;  $G$ , coefficient of dilution due to turbulent diffusion; and  $\Gamma$ , a hydrodynamic parameter (a tabulated function).

The development of flow turbulence by the water flow proper and the mixing by wind-induced waves have been taken into account in Eq. (4). For this purpose the velocity  $v^*$  was introduced; this velocity is equal to the sum of the transport velocity and the orbital velocity calculated with the formula  $v_{\text{orb}} = 2h/T[\text{sh}(2\pi H/L)]$ , where  $v_{\text{orb}}$  denotes the orbital velocity caused by undulation;  $h$ , height of a wind-induced wave;  $T$ , wave period;  $H$ , depth of the water reservoir; and  $L$ , wavelength.

The relation between the stationary contamination of the bottom sediments due to the precipitation of suspended particles and the contamination of the water by suspended radioactive material is obtained from the condition of the balance of undissolvable material in the water flow

$$\sigma(x) = \frac{Hw}{\lambda + \varphi} \frac{\partial q}{\partial x} \Big|_{G=\text{const}},$$

where  $\lambda$  denotes the decay constant; and  $\varphi$  denotes the constant volume corresponding to the drag of the bottom load [7].

It is assumed that the speed of motion of the dissolved materials in the filtration through the ground is below the flow rate of the water due to sorption by ground particles. The velocity ratios were taken from [9].

Three additional simplifications were introduced in addition to the basic assumptions listed above:

an estimate has shown that the rate of mixing of the water masses in the coolant water reservoir by wind-induced currents is much greater than the rate of the exchange between the water masses of the coolant water reservoir and the external reservoir; therefore the assumption that the dissolved material is uniformly distributed over the volume of the coolant water reservoir was made in the calculations;

it was assumed that streams of contaminated water are formed in the exit into the external water reservoir and that the specific activity of the water in the streams is characterized by a Gauss distribution [6]:

$$\rho(x, y) = \tilde{\rho}(x) \exp \left\{ -y^2 / \left[ 2D \int_0^x \left( \frac{dx}{v} \right) \right] \right\},$$

where  $\bar{a}$  is the specific water activity averaged over the depth;  $r$ , distance from the center line of the vortex in the transverse direction;  $x$ , distance along the central axis of the vortex;  $v$ , flow rate in the region of the center line;  $D$ , coefficient of turbulent diffusion; and  $\bar{\rho}(x)$ , normalizing function which is proportional to the concentration of the contamination at the beginning of the stream.

5. Stable local whirls have been disregarded.

The model described above was used to calculate the radiation capacity in the case of  $^{137}\text{Cs}$  (see Table 1). The calculation has shown that the matrix elements corresponding to coarse particles (fractions with a diameter of 1-0.05 mm) are negligibly small and therefore they have not been listed in the table.

We state as an example the AWR value calculated for the model water system. The monitored concentrations of [10] were used for the external water reservoir; the monitored concentrations for the coolant water reservoir were taken from Radiation Safety Standard NRB-76. The quantities were corrected taking into account the SP-AES-79 requirements, i.e., the quantities were normalized to an equivalent dose rate of  $5 \cdot 10^{-5}$  Sv/yr of the ionizing radiation. Thus, it was assumed that the monitored concentration of the coolant water reservoir is  $5.5 \cdot 10^3$  Bq/m<sup>3</sup>, and 740 Bq/m<sup>3</sup> in the water of the external water reservoir; the monitored concentration in the ground of the external water reservoir was assumed as 260 Bq/kg.

In the water system described above,  $\text{AWR} = 5.5 \cdot 10^8$  Bq/yr in the case of  $^{137}\text{Cs}$ . When the interrelation between the internal and the external water reservoirs is disregarded, we obtain  $\text{AWR} = 8.1 \cdot 10^{11}$  Bq/yr.

The calculations have shown that the accumulation of contaminants by bottom sediments near the exit point of the pond water is the main process limiting in the particular case the maximum release of waste. Therefore the AWR value depends only slightly upon the monitored concentration in the coolant water reservoir. When we assume that the monitored concentration in this reservoir is equal to the monitored concentration in the water of the external water reservoir, the AWR value changes by only 1%.

Let us note that these results are only illustrative because both the characteristics of the water reservoir and the monitored concentrations were randomly assumed. Nevertheless, the results show qualitatively that when the AWR is calculated, the influence of an atomic power station upon the entire water system must be taken into account rather than considering only the influence upon the water reservoir into which the direct release takes place.

Let us note in conclusion that the matrix technique employed in the present paper for calculating the AWR does not reduce in the general case the amount of calculations and does not simplify the computational formulas. But the advantages of the matrix notation become obvious when changes are introduced in the water supply circuit. The notation method used in the present work makes it possible to introduce corrections only in the matrix elements which relate to changes in the water system. This simplifies the derivation of corrected results and makes the calculations more flexible when the arrival paths are properly selected.

#### LITERATURE CITED

1. A. L. Kononovich, M. A. Baranov, N. I. Sinyukova, and L. P. Kham'yanov, "On the relation of the monitored values of the release of liquid radioactive waste and the monitored concentrations of radionuclides in the water of open water reservoirs," *At. Energ.*, **50**, No. 1, 50 (1981).
2. D. I. Gusev and O. A. Pavlovskii, "Basic assumptions of the method of calculating the greatest admissible release of radioactive materials into surface water reservoirs," in: *Radiation Safety and Protection of Atomic Power Stations* [in Russian], Énergoizdat, Moscow (1982), pp. 157-164.
3. A. N. Marei, *Public Health Measures to Prevent the Contamination of Water Reservoirs with Radioactive Materials* [in Russian], Atomizdat, Moscow (1976).
4. G. A. Petukhov, "The dependence of the volume weight of bottom sediments upon their granulometric composition," *Trudy GGI*, No. 132, 87-89 (1966).
5. V. M. Prokhorov and N. G. Safronova, "The kinetics of self-cleaning of a water reservoir as a result of the absorption of a radionuclide by the bottom ground," *Ekologiya*, No. 2, 12 (1973).

6. Declassified and Approved For Release 2013/02/20 : CIA-RDP10-02196R000300070003-2 ,  
York-London (1979).
7. A. V. Karaushev, Problems of the Dynamics of Natural Water Currents [in Russian], Gidrometizdat, Leningrad (1960).
8. V. N. Goncharov, The Dynamics of Fluvial Currents [in Russian], Gidrometizdat, Leningrad (1962).
9. E. I. Orlova, V. A. Smrennaya, and R. A. Chelyshev, "Behavior of some long-life isotopes in rocks in the contamination with nontechnological run-offs of atomic power stations," Sanitaryia Gigiena, No. 12, 65 (1973).
10. D. I. Gusev, "Sanitary criteria in the evaluation of the contamination of coastal sea waters with radionuclides," in: Impact of Nuclear Releases in the Aquatic Environment [in Russian], IAEA, Vienna (1975).

CHOOSING THE METHOD OF CALCULATING THE IMPURITY SCATTERING  
IN THE ATMOSPHERE WITH NORMALIZATION OF THE RADIONUCLIDE  
EMISSION FROM HIGH SOURCES

N. E. Artemova

UDC 621.039.583:551.5

The maintenance of environmental-quality standards in the operation of commercial and power installations releasing radionuclides into the atmosphere depends significantly on whether correct account is taken of the meteorological factors determining the propagation of impurities in the atmosphere.

Systematic investigation of atmospheric diffusion accompanying the release of harmful chemical materials has led to the development of the two most widespread models of impurity scattering in the atmosphere and engineering methods of calculating the concentration. One of these is a model based on solving the semiempirical equation of turbulent diffusion and applying the results of studying moisture and heat transfer, the boundary-layer structure of the atmosphere, and the distribution laws of meteorological elements in the ground layer of the air. The other (Gaussian) model is constructed using statistical laws and describes the vertical and transverse scattering of impurities by a normal Gaussian law with empirical dispersions depending on the meteorological conditions and the distance to the source of the emission.

In the USSR, the development of a model of contaminant scattering in the atmosphere has always been subordinate to the idea of monitoring and preventing industrial contamination of the atmosphere. The development of a theoretical apparatus based on modern concepts of the theory of atmospheric diffusion [1] was primarily aimed at the construction of a well-founded practical scheme for calculating the control characteristic of air pollution: the maximum one-time ground-level concentration. The scattering model described in [1] allows the release to the atmosphere  $Q$  to be related to the maximum one-time (20-min) concentration  $q_{\max}$  by a dependence of the form  $Q = K_{\min} q_{\max}$ , where  $K_{\min} = H^2 \sqrt{V \Delta T / (A F m n)}$  is the minimum one-time dilution coefficient;  $H$  is the height of emission;  $A$ ,  $F$ ,  $m$ ,  $n$ ,  $V$ ,  $\Delta T$  are parameters characterizing the features of the contamination flare.

In accordance with this model, which forms the basis of the pronouncements of the Office of State Construction of the USSR in Notes on the Calculation of Scattering (SN369-74) [2], the degree of contamination of the ground layer of the atmosphere by releases of harmful materials from high continuously acting sources is estimated from the maximum value of the one-time ground-level concentration  $q_{\max}$ , which is established at a definite distance  $x_M$  from the point of release, with unfavorable meteorological conditions (the wind speed reaches a dangerous value  $u_M$  and there is developed turbulent exchange). The parameters required to calculate  $K_{\min}$ ,  $u_M$ ,  $x_M$  are estimated from the formulas in [2].

---

Translated from Atomnaya Énergiya, Vol. 59, No. 3, pp. 216-221, September, 1985. Original article submitted August 13, 1984.

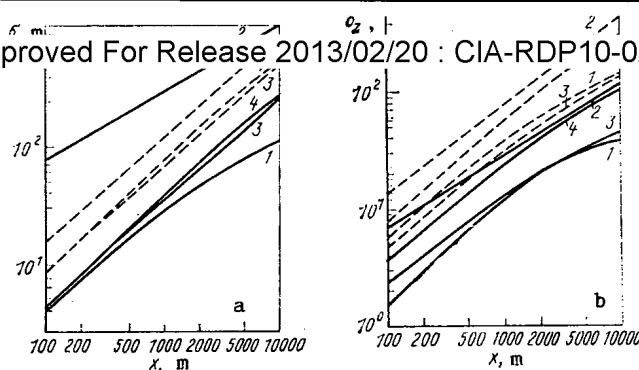


Fig. 1. Dependence of the transverse (a) and longitudinal (b) dispersion on the distance to the source determined according to Briggs (1), Vogt (2), Pasquill-Gifford (3), Smith (4) [6, 15]: the dashed curves correspond to category D (neutral stratification) and the continuous curves to category F (moderate stability).

Comparison of  $q_{\max}$  with the limiting permissible concentration (LPC) of chemical materials provides the criterion of purity of the ground-level atmosphere in the region of action of a particular source of chemical contamination. On the basis of this method, the minimum height of the plant smoke-stack may be determined, as well as the limiting permissible release (LPR) ensuring maintenance of the health norms regarding the content of harmful materials in the ground-level air and the boundaries of the sanitary-protection zone around the plant.

The general laws of turbulent scattering of impurity in the atmosphere do not depend on the form of material released. The difference between radioactive and chemical materials is that the action of radionuclides on living organisms is long-term and the radiation dose accumulates over time; therefore, their permissible concentration (PC) leads to an annual averaging period. The formula used to calculate the annual mean dilution coefficient is [3, 4]:

$K_{\min} = H^2 \sqrt{V \Delta T} / (A F m n \alpha P / P_0)$ , where  $\alpha P / P_0$  is the conversion factor from 20-min averaging ( $\tau_{ot}$ ) to the annual mean  $\tau_y$ ;  $P / P_0$  is the elongation index of the annual mean wind rose;  $\alpha = (1/2) \cdot (\tau_{ot} / \tau_y)^{0.2}$ .

When the wind velocity  $u$  differs from  $u_m$  and also along and perpendicular to the carrier wind,  $K_{\min}$  is determined using the functions  $r$ ,  $S_1$ ,  $S_2$  [2].

For the given model, a great mass of experimental data has been accumulated, confirming the theoretical concentration values for metallurgical, chemical, and energy plants as well as those releasing radionuclides [3-5]. This material forms the basis for specialist method PDV-83 developed by the State Commission on Hydrometeorology (SCHM).

Other methods of calculating the ground-level concentrations of radionuclides or the dilution factors used in the USSR by some scientific-research and design organizations traditionally follow the recommendations of the International Agency on Atomic Energy regarding estimates of the radiation safety of atomic power plants, in most cases [6]. A particular modification of the Gaussian statistical model is used, characterized by the methods of determining the stability of the atmosphere, the parameters of lateral and vertical dispersion  $\sigma_y$  and  $\sigma_z$ , and the additional height of flare release  $\Delta h$  on account of the thermal and dynamic lift of the jet. The one-time ground-level concentration  $q$  normalized per unit release  $Q$  (i.e., the reciprocal of  $K_{\min}$ ) may be written in the form

$$\left(\frac{q}{Q}\right)_y = \frac{1}{\pi u \sigma_y \sigma_z} \exp\left(-\frac{y^2}{2\sigma_y^2}\right) \exp\left(-\frac{(H + \Delta h)^2}{2\sigma_z^2}\right),$$

where  $u$  is the wind velocity at the level of the release, m/sec.

The normalized annual mean concentration may be determined in accordance with the expression

$$\left(\frac{q}{Q}\right)_{jy} = \frac{2}{\sqrt{2\pi} x \Theta} \sum_{ih} \frac{N_{ijk}}{\sigma_{zi} U_k} \exp\left(-\frac{H_{ih}^2}{2\sigma_{zi}^2}\right),$$

TABLE 1. Compound Table of the Most Satisfactory Formulas for Determining  $\sigma_y$  and  $\sigma_z$ 

Author	$\sigma_y$	$\sigma_z$
Smith	$C_3 x / \sqrt{1 + 10^{-4} x}$	$f(z_0, x) g(x)$ when $f(z_0, x) g(x) \leq \sigma_z^{\max}$ ; $\sigma_z^{\max}$ when $f(z_0, x) g(x) > \sigma_z^{\max}$ ; $g(x) = a_1 x^{b_1} / (1 + a_2 x^{b_2})$ ; $f(z_0 x) = \begin{cases} \ln [C_1 x^{d_1} (1 + C_2 x^{d_2})] & \text{when } z_0 > 10 \text{ cm} \\ \ln [C_1 x^{d_1} (1 + C_2 x^{d_2})^{-1}] & \text{when } z_0 \leq 10 \text{ cm} \end{cases}$
Vogt	$P_y x^{q_y}$	$P_z x^{q_z}$
Briggs	$C_1 x (1 + 0,0001 x)^{-1/2}$	$C_1 x$ for categories A and B; $C_1 x (1 + 0,0002 x)^{-1/2}$ " C and D; $C_1 x (1 + 0,0015 x)^{-1/2}$ " D; $C_1 x (1 + 0,0003 x)^{-1}$ " E and F

Note. The numerical values of  $C_1$ ,  $C_2$ ,  $C_3$ ,  $P$ ,  $q$ ,  $d_1$ ,  $d_2$  are determined by the stability class.

TABLE 2. Formulas for Determining the Additional Lift Height  $\Delta h$ 

Recommending organization	Stratification of the atmosphere			
	unstable	neutral	stable	
			no wind	wind
Institute of Biophysics	$\Delta h = 1,44 D \left( \frac{w_0}{u} \right)^{2/3} \times \left( \frac{x}{D} \right)^{1/3} + \frac{2}{u} \Phi^{1/3} x^{2/3}$ ; $\Phi = \frac{\Delta T}{T_s} g w_0 \frac{D^2}{4}$	$\Delta h^{\max} = \frac{3 w_0 D}{u} \left[ 2,5 + \left( 3,3 g \frac{D}{2 u^2} \right) \frac{\Delta T}{T_s} \right]$	$\Delta h^{\max} = 5,1 \Phi^{1/4} S^{3/8}$ ; $S = \frac{g}{T_s} \frac{\partial \Theta}{\partial z}$	$\Delta h^{\max} = 1,5 S^{-1/6} \times \frac{w_0 D}{2 u^2} + 2,6 \left( \frac{\Phi}{u S} \right)^{1/3}$
A. I. Voeikov Principal Geophysical Observatory International Agency on Atomic Energy World Meteorological Organization	$\Delta h = \frac{1,5 w_0 R_0}{u \Phi} \left( 2,5 + \frac{3,3 g R_0 \Delta T}{T_s u \Phi^2} \right)$ $\Delta h_1 = 1,44 D_i \left( \frac{w_0}{u} \right)^{2/3} \left( \frac{x}{D_i} \right)^{1/3} - C$ $C = 3 \left( 1,5 - \frac{w_0}{u} \right) D_e$ when $w_0 \leq 1,5 u$ $\Delta h_2 = 3 \frac{w_0}{u} D_i$ ; $\Delta h = \min (\Delta h_1, \Delta h_2)$		$\Delta h_1 = 1,44 D_i (w_0/u)^{2/3} (x/D_i)^{1/3} - C$ ; $C = 3 (1,5 - w_0/u) D_e$ ; $\Delta h_2 = 4 (F_m/S)^{1/4}$ ; $F_m = w_0^2 (D/2)^2$ ; $\Delta h_3 = 1,5 S^{-1/6} (F_m/u)^{1/3}$ ; $\Delta h = \min (h_1, h_2, h_3)$	
I. V. Kurchatov Institute of Atomic Power		$\Delta h = 1,54 (F_0/u u_*^2)^{2/3} h_s^{1/3}$ $\Delta h = 3,0 M_0^{1/2} / u + A F_0 / u^3$ $\Delta h = A \left( 2,61 \frac{\sqrt{Q} h}{u} - 0,029 \frac{w_0 D}{u} \right)$	$\Delta h = 5,3 F_0^{1/4} S^{3/8} - R_0$	$\Delta h = 2,6 (F_0/u S)^{1/3}$ ; $F_0 = w_0 R_0^2 g / T (T - T_s)$ ; $S = \frac{g}{T_s} \left( \frac{\partial T_s}{\partial z} + 0,01 K \right)$

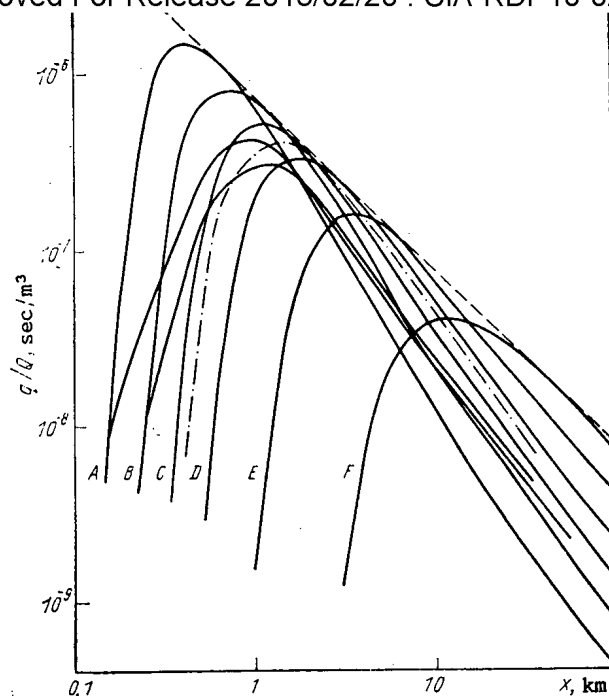


Fig. 2. Normalized concentrations in conditions of different stratification: dashed curves show the envelope and dash-dot curves show 100% repeatability of category C-D or "average weather."

where  $N_{ijk}$  is the repeatability of the  $i$ -th stability class, the  $j$ -th sector of wind direction, and the  $k$ -th class of wind velocity;  $\theta$  is the sector of wind direction adopted.

To determine the stability classes of the atmosphere and also the values of  $\sigma_y$ ,  $\sigma_z$ , and  $\Delta h$  corresponding to these classes, various recommendations and formulas are applied; the diversity of these methods may be one reason for the pronounced discrepancies in the calculation results.

The stability condition of the atmosphere is determined by the methods of [7-11], from the vertical temperature and wind-velocity gradients at the weathercock (in some modifications) [12], and so on. At the Leningrad Hydrometeorological Institute (LHMI), gradation of the stratification  $\mu$ , and the velocity of the geostrophic wind  $G$  is used for this purpose [13]. In determining the stability classes by different methods, two of the classes may show a discrepancy [12, 14].

Depending on the stability class,  $\sigma_y$  and  $\sigma_z$  are estimated (Table 1, Fig. 1). The theoretical values of the dispersion for the same distances differ by a factor of 2-10. Determining  $\Delta h$  by the most satisfactory formulas (Table 2) in some cases leads to significant (up to an order of magnitude) discrepancy in the theoretical values. In [15], it was noted that the efficiency of the model may be determined by comparing a series of model predictions of scattering (calculation) with a series of observations or predictions made by another model. The results of any comparison of models depend on the form of the curves of  $\sigma_y$  and  $\sigma_z$  employed.

In all scattering methods based on the Gaussian model, the annual mean concentration or the annual mean dilution coefficient is calculated taking account of the annual mean repeatability of the various stability categories of the atmosphere, the wind direction, and the gradation of its velocity. Remember that determining the repeatability as a statistically reliable annual mean quantity requires laborious analysis of a large mass of data, the representativeness of which must be ensured. In any case, the calculation of an annual mean dilution coefficient such as to ensure that the limiting permissible levels of atmospheric contamination are not exceeded in any specific annual period and such as to form the basis for LPR calculation is not guaranteed.

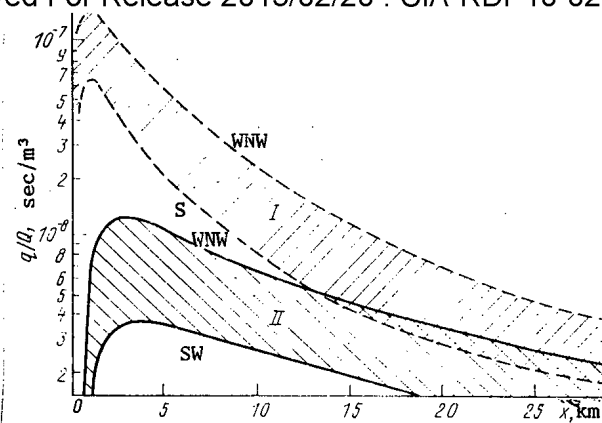


Fig. 3. Dependence of the normalized annual mean concentration on the distance to the source: S, N, W) southern, northern, and western wind directions.

Curves of the change in annual mean normalized ground-level concentration corresponding to 100% repeatability of each of six Pasquill stability classes (curves A-F) under conditions of equiprobability of all the wind directions for a source of height 100 m are shown in Fig. 2. Envelopes and curves corresponding to the real annual mean distribution of the repeatability of various stability categories for Great Britain (I) and the middle section of the European USSR (II) are plotted, as well as a curve corresponding to 100% repeatability of category C-D or conditions of "average weather."

Comparison of the curves shows slight difference in curves C-D, I and II at distances of more than 1 km. On the other hand, these curves (especially at large distances) differ from the envelope, according to which the annual mean ground-level concentration is taken to be the maximum of all possible values for each distance, i.e., 100% repeatability of each stability class is assumed simultaneously. The envelope method is sometimes used in conservative estimates; it gives significant overestimates of the annual mean concentrations for distances outside the range 1-10 km.

Observations show [12, 14, 16] that, for the predominant majority of geographical regions, slight (of the orders of a few or a few fractions of a percent) repeatability of stability categories A and B is characteristic, in connection with which category C-D (conditions of developed turbulent transfer) is closest to the upper limit of the annual mean stability conditions and may be regarded as the category forming the annual mean concentration (Fig. 2).

The results of calculating the normalized annual mean concentration for all wind directions for the Chernobylsii atomic power plant (RBMK-1000 reactor, source height 150 m) by the Pasquill-Gifford [17] (region I) and LHMI [13] (region II) methods are shown in Fig. 3. The theoretical normalized concentrations (and hence the dilution coefficients) in the region of the maximum and beyond, to a distance of 5-10 km, differ by more than a factor of 10 for the same wind directions.

The problem of the priority of a particular model used in calculating impurity scattering in the atmosphere in connection with problems of design and use must be solved primarily as a function of such indices as the region of reliability of the model determined by the empirical coefficients which it includes, the averaging period of the input meteorological data, and the confirmation of the method by full-scale measurements. The Gaussian model is relatively simple, clear, and convenient; however, the concentration determined by this method for extreme stability classes, remote distances, and different geographic regions may have a large error [7, 15]. The modifications of the Gaussian model used in the USSR (Pasquill-Gifford, Smith-Hosker, Briggs) have not been tested for specific objects or in specially formulated experiments. The empirical Gaussian model does not permit generalization to a wider class of conditions, in particular, it is inapplicable for complex local relief and does not take account of the dependence of the dispersion on the height of release. At the same time in the class of scientific-research problems, such as studying the separate influence of small- and large-scale turbulence, it is convenient and allows diffusion processes

In LHMI method, a model of a neutral boundary layer is used - that is, the profiles  $K(Z)$  and  $u(Z)$  correspond to the approximations for neutral conditions - and hence it is not adequately correct to calculate the annual mean concentration from the contributions of different stability categories. Comparison of the theoretical data obtained by the LHMI and Pasquill-Gifford methods (Fig. 3) shows significant discrepancy between the results of calculation for the same source, and the lack of corresponding experimental data prevents the assignment of a preference to one method or the other in the present case. Regrettably, the literature has no information on the experimental confirmation of calculations by the LHMI method.

It is expedient, in developing methods of normalizing radionuclide releases, to use the method of calculating the dilution coefficient developed by SCHM [18]; this method combines radioactive and chemical contaminants into a single calculation scheme and is characterized by uniqueness of the requirements on practical calculations. It is aimed at establishing a scientifically based value of the release ensuring maintenance of the radiation-safety norms with any weather conditions (with release from a high source). In the method, all types of continuously acting high sources (and also short-term increased releases) are considered, and account is taken of summation over sources and nuclides and of the specifics of the particular regions within the territory of the USSR; it is applicable for sources of height 40-320 m, releasing hot and cold impurities. The mathematical model on which it is based allows the problem of impurity propagation over a region of complex terrain and in anomalous meteorological conditions to be solved. The method is tested using large quantities of experimental material at a series of plants and in specially organized experiments [1, 4, 5]. Its limitation is that at present it does not include, like other methods, recommendations on the means of calculating the scattering with a sharp qualitative change in the underlying surface.

The introduction of a GOST state standard on limiting permissible releases of material contaminating the atmosphere [19] poses the problem of unifying the calculation methods and creating a single engineering method of determining LPR. This problem has been solved, to a considerable extent, by the development and introduction of Specialized Methodological Notes on the Calculation of Limiting Permissible Releases of Radioactive and Chemical Materials Contaminating the Atmosphere, using the principles of the SCHM method.

#### LITERATURE CITED

1. M. E. Berlyand, Modern Problems of Atmospheric Diffusion and Contamination [in Russian], Gidrometeoizdat, Leningrad (1975).
2. Notes on the Calculation of the Scattering of Harmful Materials Included in Plant Releases in the Atmosphere [in Russian], Publication SN 369-74, Moscow (1975).
3. N. E. Artemova and E. N. Teverovskii, "Principles of the normalization of releases of radioactive products from the smoke-stacks of atomic-industry and power plants (meteorological aspects)," *At. Energ.*, 31, No. 6, 573-576 (1971).
4. E. N. Artemova, I. N. Ruzhentsova, and R. V. Semova, "Dependence of the ground-level concentration of smokestack-released radionuclides on the averaging time," *At. Energ.*, 51, No. 2, 112-116 (1981).
5. Proceedings of A. I. Voeykov Main Geophysical Observatory [in Russian], No. 387, Gidrometeoizdat, Leningrad (1977), No. 373 (1976); No. 417 (1979); No. 450 (1982).
6. Safety Handbook of the International Agency on Atomic Energy. Taking Account of the Dispersional Parameters of the Atmosphere in Selecting Areas for Atomic Electric-Power Stations. Series of Texts on Safety, No. 50-SG-S3 [in Russian], IAEA, Vienna (1982).
7. F. Pasquill, Atmospheric Diffusion, Pergamon, London (1962).
8. B. Turner, *Int. J. Air Poll.*, 11, No. 10, 15 (1961).
9. S. Ulig, *Mitt. Deutsch. Wetterdienst.*, No. 35, 436 (1965).
10. F. B. Smith, in: Third Meeting of the Expert Panel on Air Pollution Modeling, WMO, Paris (1972), p. 18.
11. R. Hosker, in: Third Meeting of the Expert Panel on Air Pollution Modeling, WMO, Paris (1972), p. 29.
12. N. A. Byzova, Impurity Scattering in the Boundary Layer of the Atmosphere [in Russian], Gidrometeoizdat, Moscow (1974).

- Declassified and Approved For Release 2013/02/20 : CIA-RDP10-02196R000300070003-2
13. E. S. Ginzburg, A. I. Glushchenko, G. A. Natanzon, et al., "Methods of calculating and propagation of gas-aerosol releases of atomic-power stations into the atmosphere," in: Atomic Electric Power Stations [in Russian], No. 6, Energoatomizdat, Moscow (1983), pp. 11-18.
  14. P. Bryant, Report AHSB (RP), R42, UKAEA (1964).
  15. S. R. Hanna, WMO Technical Note No. 177. Review of Atmospheric Diffusion Models for Regulatory Applications, WMO-581, Geneva (1982).
  16. M. A. Padron, Kh. M. Rodrigues, and Kh. Ernandes, "Some problems of radiation safety of the first atomic power plant in the Republic of Cuba," in: Radiation Safety in the Operation of Atomic Power Plants [in Russian], Vol. 5, Energoatomizdat, Moscow (1984, pp. 112-119.
  17. A. I. Glushchenko, E. S. Ginzburg, G. A. Natanzon, and O. G. Petrov, "Annual mean concentration field of radioactive impurities from the smoke-stack of the Chernobylskii atomic power plant," At. Energ., 49, No. 6, 392-393 (1980).
  18. N. E. Artemova, A. A. Bondarev, V. I. Karpov, et al., Permissible Releases of Radioactive and Harmful Chemicals in the Ground Layer of the Atmosphere [in Russian], Atomizdat, Moscow (1980).
  19. State Standard GOST 17.2.3.02-78. Environmental Protection. The Atmosphere. Rule for Establishing Permissible Releases of Harmful Materials from Industrial Plants [in Russian].

# DISTRIBUTION OF $^{137}\text{Cs}$ IN SAMPLES OF OCEAN BOTTOM SEDIMENTS OF THE BALTIC SEA IN 1982-1983

L. I. Gedeonov, L. M. Ivanova,  
K. A. Kostandov, and V. M. Flegontov

UDC 551.464.6.02

Measurements of the concentration of radionuclides in ocean bottom sediments are one of the complicated problems in the investigation of the radioactive contamination of the Baltic Sea. Obtaining a representative sampling technique is one of the important conditions in the solution of the problem. Extracting soil together with material suspended near the ocean bottom or without such material or with a partial loss of this material can significantly influence the results. The concentration of  $^{137}\text{Cs}$  in samples of ocean bottom sediments picked up in 1979 in the Gulf of Finland with a geological nozzle pipe varied within a wide interval of values: from 500 Bq/m<sup>2</sup> to 1600 Bq/m<sup>2</sup> in the layer 0-5 cm [1], and 3500 Bq/m<sup>2</sup> in the layer 0-25 cm [2]. The results could indicate nonuniformity of the  $^{137}\text{Cs}$  distribution in ocean bottom sediments as well as the penetration of significant amounts of  $^{137}\text{Cs}$  to large depths. The main error resulted from the sampling technique employed because the upper part of the sediment could be lost.

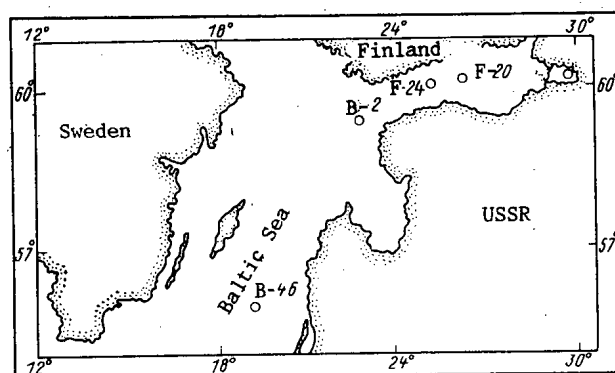
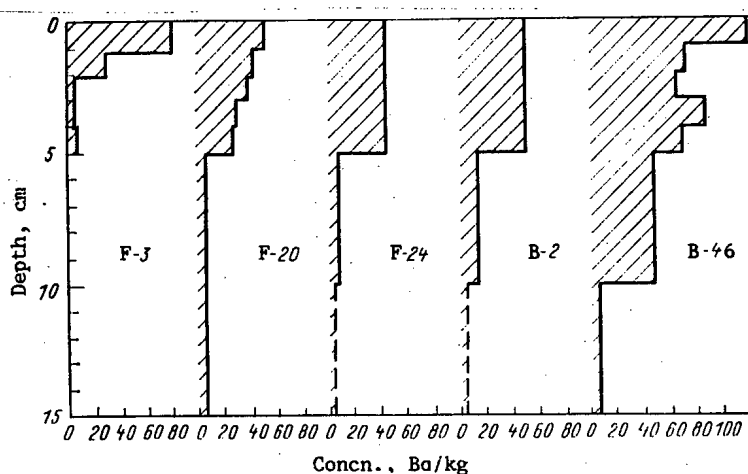


Fig. 1. Schematic map of the points at which samples of ocean bottom sediments were taken (○).

Translated from Atomnaya Energiya, Vol. 59, No. 3, pp. 221-223, September, 1985. Original article submitted January 15, 1985.

TABLE 1.  $^{137}\text{Cs}$  Concentration in Samples of Ocean Bottom Sediments of the Gulf of Finland and of the Baltic Sea in 1982-1983 (area of taking samples  $56.7 \text{ cm}^2$ )

Sample identification	Time of sampling	Layer (cm) of sampling	Volume, $\text{cm}^3$	Dry mass, g	$^{137}\text{Cs}$ concn., Bq		
					in the sample	per 1 kg of the dry mass	per $\text{m}^2$
F-3	July 1983	0-1	56,7	30	$2,4 \pm 0,3$	$80 \pm 20$	$430 \pm 70$
		1-2	56,7	77	$2,0 \pm 0,3$	$27 \pm 5$	$360 \pm 60$
		2-3	56,7	78	$0,4 \pm 0,1$	$6 \pm 2$	$75 \pm 10$
		3-4	56,7	55	$0,3 \pm 0,1$	$5 \pm 2$	$50 \pm 8$
		4-5	56,7	60	$0,4 \pm 0,1$	$7 \pm 2$	$75 \pm 10$
F-20	July 1983	Total in layer 0-5					985
		0-1	56,7	35	$1,7 \pm 0,3$	$48 \pm 7$	$300 \pm 50$
		1-2	56,7	35	$1,4 \pm 0,3$	$40 \pm 6$	$250 \pm 40$
		2-3	56,7	29	$1,0 \pm 0,2$	$35 \pm 5$	$180 \pm 25$
		3-4	56,7	22	$0,5 \pm 0,2$	$24 \pm 7$	$95 \pm 20$
		4-5	56,7	34	$0,8 \pm 0,2$	$23 \pm 7$	$135 \pm 20$
		0-5					$960 \pm 140$
		5-10	283,5	200	$0,6 \pm 0,1$	$3 \pm 1$	$105 \pm 15$
		10-15	283,5	175	$0,6 \pm 0,1$	$3 \pm 1$	$90 \pm 15$
		Total in layer 0-15					1155
F-24	June 1982	0-5	283,5	133	$6 \pm 1$	$45 \pm 6$	$1060 \pm 160$
		5-10	283,5	183	$0,9 \pm 0,2$	$5 \pm 1$	$160 \pm 24$
		10-15	283,5	155	$< 0,3$	$< 1,5$	$< 40$
		Total in layer 0-15					$\sim 1260$
B-2	July 1982	0-5	283,5	75	$8 \pm 2$	$100 \pm 15$	$1320 \pm 150$
		5-10	283,5	100	$1,3 \pm 0,2$	$13 \pm 3$	$230 \pm 55$
		10-15	283,5	130	$< 0,2$	$< 1,5$	$< 40$
		Total in layer 0-15					$\sim 1550,0$
B-46	July 1983	0-1	56,7	14	$1,7 \pm 0,3$	$120 \pm 20$	$300 \pm 45$
		1-2	56,7	13	$1,0 \pm 0,2$	$77 \pm 13$	$170 \pm 25$
		2-3	56,7	15	$1,0 \pm 0,2$	$67 \pm 10$	$170 \pm 25$
		3-4	56,7	11	$1,0 \pm 0,2$	$90 \pm 15$	$170 \pm 25$
		4-5	56,7	17	$1,3 \pm 0,2$	$75 \pm 13$	$220 \pm 30$
		0-5					1030
		5-10	283,5	67	$3,2 \pm 0,5$	$50 \pm 8$	$560 \pm 80$
		10-15	283,5	146	$0,8 \pm 0,2$	$6 \pm 1$	$140 \pm 20$
		Total in layer 0-15					1730
		Total in layer					

Fig. 2.  $^{137}\text{Cs}$  distribution over the depth of layers of ocean bottom sediments in the Gulf of Finland and the Baltic Sea.

In 1982, a special ground-sampling device, with which the upper layer of sediments in the water layer close to the ocean bottom could be sampled, was tested in the Gulf of Finland and the Northeastern part of the Baltic Sea; the device had been developed in the V. G. Khlopin Radium Institute. The points at which samples were taken are shown in Fig. 1. The samples of the ocean bottom sediments were divided into 5-cm layers, the water layer near the ocean bottom was decanted, and the suspended material was filtered, burnt to ashes at a temperature not exceeding 400°C, and combined with the upper layer of the sediments. The sea bottom samples were dried and subjected to gamma spectrometric analysis.

The results of a layerwise (5-cm layers) determination of the  $^{137}\text{Cs}$  concentration in samples of ocean bottom sediments of the Gulf of Finland and of the Baltic Sea are listed in Table 1 for 1982. It was established that  $^{137}\text{Cs}$  is present mainly in the upper 5-cm layer. When calculated per unit mass, the  $^{137}\text{Cs}$  concentration in this layer amounted to 87-89%; when calculated per unit surface (taking into account varying densities of the layers), the  $^{137}\text{Cs}$  concentration amounted to 80-85% of the total concentration in the 0-15-cm layer.

In the samples taken in 1983, the upper 5-cm layer was divided into 1-cm layers and in each of these the  $^{137}\text{Cs}$  concentration was analyzed. The results are compiled in Table 1 and shown in Fig. 2. It was noted in three samples analyzed in this way that the upper 0-1-cm layer contains the greatest amount of  $^{137}\text{Cs}$ . Various forms of a decreasing  $^{137}\text{Cs}$  concentration are observed in the other layers: a gradual concentration decrease (sample F-20), a more pronounced decrease (sample F-3), or a nonuniform decrease (sample B-46). These differences may be caused by errors in the separation of samples into layers. It was established in a comparison that the  $^{137}\text{Cs}$  distribution in 5 cm sediment layers (1983) amounted to 83% in the Gulf of Finland in the 0-5-cm layer, to 9% in the 5-10-cm layer, and to 8% in the 10-15-cm layer; in the Baltic Sea, the corresponding figures were 59, 32, and 8%, respectively. The  $^{137}\text{Cs}$  concentration referred to unit surface at a layer depth of 0-15 cm was 1160-1730 Bq/m<sup>2</sup>.

So far we have only few results which characterize only isolated regions. The results do not allow a quantitative assessment of the  $^{137}\text{Cs}$  concentration in ocean-bottom sediments of the large water area of the sea. The pattern established for the  $^{137}\text{Cs}$  distribution leads to the assumption that the new soil-sampling device for picking samples of ocean sediments of undisturbed stratification will allow a correct determination of the radionuclide accumulation in the upper layers of ocean bottom sediments in the Baltic Sea.

#### LITERATURE CITED

1. A. Salo, M. Pukhakainen, R. Saksen, et al., Investigation of the Radioactive Contamination of the Baltic Sea in 1979-1980 [in Russian], Preprint RI-176, Leningrad (1983).
2. Studies on Environmental Radioactivity in Finland 1979, STL-A34, Institute of Radiation Protection, Helsinki (1981).

CORROSION RESISTANCE OF OKh18N10T STEEL IN GADOLINIUM  
NITRATE SOLUTIONS IN THE LIQUID REGULATION OF THE REACTIVITY  
OF NUCLEAR REACTORS

V. D. Ganzha, K. A. Konoplev,  
V. P. Mashchetov, S. P. Orlov,  
and A. A. Ukhanev

UDC 620.193.28:621.039.53

This study was carried out in connection with the preparation of the design for the PIK research reactor [1]. It should also be noted that the literature does not contain any data on the corrosion resistance of OKh18N10T steel in gadolinium nitrate solutions.

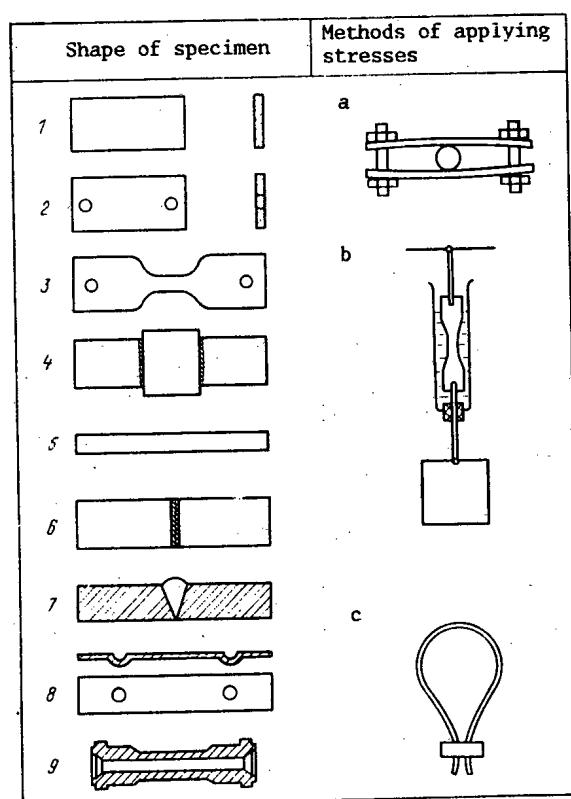


Fig. 1. Shapes of specimens for corrosion tests and methods for applying mechanical stresses to them: 1) flat; 2) flat with holes; 3) flat with neck; 4) with welded lap joint; 5) loop-shaped; 6) with welded butt joint; 7) a cut in the weld; 8) with indentations; 9) bushing with neck; a) specimens of shape 2 deformed within the elastic limit; b) specimens of shape 3 in a corrosive medium and subjected to tensile force at the neck (200 MPa); c) specimens of shape 5 deformed within the elastic limit.

Translated from Atomnaya Énergiya, Vol. 59, No. 3, pp. 224-226, September, 1985. Original article submitted January 16, 1984; revision submitted January 10, 1985.

Declassified and Approved For Release 2013/02/20 : CIA-RDP10-02196R000300070003-2  
of the flat and cylindrical specimens and the methods of applying mechanical stresses to them. The specimens were made of materials certified by the production plant and showed no tendency to intercrystallite corrosion after tests in standard solutions.

Before testing, the specimens were degreased with ethyl alcohol, washed with desalinated water, dried to constant mass, and stored in a desiccator. After testing, they were washed with desalinated water and dried to constant mass. The solutions were prepared with chemically pure gadolinium nitrate and desalinated water. The nature of the local forms of corrosion was evaluated visually with the aid of an MIM-8 microscope. The total corrosion rate was determined from the change in the mass of the specimens and also from the amount of corrosion products present in the solutions.

The experimentally obtained values of the total corrosion rate in this study are arithmetic means for series of 3-6 measurements with a confidence limit of 0.78.

At all stages of the tests, we investigated the effect produced on the corrosion processes by factors related to the technology of preparation of the equipment (mechanical working of the surfaces, welding, sensitizing annealing, stressed state of the material, cracks, etc.).

Under laboratory conditions we tested polished specimens of shapes 1-3 (see Fig. 1). The tests showed that at a gadolinium nitrate concentration of 0.01-1.0 mole/liter and under tensile mechanical stresses maintained for a test period of 30,000 h at 20°C and 1500 h at 70-80°C no failure was observed in any specimen of shape 3.

The rate of total corrosion of specimens of shape 2 in a boiling 0.5 mole/liter solution of gadolinium nitrate after 300 h of testing does not exceed  $1.9 \pm 1.1 \text{ mg}/(\text{m}^2 \cdot \text{h})$  and, as can be seen from the data of [2], is equal to the rate of corrosion of steel in distilled water. The rate of total corrosion of specimens of shape 1 under the same conditions was  $0.7 \pm 0.6 \text{ mg}/(\text{m}^2 \cdot \text{h})$ .

Ampule tests were conducted in order to determine the effect produced by reactor radiation and shutdown regimes on the corrosion resistance of the steel. Specimens of shapes 1, 2, 4, and 5 were placed in special ampules made of OKh18N10T steel which were filled with gadolinium nitrate solutions of various concentrations, sealed, and irradiated for a long period in the core of the VVR-M reactor at a temperature of 20-50°C. The results of the ampule tests are shown in Table 1.

The concluding stage of the corrosion investigations was testing in the loop of the VVR-M reactor under conditions as close as possible to the operating conditions of the system of liquid regulation.

The volume of circulating solution in the loop was 15-30 liters, the pressure 1.6 MPa, the temperature 20-60°C, and the flow rate 150-360 liters/h. All the equipment in the loop was made of OKh18N10T steel.

In the loop we set up two channels with specimens for corrosion tests, one of which was placed directly in the reactor core.

In each channel we set up three specimens of shape 9, which served simultaneously as tubing, and two cassettes with specimens of shapes 1, 6, 7, and 8 (see Fig. 1). The tensile stress (200 MPa) on the neck of each specimen 9 was produced by the hydraulic pressure of the loop. One end of the tubing with the specimens of shape 9 welded into it was rigidly attached to the bottom of the channel, and the second one could be moved, by means of a syphon and a piston, when the hydraulic pressure in the channel increased. A microswitch with an indicator to show when one of the three specimens failed was placed along the piston path.

The conditions of the loop tests are shown in Table 2. The concentrations of the water radiolysis products ( $\text{H}_2$ ,  $\text{O}_2$ , and  $\text{H}_2\text{O}_2$ ) correspond to the equilibrium values when the reactor is operating at a power of 16 MW.

The results of the loop tests are shown in Table 3.

Thus, the investigations showed that the corrosion of OKh18N10T steel in solutions of gadolinium nitrate is uniform, regardless of the state of the surface, the concentration of gadolinium nitrate, the duration of the tests, the action of the reactor radiation under static and dynamic conditions, and the presence of mechanical stresses. Local forms of corrosion such as corrosion cracking, intercrystallite corrosion, pitting corrosion, crack corrosion, notch corrosion in the region of welded seams, point corrosion, and other types are

TABLE 1. Results of Ampule Tests

Characteristics of specimens			Test conditions		Test time, h		Type of corrosion	Total corrosion rate, mg/(m <sup>2</sup> ·h)	
Shape of specimen (see Fig. 1)	Preliminary processing	Additional processing	concn. of Gd(NO <sub>3</sub> ) <sub>3</sub> , moles/liter	Fluence of neutrons, cm <sup>2</sup> (E > 1 MeV)	In neutron flux	Total		According to change in specimen mass	According to corrosion-product content of soln.
I; 2; 5	As delivered	Mechanical polishing	Desalinated water	5,22·10 <sup>20</sup>	2264	14 400	Uniform	0,52±0,26	0,3±0,1
I; 2; 5	The same	The same	0,011	5,22·10 <sup>20</sup>	2264	14 400	»	0,37±0,12	0,2±0,1
I; 2; 5	» »	» »	0,1	2·10 <sup>20</sup>	1080	14 400	»	0,05±0,01	0,25±0,06
I; 2; 5	» »	» »	1,22	2·10 <sup>20</sup>	1080	14 400	»	0,22±0,05	—
I; 2; 5	» »	» »	Saturation	2·10 <sup>20</sup>	1080	14 400	»	0,023±0,022	—
I; 2; 5	» »	» »	0,14	5,2·10 <sup>20</sup>	2264	14 400	»	—	0,15±0,04
Ampule without specimens I; 4	» »	Welded joints	0,1—0,7	3,4·10 <sup>20</sup>	2136	6 336	»	—	0,04±0,02

TABLE 2. Conditions of the Loop Tests

Stage	Chemical composition of the medium							Duration of tests, h*		
	Gd(NO <sub>3</sub> ) <sub>3</sub> , moles/liter	pH	Cl <sup>-</sup> , mg/liter	Fe <sup>3+</sup> , mg/liter	H <sub>2</sub> , moles/liter	O <sub>2</sub> , moles/liter	H <sub>2</sub> O <sub>2</sub> , moles/liter	With reactor operating at power	With reactor suppressed	Total
Desalinated water	0	6,0	0,15	0,5—1,0	4,0·10 <sup>-4</sup>	0,6·10 <sup>-3</sup>	0,6·10 <sup>-3</sup>	378	222	600
Gadolinium nitrate solution	0,15—0,33	5—5,5	5—10	2—20	7·10 <sup>-3</sup>	2·10 <sup>-3</sup>	2·10 <sup>-3</sup>	790	3722	4512

\*The total duration of the testing of the specimens when the reactor was operating at power was 1168 h, and the duration of the testing when the reactor was suppressed was 3944 h, making a total of 5112 h.

TABLE 3. Results of the Loop Tests

Characteristics of specimens			Total corrosion rate, mg/(m <sup>2</sup> ·h)		Type of corrosion
Shape of specimen (see Fig. 1)	Preliminary processing	Additional processing	Inside the reactor core	Outside the reactor core	
1	Rolled metal, as delivered	Sensitizing annealing	0,36±0,04	0,320±0,060	Uniform
1	One side polished, the other mechanically worked	The same	0,30±0,05	0,390±0,044	»
1	Both surfaces rolled metal, as delivered	—	0,30±0,10	0,06±0,05	»
1	One side polished, the other mechanically worked	—	0,20±0,15	0,08±0,04	»
6	Rolled metal, as delivered	Butt welding	0,18±0,05	0,026±0,012	»
7	Polishing	Transverse cut in welded seam	0,29±0,01	0,065±0,057	»
8	Rolled metal, as delivered	With indentations	0,24±0,08	0,07±0,03	»
9	Mechanical working, polishing	—	—	—	No corrosion cracks were observed

The observed tendencies of the total corrosion to vary with particular factors when the absolute values are small play practically no role. We found that OKh18N10T steel in a gadolinium nitrate solution has high corrosion resistance and can be used as structural material for the manufacture of equipment for liquid regulation systems that govern the reactivity of nuclear reactors.

The authors express their gratitude to V. M. Sokolov for developing the design of the corrosion channels.

#### LITERATURE CITED

1. A. N. Erykalov, I. A. Kondurov, K. A. Konoplev, et al., LIYaF Preprint No. 376 [in Russian], Leningrad (1977), p. 6.
2. V. A. Gerasimov, Corrosion of Reactor Materials [in Russian], Atomizdat, Moscow (1980).

#### EFFECT OF CORROSION OF FUEL-ELEMENT JACKETS OF FAST REACTORS ON THEIR MECHANICAL PROPERTIES

E. F. Davydov, F. N. Kryukov,  
and V. K. Shamardin

UDC 621.039.54

During intense burn-up (depletion) of the uranium oxide or uranium plutonium oxide fuel, its physicochemical interaction with the stainless steel jacket (can) of the fuel elements of the fast reactors is accompanied by corrosive damage of the internal surface of the jacket and a reduction in its mechanical properties. These facts must be considered in the fuel element design. The results of out-of-reactor experiments show that in this case, the strength of the jacket may be found to be lower than that calculated only from the considerations of reduction its wall thickness because of corrosion [1, 2]. In view of this, it was of interest to obtain a quantitative evaluation of the effect of corrosion on the mechanical properties of the fuel elements subjected to irradiation in a BOR-60 reactor.

The fuel-element jackets (external diameter 6 mm and wall thickness 0.3 mm) were made from the austenitized stainless steel OKh16N15M3BR. The fuel elements having a uranium dioxide core were irradiated up to a maximum depletion of 8% heavy atoms at a maximum linear intensity (power) of 42 kW/m. The calculated maximum temperature of the jacket without taking

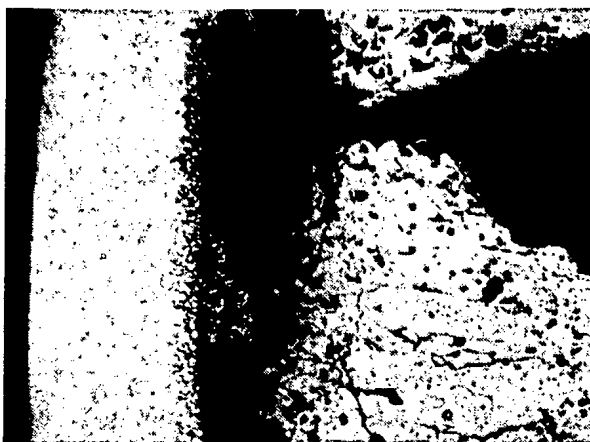


Fig. 1. Microstructure of the corroded layer of the fuel-element jacket,  $\times 100$ .

Translated from Atomnaya Energiya, Vol. 59, No. 3, pp. 226-227, September, 1985. Original article submitted August 27, 1984.

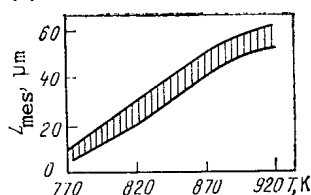


Fig. 2

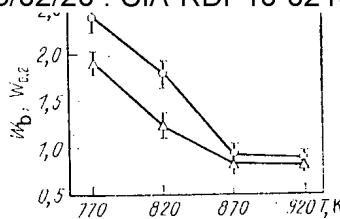


Fig. 3

Fig. 2. Temperature dependence of the depth of corrosion of the fuel-element jackets.

Fig. 3. Temperature dependence of the coefficients of weakening  $W_b$  ( $\circ$ ) and  $W_{0.2}$  ( $\Delta$ ) of the jacket material.

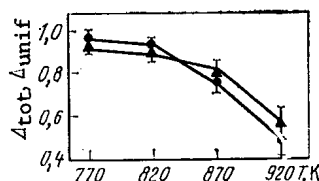


Fig. 4. Temperature dependence of the coefficients of ductility loss  $\Delta_{tot}$  ( $\bullet$ ) and  $\Delta_{unif}$  ( $\blacktriangle$ ) of the jacket material.

overheating into account was equal to  $920 \pm 30^\circ\text{K}$ . The neutron fluence in the central plane of the fuel-element core amounted to  $6.3 \cdot 10^{26} \text{ m}^{-2}$ .

In order to study the temperature dependences of the corrosion depth and the mechanical properties, from each one of the jackets of two fuel elements we cut out six ring-shaped specimens measuring 3 mm in height that belong to four regions corresponding to the jacket-temperatures 770, 820, 870, and  $920^\circ\text{K}$ . Corrosion depth in the jackets was measured within an error of  $\pm 5 \mu\text{m}$  by examining the unetched sections under a MIM-15 microscope. The mechanical properties of the jackets were determined from the transverse rupture tests [3] conducted on the ring-shaped specimens at the service temperature in a MM-150 D machine maintaining an active grip-displacement rate of 1 mm/min. In order to study the effect of corrosion on the short-term strength and the ductility of the jackets, we carried out comparative (reference) mechanical tests on the ring-shaped specimens cut out from neighboring regions of the fuel elements having uncorroded internal surfaces. After removing the fuel residues from the internal surface, a 100- $\mu\text{m}$ -thick layer was etched out electrochemically and the mechanical tests were carried out.

In view of the fact that in the general case, the change in the strength does not correspond to the corrosion-induced reduction in the thickness of the working portion of the specimens [2], it is of practical importance to determine the effective depth of corrosion from the condition of equality of the ultimate and the yield strengths ( $\sigma_b$  and  $\sigma_{0.2}$ ) of a ring-shaped specimen having a corroded layer and a specimen whose internal layer is removed ( $\Delta d_{bef}$  and  $\Delta d_{0.2,ef}$ , respectively). From this two distinct relationships emerge:

$$\Delta d_{bef} = d - \frac{P_{b,corr}}{P_{b,et}} \frac{h_{et}}{h_{corr}} (d - d_{et});$$

$$\Delta d_{0.2,ef} = d - \frac{P_{0.2,corr}}{P_{0.2,et}} \frac{h_{et}}{h_{corr}} (d - d_{et}),$$

where  $P_{b,corr}$ ,  $P_{b,et}$ ,  $P_{0.2,corr}$ , and  $P_{0.2,et}$  are the values of the loads corresponding to the ultimate strength and the conditional yield strength of the specimens with a corroded layer and with an etched internal layer;  $h_{corr}$  and  $h_{et}$ , heights of the corresponding ring-shaped specimens; and  $d$  and  $d_{et}$ , wall thickness of the jacket in the original state and the thickness of the etched corrosive layer, respectively.

the coefficients of weakening that are equal to the ratio of the effective corrosion depth to the depth measured using an optical microscope,

$$W_b = \Delta d_{\text{bef}} / \Delta d_{\text{opt}};$$
$$W_{0.2} = \Delta d_{0.2, \text{ef}} / \Delta d_{\text{opt}}$$

and the coefficients of reduction in ductility of the jacket material which are equal to the ratios of the total and the uniform elongations of the specimens having a corroded layer to those of the specimens with an etched out internal layer

$$\Delta_{\text{tot}} = \delta_{\text{tot, corr}} / \delta_{\text{tot, et}};$$
$$\Delta_{\text{unif}} = \delta_{\text{unif, cor}} / \delta_{\text{unif, et}}.$$

Figure 1 shows the microstructure of the corroded layer of the jacket-material, and Fig. 2 shows the temperature dependence of the depth of corrosion of the material measured on the specimens cut out from different regions along the height of the fuel elements. Figures 3 and 4 show the average values of the coefficients  $W_b$ ,  $W_{0.2}$ ,  $\Delta_{\text{tot}}$ , and  $\Delta_{\text{unif}}$  of the jacket material calculated from the test results obtained on the series consisting of six specimens for each of the regions along the height of the fuel element.

While at the temperatures 770 and 820°K the effective depth of corrosion is considerably greater than the depth measured using an optical microscope, at 870 and 920°K the zone of corrosive damage contributes to the total strength of the jacket (see Fig. 3). Ductility loss is a distinguishing feature in the specimens having a corroded layer (see Fig. 4). The notch effect of the corroded grain boundaries increases with increasing irradiation and testing temperatures (see Fig. 3).

In future investigations, it is advisable to study the dependence of the aforementioned characteristics on different technological and operational parameters so as to make use of them in the design calculations of fuel elements.

#### LITERATURE CITED

1. O. Götzmann, "Fuel and cladding interaction, out-of-pile experiments," Technical Committee Meeting on Fuel and Cladding Interaction, IWGFR/16, IAEM, Tokyo (1977), pp. 37-40.
2. L. Schäfer and P. Hofmann, "Tensile properties of 1.4970 austenitic stainless steel after corrosion caused by uranium dioxide and simulated fission products," J. Nucl. Mater., 115, Nos. 2-3, 169-177 (1983).
3. V. N. Prokhorov, A. G. Fin'ko, and R. I. Mineev, "Experimental determination of the working length of circular specimens made from the fuel-element cans under transverse tension," Preprint NIIAR, P-23 (317) (1977).

# MAGNETIC RESONANCE METHODS USED TO STUDY THE MOBILITY OF LITHIUM IONS AND THE FORMATION OF GAMMA RADIOLYSIS PRODUCTS IN LITHIUM SILICATES

I. S. Pronin, A. A. Vashman,  
and A. S. Nikiforov

UDC 546.66.085:535.34.083.2

Inorganic lithium compounds are among the promising materials for winning tritium in thermonuclear reactions [1-3], and it is therefore necessary to have information on both the physical and chemical properties of these compounds. We present in this paper the results of research on the mobility of lithium ions and the formation of radiation-induced paramagnetic centers in the gamma radiolysis of lithium ortho- and metasilicates; nuclear magnetic resonance of  $^7\text{Li}$  and electroparamagnetic resonance were used in the studies.

We used in the experiments a screened fraction ( $-250$  and  $+80$   $\mu\text{m}$ ) of powders with a purity for chemical analysis; in these powders, the total mass fraction of the metal impurities

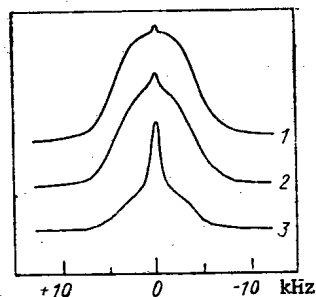


Fig. 1

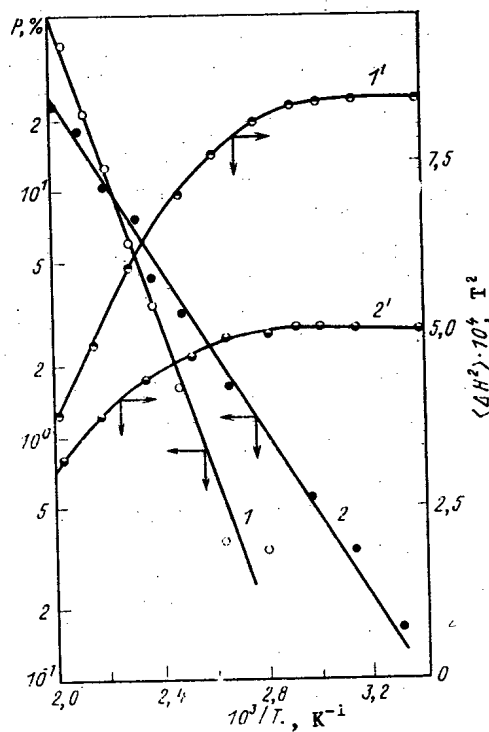


Fig. 2

Fig. 1. Typical normalized spectra of the  $^7\text{Li}$  nuclear magnetic resonance of lithium metasilicate at: 1) 320, 2) 400, and 3) 480°K.

Fig. 2. Temperature dependencies of the relative fraction  $P$  (curves 1 and 2) of the narrow component and of the second moment  $\langle \Delta H^2 \rangle$  (curves 1' and 2') of the broad component of the nuclear magnetic resonance spectra of  $^7\text{Li}$ : 1 and 1' refer to lithium orthosilicate and 2 and 2' to lithium metasilicate.

Translated from *Atomnaya Energiya*, Vol. 59, No. 3, pp. 227-229, September, 1985. Original article submitted August 27, 1984.

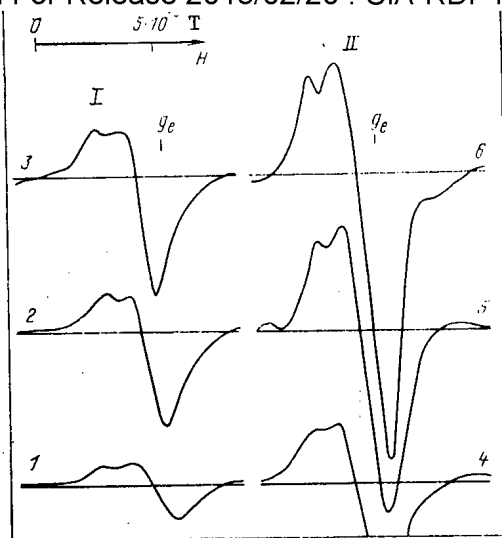


Fig. 3. EPR spectra of: I) lithium orthosilicate and II) lithium metasilicate with an irradiation dose of 1) 13, 2) 77, 3) 155, 4) 258, 5) 851, and 6) 1039 Mrad.

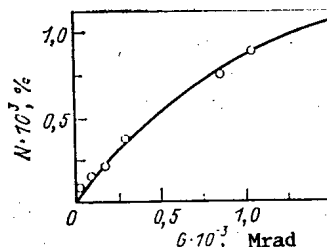


Fig. 4. Dependence of the accumulation of paramagnetic centers upon the irradiation dose: —) theory; O) experiment.

(Cu, Al, Fe, Mn, Mg, Ti, and Mo) did not exceed 0.35% in the case of lithium orthosilicate and 0.12% in the case of lithium metasilicate. The  $^7\text{Li}$  nuclear magnetic resonance spectra were recorded with a Brooker SKhR-100 spectrometer used in high-power operation with external stabilization of the magnetic field in the temperature range 300-500°K. The EPR spectra of the powders which had been irradiated at room temperature with a  $^{60}\text{Co}$  gamma beam were recorded with an RE-1301 spectrometer at 77 and 295°K. In order to determine the concentration of the primary radiolysis products which appear as paramagnetic centers, we used an external standard, namely a copper chloride single crystal with  $2 \cdot 10^{17} \text{ Cu}^{2+}$  ions.

The  $^7\text{Li}$  nuclear magnetic resonance spectra of lithium ortho- and metasilicates are a superposition of two lines with identical chemical shifts but with different widths. When the sample temperature is raised, the intensity of the broad component of the spectrum decreases, whereas the intensity of the narrow component increases (see Fig. 1). The total intensity and the form of the lines do not change. A graphic analysis of the line contours of lithium ortho- and metasilicates was used to determine the intensity, the widths of the broad and the narrow components at various temperatures, the fraction  $P = S_1/(S_1 + S_2)$  of the narrow component in the total spectral intensity ( $S_1$  and  $S_2$  denote the intensity of the narrow and the broad component, respectively), and the second moment  $\langle \Delta H^2 \rangle$  of the broad component of the  $^7\text{Li}$  nuclear magnetic resonance line (Fig. 2).

The two-component spectra of the  $^7\text{Li}$  nuclear magnetic resonance indicate that the lithium ions move with different velocities in the solid matrix of the silicates examined. When the temperature is increased, the slow movement (broad component of the spectrum) of the lithium ions is gradually replaced by a fast motion (narrow component of the spectrum).

The a Declassified and Approved For Release 2013/02/20 : CIA-RDP10-02196R000300070003-2  
 endence in  $P = f(10^3/T)$  is  $E_{\text{ort}} = 142 \pm 2$  kJ/mole in the case of the orthosilicate and  $E_{\text{met}} = 75 \pm 2$  kJ/mole in the case of the metasilicate of lithium. The average length  $R$  of a diffusion jump of a lithium ion in the silicate matrix is given by the distance between the Li-Li nuclei and can be calculated with the Van Vleck formula for the second moment of the nuclear magnetic resonance line of a rigid lattice:

$$R = [6\gamma^2 h^2 I(I+1)/5n \langle \Delta H^2 \rangle]^{1/6},$$

where  $\gamma$  and  $I$  denote the gyromagnetic ratio and the spin of the  $^7\text{Li}$  nucleus, respectively; and  $n$  denotes the number of nuclei with dipole-dipole interaction. For  $I = 3/2$ ,  $n = 2$ ,  $\langle \Delta H^2 \rangle_{\text{ort}} = 8.2 \cdot 10^{-8} \text{ T}^2$ , and  $\langle \Delta H^2 \rangle_{\text{met}} = 5.0 \cdot 10^{-8} \text{ T}^2$ , we obtain  $R_{\text{ort}} = 0.179 \pm 0.001 \text{ nm}$  and  $R_{\text{met}} = 0.193 \pm 0.001 \text{ nm}$ .

The EPR spectra of lithium ortho- and metasilicates irradiated with  $^{60}\text{Co}$  are identical and correspond to a singlet with an axisymmetric  $g$  factor having the components  $g_{\perp} = 2.002 \pm 0.0015$  and  $g_{\parallel} = 2.020 \pm 0.0015$ . The typical EPR spectra of paramagnetic centers of gamma-irradiated lithium silicates are indicated in Fig. 3. Such spectra are characteristic of "oxygen" radicals of the  $\text{O}_2^-$  type formed in  $2\text{Li}_2\text{O} \cdot \text{SiO}_2$  and  $\text{Li}_2\text{O} \cdot \text{SiO}_2$  silicates upon gamma irradiation. The accumulation of paramagnetic centers in the silicate matrix during the irradiation at  $\sim 300^\circ\text{K}$  can be represented by the formula

$$N = N_0 [1 - \exp(-G/g)],$$

where  $G$  denotes the irradiation dose;  $N_0$ , concentration of the paramagnetic centers for  $G \rightarrow \infty$ ; and  $g$ , a constant the inverse of which is a measure of the accumulation rate of paramagnetic centers.

The resulting expression satisfactorily describes the experimental  $N$  values which were determined from the intensity of the lines of the EPR spectra with  $N_0^{\text{ort}} = 11 \cdot 10^{20}$  paramagnetic centers per kg and  $N_0^{\text{met}} = 3.6 \cdot 10^{20}$  paramagnetic centers per kg and  $g = 1000 \text{ Mrad}$  ( $1 \text{ rad} = 0.01 \text{ Gy}$ ). When we relate the concentration of the paramagnetic centers to the number of Li-O bonds per gram-mole of the corresponding lithium silicate, we obtain  $N_0^{\text{ort}}/N_0^{\text{met}} = 2$ . Figure 4 illustrates the function  $N = f(G)$  for  $N_0 = 1.38 \cdot 10^{-3} \%$  and  $g = 1000 \text{ Mrad}$ . This function agrees with the experimental  $N$  values reduced by a factor of 4 in the case of lithium orthosilicate and by a factor of 2 in the case of lithium metasilicate. We can therefore assume that the number of stable paramagnetic centers which are formed upon gamma irradiation of lithium silicates is proportional to the number of  $\text{Li}_2\text{O}$  groups in the  $\text{Li}_4\text{SiO}_4$  and  $\text{Li}_2\text{SiO}_3$  molecules. When the temperature during irradiation is increased, the number of stable paramagnetic centers must decrease by recombination. The average distance  $l$  between paramagnetic centers which are stabilized in the silicate matrix at the irradiation temperature is

$$l = N_0^{-1/3} \cdot (6M/\pi\rho A)^{1/3},$$

where  $N_0$  denotes the concentration of paramagnetic centers per  $\text{m}^3$  for  $G \rightarrow \infty$ ;  $M$ , molecular mass of the lithium silicate (atomic mass units);  $\rho$ , density of lithium silicate; and  $A$ , Avogadro number. For  $M_{\text{ort}} = 120$ ,  $\rho_{\text{ort}} = 2.58 \cdot 10^3 \text{ kg/m}^3$ ,  $M_{\text{met}} = 90$ , and  $\rho_{\text{met}} = 2.52 \cdot 10^3 \text{ kg/m}^3$ , we obtain  $l_{\text{ort}} = 6.6 \text{ nm}$ ,  $l_{\text{met}} = 9.8 \text{ nm}$ .

#### LITERATURE CITED

1. E. P. Velikhov, V. A. Glukhikh, V. V. Gur'ev, et al., Thernonuclear Hybrid Tokamak Reactor for Producing Fissionable Fuel and Electric Energy, Reports of the All-Union Conf. on Engineering Problems of Thernonuclear Reactors [in Russian], Vol. 1, NIIÉFA, Leningrad (1977), pp. 15-18.
2. V. Kotov and G. Shatalov, in: Proc. US-USSR Symp. Fusion-Fission Reactors, Conf. 760733, p. 129, July 13-16 (1976).
3. V. G. Vasil'ev, S. R. Borisov, N. N. Ryazantseva, and A. A. Vashman, "Investigation of the physicochemical properties of irradiated inorganic lithium compounds: lithium oxides, aluminates, and silicates," At. Energ., 48, No. 6, 392 (1980).

# MEASURING THE CONTENT BY VOLUME OF DEUTERIUM IN HEAVY WATER WITH CARBON DIOXIDE DISSOLVED IN IT\*

T. I. Efimova, V. F. Kapitanov,  
and G. V. Levchenko

UDC 621.039.52

Heavy water and carbon dioxide are extensively used in nuclear power engineering. Heavy water is the best moderator of all if we just take account of neutron braking and its insignificant levels of absorption. However, it is inevitable for there to be some contact between the moderator and the carbon dioxide coolant in a reactor, as a result of which we get them entering into solution with each other. The intrusion of the carbon nuclei in solution with the heavy water changes the volume content of the deuterium, and so varies its properties as a moderator (the thermophysical characteristics of  $D_2O$  and  $CO_2$  are generalized in [1, 2])

\*In the original paper the authors used the term "nuclear density," by which the density of the matter within the nucleus is denoted in physics; for all nuclides this quantity, as is known, is approximately equal to  $5 \cdot 10^{14}$  g/cm<sup>3</sup> - Editor.

TABLE 1. Density of  $CO_2$ - $D_2O$  Solutions on a Scale of 100%  $D_2O$ , in g/cm<sup>3</sup>

T, K	Pressure, MPa				
	3	6	10	15	20
303	1,119000	1,126010	—	—	—
323	1,106165	1,115558	1,121772	1,130386	1,139336
343	1,092728	1,097366	1,106748	1,115242	1,124200
373	1,069903	1,073943	1,082768	1,089864	1,097798
393	1,052081	1,055217	1,064315	1,071546	1,078717
413	1,032172	1,036013	1,044503	1,051367	1,058460
423	1,010372	1,014258	1,022493	1,029542	1,036409
453	0,986888	0,990889	0,998901	1,006389	1,013306
473	0,961712	0,965734	0,973414	0,981720	0,988969

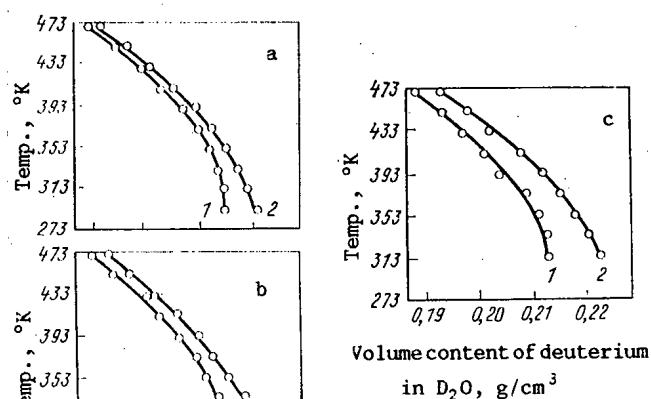


Fig. 1. Isobars of volume content of deuterium for a saturated solution of carbon dioxide in heavy water (1) and for heavy water alone (2) at pressures of 5 MPa (a), 10 MPa (b), and 20 MPa (c).

Translated from Atomnaya Énergiya, Vol. 59, No. 3, pp. 229-230, September, 1985. Original article submitted September 11, 1984.

article is an attempt to measure the density of a solution of carbon dioxide in heavy water at increased temperatures and pressures, and also to determine the effect of the solubility of carbon dioxide in heavy water on the volume content of deuterium. Investigations have been carried out over the temperature range 303-473°K and the pressure range 3-20 MPa by the autoclave method. The heavy water was poured into the autoclave and the carbon dioxide introduced. The heavy water was saturated with carbon dioxide to a state of equilibrium at the specific temperature and pressure concerned by agitation. A sample of the liquid phase was then withdrawn in an ampoule, weighed and the density of the solution calculated.

From the data on the density of solutions of  $\text{CO}_2$ - $\text{D}_2\text{O}$  and experimental data on the solubility of  $\text{CO}_2$  in  $\text{D}_2$  in a  $\text{CO}_2$ - $\text{D}_2\text{O}$  system [3] (which we obtained earlier), we calculated the volume content of deuterium in heavy water saturated with carbon dioxide.

Figure 1 shows the relationship of the volume content of deuterium in a saturated solution of carbon dioxide in heavy water against temperature and pressure, compared with the volume content of deuterium in heavy water alone at the same parameters. Figure 1 shows that the volume content of deuterium in heavy water with carbon dioxide dissolved in it is markedly lower. This reduction becomes more pronounced with an increase in pressure. At increased pressures, the volume content of deuterium is reduced, both for heavy water and for a saturated solution of carbon dioxide in heavy water.

#### LITERATURE CITED

1. Heavy Water, Its Thermophysical Properties [in Russian], Goskhimizdat, Moscow (1963), p. 171.
2. M. P. Vukalovich and V. V. Altunin, The Thermophysical Properties of Carbon Dioxide [in Russian], Atomizdat, Moscow (1965), p. 360.
3. V. F. Kapitanov and O. M. Shcherbakova, "Studying the solubility of carbon dioxide in heavy water," Zh. Fiz. Khim., 57, No. 7, 1785-1787 (1983).

# USING THE THEORY OF SMALL PERTURBATIONS IN PERFORMANCE CALCULATIONS OF THE RBMK

N. V. Isaev, Yu. V. Shmonin,  
L. R. Pogosbekyan, and V. E. Druzhinin

UDC 621.039.51.15

When performance calculations of the RBMK are made [1], it is often necessary to select optimal parameters for the reactor core (for example, when the field of energy generation is to be kept within certain limits, when the reloading and transposition of fuel elements is being planned, etc.). For this purpose one usually must consider many versions of reactor conditions. For solving such problems one traditionally employs the theory of small perturbations in reactor physics [2]. The theory is usually applied to simple one-dimensional models. In two-dimensional calculations of the RBMK, the theory of small perturbations to date has not been employed though it had been necessary for a long time.

Formulation of the Problem. We state in matrix-vector form the equations for the direct problem and the conjugated problem in the two-group diffusion approximation which is usually employed in calculations of the RBMK-1000:

$$M\Phi = \frac{1}{K_{\text{eff}}} F\Phi; \quad (1)$$

$$M^+\Phi^+ = \frac{1}{K_{\text{eff}}} F^+\Phi^+, \quad (2)$$

where  $\Phi$  and  $\Phi^+$  denote the solution of the direct problem and the conjugated problem;

$$M = \begin{pmatrix} -\text{div } D^{(1)}\nabla + \Sigma_{ad}^{(1)} & 0 \\ -\Sigma_d^{1+2} & -\text{div } D^{(2)}\nabla + \Sigma_a^{(2)} \end{pmatrix};$$

$$F = \begin{pmatrix} \nu_f \Sigma_f^{(1)} & \nu_f \Sigma_f^{(2)} \\ 0 & 0 \end{pmatrix};$$

$$M^+ = \begin{pmatrix} -\text{div } D^{(1)}\nabla + \Sigma_{ad}^{(1)} & -\Sigma_d^{1+2} \\ 0 & -\text{div } D^{(2)}\nabla + \Sigma_a^{(2)} \end{pmatrix};$$

$$F^+ = \begin{pmatrix} \nu_f \Sigma_f^{(1)} & 0 \\ \nu_f \Sigma_f^{(2)} & 0 \end{pmatrix};$$

$$\Phi = \{\Phi_1, \Phi_2\}; \quad \Phi^+ = \{\Phi_1^+, \Phi_2^+\}.$$

The generally accepted notation is employed [2];  $\chi^{(1)} = 1$  and  $\chi^{(2)} = 0$ . In order to solve the conjugated problem with the BOKR-BIS program of [3], Eq. (2) is conveniently rewritten in the form

$$\begin{pmatrix} -\text{div } D^{(2)}\nabla + \Sigma_a^{(2)} & 0 \\ -\Sigma_d^{1+2} & -\text{div } D^{(1)}\nabla + \Sigma_{ad}^{(1)} \end{pmatrix} \begin{pmatrix} \Phi_2^+ \\ \Phi_1^+ \end{pmatrix} = \frac{1}{K_{\text{eff}}} \begin{pmatrix} 0 & \nu_f \Sigma_f^{(2)} \\ 0 & \nu_f \Sigma_f^{(1)} \end{pmatrix} \begin{pmatrix} \Phi_2^+ \\ \Phi_1^+ \end{pmatrix}. \quad (3)$$

Let us calculate the change in the reactivity,  $\Delta\rho$ , caused by a perturbation (change in the position of a control rod, reloading of a channel, etc.). Assume that the equation for the solution of this problem is of the form

$$M'\Phi' = \frac{1}{K_{\text{eff}}} F'\Phi', \quad (4)$$

where

$$M' = M + \delta M, \quad F' = F + \delta F, \quad \Phi' = \Phi + \delta\Phi.$$

Translated from *Atomnaya Energiya*, Vol. 59, No. 3, pp. 230-232, September, 1985. Original article submitted September 14, 1984.

Form of reloading	Theory of small perturbations	"Improved" theory
AA → FR	-110	-25
IFE → FR	-10	-8
CW → FR	-100	-30
AAJ → FR	-100	-26
AAJ → AA	-10	-8
AAJ → IFE	-20	-15

Remark: IFE) irradiated fuel element; CW) water column; and AAJ) additional absorber with a jacket.

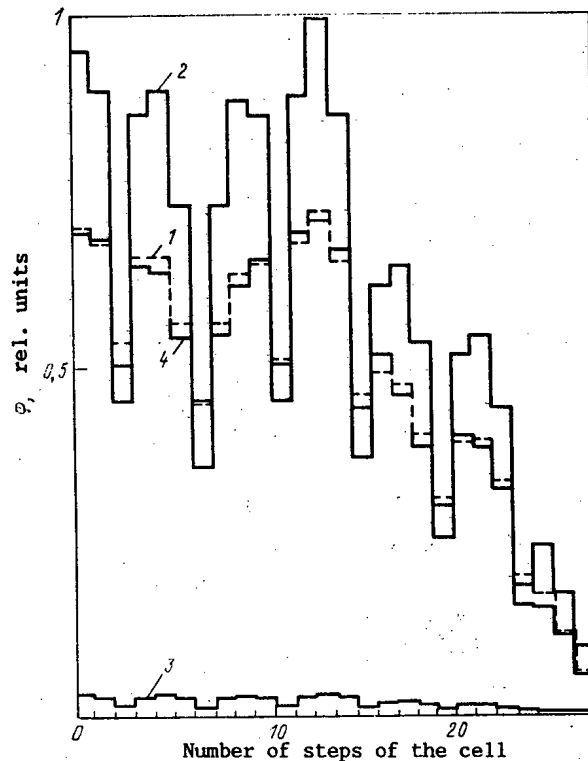


Fig. 1. Histogram of the distributions of  $\phi$  and  $\phi^+$  over the radius of the RBMK-1000: 1)  $\phi^+$ ; 2)  $\phi_2^+$ ; 3)  $\phi_1$ ; 4)  $\phi_2$ .

When we use the formalism of the theory of small perturbations, we can state a formula for the change in the reactivity due to small changes in two-group macroscopical cross sections:

$$\Delta\rho \approx \left\{ \phi^+, \left( -\frac{1}{k_{\text{eff}}} \delta F - \delta M \right) \phi \right\} / \{ \phi^+, F\phi \}. \quad (5)$$

**Description of the Program.** In order to solve the conjugated problem of Eq. (2), which is actually expressed by Eq. (3), it suffices to exchange the positions of  $\phi_1$  and  $\phi_2$ ,  $D^{(1)}$  and  $D^{(2)}$ , and  $\Sigma_{\text{ad}}^{(1)}$  and  $\Sigma_{\text{d}}^{(2)}$  when the algorithm for solving the direct problem of Eq. (1) is employed. For solving the problems stated in Eqs. (1) and (2) and for calculating the  $\Delta\rho$  values, the RERO program is employed; the basis of this program is the BOKR-BIS program. The program is written in the FORTRAN IV language for an ES series computer with an ES operational system (version 6.1). The calculation time for one version of the RBMK-1000 with the RERO program is 5 min on an ES-1052 computer.

The operational memory required for the RERO program must have 350 kbyte.

Numerical Examples. The RBMK program was used for calculating the RBMK-1000 of the first block of the Smolensk Atomic Power Station in the reactor state corresponding to Dec. 14, 1983. We have for the direct problem of Eq. (1):  $K_{\text{eff}} = 0.99928$ ,  $K_r = 1.5365$ ,  $n = 41$ ; we have for the conjugated problem of Eq. (2):  $K_{\text{eff}} = 0.99926$ ,  $K_z = 1.5342$ , and  $n = 57$ , where  $K_{\text{eff}}$  denotes the calculated value of the real state of the critical reactor wherein the errors of the cross sections and of the computational model have been taken into account;  $K_r$  denotes the coefficient of the nonuniformity of energy liberation in the reactor; and  $n$  denotes the number of external iterations with an accuracy of  $10^{-5}$  in the  $K_{\text{eff}}$  calculation. Figure 1 represents histograms of the  $\phi$  and  $\phi^+$  distributions for the center-line series of reactor cells, starting from cell 37-40 and ending with cell 37-73. The "dips" on the figure correspond to cells with additional absorbers (AA).

We will demonstrate the determination of the reactivity effects in reloading operations by a sample calculation of the first block of the Smolensk Atomic Power Station in its state of April 19, 1984. In order to assess the relative error  $\epsilon$  corresponding to the theory of small perturbations, the  $\Delta\rho$  value obtained with Eq. (5) is compared with the  $\Delta\rho$  values obtained with the solution of the direct "perturbed" (Eq. (4)) problem and the "unperturbed" (Eq. (1)) problem. Let us calculate the reactivity  $\Delta\rho_{\text{AA} \rightarrow \text{FR}}$  when an additional absorber (AA) is replaced by a fresh fuel rod (FR). The results of the calculation depend strongly upon the coordinates of the channel which is being reloaded. For example, for the center-line series (cells 37-12, 37-16, 37-26, 37-32, 37-36, 37-42, 37-46, 37-52, 37-56, and 37-62), the  $\Delta\rho_{\text{AA} \rightarrow \text{FR}}$  values are ( $\cdot 10^{-5}$ ): 29, 48, 45, 57, 67, 42, 46, 44, 51, and 39, respectively. For the vertical series (cells 57-36, 53-36, 47-36, 43-36, 37-36, 33-36, 27-36, 23-36, 17-36, and 13-36) the  $\Delta\rho_{\text{AA} \rightarrow \text{FR}}$  values are ( $\cdot 10^{-5}$ ): 62, 47, 58, 63, 67, 57, 43, 31, and 21, respectively. The errors  $\epsilon$  (see Table 1) were obtained for channels in which the reloading effect is greatest. The  $\Delta\rho_{\text{AA} \rightarrow \text{FR}}$  values calculated with the formulas of the theory of small perturbations are smaller than the values obtained by the solution of Eqs. (4) and (1) by a factor of about 2. The explanation may be that values of the unperturbed functions  $\phi$  and  $\phi^+$  were used in Eq. (5); in cells with an additional absorber these functions have a strong dip in comparison with the neighboring channels containing fuel rods. In a similar fashion the change in the sign of the error  $\epsilon_{\text{CW} \rightarrow \text{FR}}$  can be explained in the case of reloading a water column with a fuel rod. In a cell with a water column, a flash is observed in comparison with fuel rod cells in the unperturbed functions  $\phi$  and  $\phi^+$ . The value  $\epsilon_{\text{CW} \rightarrow \text{FR}}$  was obtained for the specific cell 43-52. With the acceptable error (10%) one can calculate  $\Delta\rho_{\text{IFE} \rightarrow \text{FR}}$  for the reloading IFE  $\rightarrow$  FR. For example, for cell 62-43 which contains an irradiated fuel element with a depletion (per fuel rod) of  $\sim 700$  MW·day, the error  $\epsilon_{\text{IFE} \rightarrow \text{FR}}$  amounts to  $\sim 10\%$ . The AAJ  $\rightarrow$  IFE reloading was calculated for cell 37-52 with a depletion of  $\sim 1100$  MW·day per irradiated fuel element (the cell loaded with fuel of repeated use was modelled).

The results of the calculations of the RBMK-1000, which are given in the present paper, indicate that all perturbations which occur in the reactivity upon unloading an additional absorber from the reactor core cannot be considered small and that the error of Eq. (5) is large. Reloading of the type IFE  $\rightarrow$  FR is described by perturbation theory with an acceptable accuracy. Using formulas of perturbation theory of  $n$ -th order is the logic way of increasing the accuracy of the  $\Delta\rho$  calculations.

In order to reduce the error of the determination of the reactivity effects in reloading channels in the RBMK-1000, a procedure which makes it possible to improve the  $\Delta\rho$  values in the theory of small perturbations was developed. The  $\phi_{i,j}$  and  $\phi_{i,j}^+$  values in the  $(i, j)$ th cell, in which a perturbation is introduced, must be replaced by the average values  $\bar{\phi}_{i,j}$  and  $\bar{\phi}_{i,j}^+$  which are calculated with the four adjacent cells:

$$\bar{\phi}_{i,j} = (\phi_{i-1,j} + \phi_{i+1,j} + \phi_{i,j-1} + \phi_{i,j+1})/4. \quad (6)$$

The  $\bar{\phi}_{i,j}^+$  value is determined in a similar manner. The results of the determination of the relative error  $\bar{\epsilon}$  with the "improved" theory of small perturbations are also listed in Table 1. In the case of reloading of the type AA  $\rightarrow$  FR, the  $\bar{\phi}_{i,j}$  and  $\bar{\phi}_{i,j}^+$  values increase in comparison with  $\phi_{i,j}$  and  $\phi_{i,j}^+$  for a cell with an additional absorber; this implies an increase in  $\bar{\Delta\rho}$  and a reduction of  $\bar{\epsilon}$  to 25%. Similarly, in the case of a reloading CW  $\rightarrow$  FR, the  $\bar{\phi}_{i,j}$  and  $\bar{\phi}_{i,j}^+$  values are smaller than  $\phi_{i,j}$  and  $\phi_{i,j}^+$  for a cell containing a water column and therefore  $\bar{\Delta\rho}$  decreases and  $\bar{\epsilon}$  is reduced to 30%.

the reloaded channels. The calculations with the RERO program have provided a map of the reactor in which for all core cells (except for the control rods) the  $\Delta\rho_{i,j}$  values arising in the replacement of the contents of the particular cell by, say, a fresh fuel rod are indicated. The personnel of the atomic power station uses the map of the reactivity effects when reloading work is planned.

Determination of the Reloading Rate. Estimates of the reloading rates  $R(\Delta t)$  of the channels in the RBMK-1000 were obtained with the theory of small perturbations and the RERO program. The procedure of calculating  $R(\Delta t)$  is as follows:

1. The energy generation  $E_{i,j}(t)$  of the channels is known at the time  $t$ . With  $W_{i,j}^{st}$  denoting the stipulated energy distribution in the reactor, we may assume that the actual energy distribution  $W_{i,j}$  is close (within  $\pm 5\%$  limits) to  $W_{i,j}^{st}$ , and therefore the energy liberation at the time  $t + \Delta t$  can be approximately defined as

$$E_{i,j}(t + \Delta t) = E_{i,j}(t) + W_{i,j}^{st} \Delta t. \quad (7)$$

2. Let us consider the perturbation which is caused by a change in the energy generation from  $E_{i,j}(t)$  to  $E_{i,j}(t + \Delta t)$  for each reactor channel during the time period  $\Delta t$  and let us estimate the corresponding reactivity changes  $\Delta\rho$  with Eq. (5). The cross sections of the cells in the RERO program are functions of  $E_{i,j}$  and  $W_{i,j}$ , and we therefore assume that the output  $W_{i,j}$  of the channel does not change during the time interval  $\Delta t$ .

3. We define the reloading rate during the time period  $\Delta t$  as

$$R(\Delta t) = \Delta\rho / \Delta t. \quad (8)$$

Let us estimate the  $R(\Delta t)$  value for the first block of the Smolensk Atomic Power Station for the reactor state of April 19, 1984. We select  $\Delta t = 10$  eff. days and  $\Delta\rho = -0.002731$  (according to the RERO program). The average reloading rate  $R(\Delta t)$  is  $-0.00027$ . When in this time period an AA  $\rightarrow$  FR reloading is performed, we obtain an average reloading rate of 0.42 channels per effective day, which within the  $\pm 10\%$  limit coincides with the result of calculations made with the OPERA program [4] or the REF-W program [5].

Estimates of the Reactivity Storage in a Control Rod. The RERO program can also be used to assess the reactivity storage in each control rod, i.e., to determine the perturbation  $\Delta\rho_k$  which is caused by a displacement of rod  $k$  from the depth  $h_k$  of immersion to level zero. The RERO program makes it possible to calculate a  $\Delta\rho_k$  map for each of the control rods. The personnel of the atomic power station uses this map in adjusting the field of energy generation in the reactor.

Summarizing, the classical theory of small perturbations implies considerable errors in calculations because the perturbations cannot be considered small. The modified theory of small perturbations can be used in atomic power stations for determining reactivity effects and reloading rates of channels in reactors and also for assessing the reactivity storage in control rods.

#### LITERATURE CITED

1. N. A. Dollezhal' and I. Ya. Emel'yanov, Channel-Type Nuclear Energy Reactor [in Russian], Atomizdat, Moscow (1980).
2. S. B. Shikhov and V. B. Troyanskii, The Theory of Nuclear Reactors. Vol. 2. The Theory of Gas Kinetics [in Russian], Énergoatomizdat, Moscow (1983), pp. 63-78.
3. A. A. Shkurpelov, V. P. Borshchev, V. P. Veselov, et al., "The BOKR-BIS program for the two-dimensional calculation of the RBMK with a series ES computer," At. Energ., 50, No. 5, 352 (1981).
4. N. V. Isaev and Yu. V. Shmonin, "A Program for Calculating Continuous Reloading Operations in the RBMK-1000 Reactor," Problems of Atomic Science and Technology, Series Physics and Technology of Nuclear Reactors [in Russian], No. 8 (37), pp. 35-40 (1983).
5. V. S. Romanenko and A. V. Krayushkin, "Computational studies of the physical characteristics of the RBMK in a transition period," At. Energ., 53, No. 6, 367 (1982).

# CHANGES IN THE MICROHARDNESS OF SiC (6H) SAMPLES IN NEUTRON IRRADIATION

V. N. Brudnyi and B. T. Tolebaev

UDC 621.039.532

When a neutron flux is incident on SiC which is used as barrier for fission products, in neutron detectors, or as a construction material, the physical properties of the material change and, in particular, the lattice parameter increases, internal stresses appear, the volume of the samples expands, and the stored energy and the thermal resistance are increased [1-3] as a consequence of the development of radiation-induced defects. Changes of the mechanical properties of SiC, e.g., of its microhardness, can develop. But the measurements performed so far have not demonstrated changes in the microhardness as a result of neutron irradiation up to a neutron flux of  $1.7 \cdot 10^{19} \text{ cm}^{-2}$  [4]. It is therefore of interest to study the microhardness of SiC (6H) crystals irradiated with reactor neutrons to a flux of  $1 \cdot 10^{17}$ – $1 \cdot 10^{21} \text{ cm}^{-2}$ .

Crystals with n-conductivity, doped with nitrogen to a concentration of  $5 \cdot 10^{17}$ – $8 \cdot 10^{18} \text{ cm}^{-3}$ , were obtained by sublimation from the gas phase. Single-crystal samples (average dimensions  $0.4 \times 0.4 \text{ cm}$ ) were cut from the ingots; these samples were cut into plates with a thickness of  $\sim 4.5 \cdot 10^{-2} \text{ cm}$ . The investigations involved samples the Laue diagrams of which revealed diffuse reflections, asterism, and other indications of structural imperfection. The irradiation took place at  $70^\circ\text{C}$  in quartz tubes inserted into the vertical channel of the VVR-K reactor of the Institute of Nuclear Physics of the Academy of Sciences of the Kazak SSR. The flux density of the thermal neutrons was  $3 \cdot 10^{13} \text{ cm}^{-2} \cdot \text{sec}^{-1}$ , that of the fast neutrons ( $E \geq 10 \text{ keV}$ ) was  $3 \cdot 10^{12} \text{ cm}^{-2} \cdot \text{sec}^{-1}$ .

The crystals were deformed by indentation on a PMT-3 microhardness tester provided with an attachment for the automatic movement of the indenter. Load was exerted upon the indenter during one measurement cycle of 5 sec. Impressions were made on the natural base face (0001)

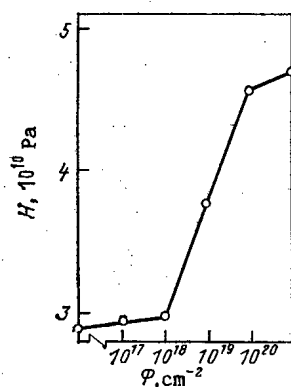


Fig. 1

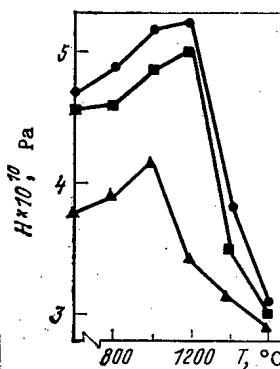


Fig. 2

Fig. 1. Dependence of the microhardness of SiC (6H) upon the neutron flux: (0001) plane;  $T = 20^\circ\text{C}$ ,  $H_0 = 2.9 \cdot 10^{10} \text{ Pa}$ .

Fig. 2. Changes in the microhardness of irradiated SiC (6H) samples with isochronous post-irradiation ( $t = 60 \text{ min}$ ) annealing:  $\Delta$ ) neutron flux  $1 \cdot 10^{19} \text{ cm}^{-2}$ ;  $\blacksquare$ )  $1 \cdot 10^{20} \text{ cm}^{-2}$ ;  $\bullet$ )  $1 \cdot 10^{21} \text{ cm}^{-2}$ .

Translated from Atomnaya Énergiya, Vol. 59, No. 3, pp. 232-233, September, 1985. Original article submitted October 10, 1984.

surface was etched for 3 min at 450°C with KOH and then washed with boiling  $\text{CCl}_4$  and  $\text{H}_2\text{O}$ . The microhardness  $H$  was calculated from the arithmetic mean of 30 measurements with arbitrary orientation of the  $\{1120\}$  slip plane relative to the faces of the diamond pyramid. The microhardness of the initial sample was  $H_0 = 2.9 \cdot 10^{10}$  Pa, which agrees with the available data [5].

As a result of neutron irradiation, the microhardness of SiC (6H) increased 1.6 times (Fig. 1) while at the same time the lattice parameter increased by about 1%. In the neutron flux range  $>1 \cdot 10^{20} \text{ cm}^{-2}$ , the microhardness reached stationary values. This is in good agreement with the changes in the lattice parameter and the volume of the sample under similar neutron flux conditions [1]. Fissures are observed in the initial samples around the impressions and most frequently at the apices. When the neutron flux is increased, both the length and the number of the fissures decrease and at a flux  $\geq 1 \cdot 10^{19} \text{ cm}^{-2}$  no damage to the material was observed in the area of the impressions.

Isochronous annealing of the irradiated samples further increased the microhardness when the samples were heated to 1000-1200°C (Fig. 2). The greatest increase in microhardness (by a factor of 1.8) was observed in samples irradiated to a neutron flux of  $1 \cdot 10^{21} \text{ cm}^{-2}$  and annealed at 1200°C. Even after heating to 1400°C, up to 30% of the microhardness increase observed at the high neutron flux is preserved.

The increased microhardness of SiC (6H) resulting from neutron irradiation can be caused by an increase in plastic-deformation stress due to the appearance of additional centers of dislocation locking. X-ray structure analysis has shown that at a neutron flux of  $\sim 1 \cdot 10^{19} \text{ cm}^{-2}$ , a sharp increase in the defect concentration and a growth of the defects take place so that a nonequilibrium stress structure develops. More particularly, there appear protracted defects of the type of dislocations with a Burgers vector in the (0001) plane or including with this plane a small angle; in addition, two-dimensional disturbances in the form of defect accumulations oriented parallel to the  $\{h\bar{0}h\}$  planes develop. The transition to the stationary microhardness value at a neutron flux  $\geq 1 \cdot 10^{20} \text{ cm}^{-2}$  occurs because a dynamic equilibrium between the development and the disappearance of radiation-induced defects has been reached. This is corroborated by measurements of the lattice parameter [1]. A further increase in the microhardness of SiC (6H) in isochronous annealing to 1000-1200°C is explained by the appearance of additional dislocation locking sites (in particular, development of dislocation loops [6]) as the result of the high defect mobility detected by EPR measurements [7] and positron annihilation [8].

The microhardness of irradiated SiH (6H) decreases upon annealing at a temperature  $>1000$ -1600°C because the concentration of radiation-induced defects decreases; this is confirmed by measurements of the electrical properties [9].

#### LITERATURE CITED

1. E. Boyce, Silicon Carbide [Russian translation], Mir, Moscow (1972).
2. W. Primak, L. Fuchs, and P. Day, Phys. Rev., 103, No. 5, 1184 (1956).
3. C. Lee, F. Pineau, and J. Corelli, J. Nucl. Mater., 108-109, 678 (1982).
4. M. D. Katrich, M. B. Reifman, and M. T. Shaskol'skaya, "Hardness testing of silicon carbide single crystals," in: Reports of the 3rd All-Union Conference on Semiconducting Silicon Carbide [in Russian], Mintsvetmet SSSR, Moscow (1970), p. 228.
5. V. A. Borisenko, G. G. Gnesin, I. V. Gridneva, et al., "The influence of temperature upon the hardness and the form of the destruction of single-crystalline silicon carbide," in: Production and Behavior of Materials in Outer Space [in Russian], Nauka, Moscow (1978), p. 207.
6. R. Stevens, Philos. Mag., 25, No. 2, 523 (1972).
7. N. M. Pavlov, M. I. Iglitsyn, M. G. Kosagonova, and V. N. Solomatin, "Centers with spin 1 in silicon carbide irradiated with neutrons and alpha particles," Fiz. Tekh. Poluprovodn., 9, No. 7, 1279 (1975).
8. V. N. Brudnyi, S. E. Ermatov, S. B. Nurmagambetov, et al., "Positron annihilation in neutron-irradiated SiC (6H)," Fiz. Tverd. Tela, 26, No. 5, 1452 (1984).
9. V. N. Brudnyi, S. E. Ermatov, M. A. Krivov, and B. T. Tolebaev, Izv. Vyssh. Uchebn. Zaved., Fiz., 26, No. 11, 122 (1983).

**MEASUREMENT TECHNIQUES**

*Izmeritel'naya Tekhnika*  
Vol. 27, 1984 (12 issues) ..... \$520

**MECHANICS OF COMPOSITE MATERIALS**

*Mekhanika Kompozitnykh Materialov*  
Vol. 20, 1984 (6 issues) ..... \$430

**METAL SCIENCE AND HEAT TREATMENT**

*Metallovedenie i Termicheskaya Obrabotka Metallov*  
Vol. 26, 1984 (12 issues) ..... \$540

**METALLURGIST**

*Metallurg*  
Vol. 28, 1984 (12 issues) ..... \$555

**PROBLEMS OF INFORMATION TRANSMISSION**

*Problemy Peredachi Informatsii*  
Vol. 20, 1984 (4 issues) ..... \$420

**PROGRAMMING AND COMPUTER SOFTWARE**

*Programmirovaniye*  
Vol. 10, 1984 (6 issues) ..... \$175

**PROTECTION OF METALS**

*Zashchita Metallov*  
Vol. 20, 1984 (6 issues) ..... \$480

**RADIOPHYSICS AND QUANTUM ELECTRONICS**

*Izvestiya Vysshikh Uchebnykh Zavedenii, Radiofizika*  
Vol. 27, 1984 (12 issues) ..... \$520

**REFRACTORIES**

*Ogneupory*  
Vol. 25, 1984 (12 issues) ..... \$480

**SIBERIAN MATHEMATICAL JOURNAL**

*Sibirskii Matematicheskii Zhurnal*  
Vol. 25, 1984 (6 issues) ..... \$625

**SOIL MECHANICS AND FOUNDATION ENGINEERING**

*Osnovaniya, Fundamenty i Mekhanika Gruntov*  
Vol. 21, 1984 (6 issues) ..... \$500

**SOLAR SYSTEM RESEARCH**

*Astronomicheskii Vestnik*  
Vol. 18, 1984 (6 issues) ..... \$365

**SOVIET APPLIED MECHANICS**

*Prikladnaya Mekhanika*  
Vol. 20, 1984 (12 issues) ..... \$520

**SOVIET ATOMIC ENERGY**

*Atomnaya Energiya*  
Vols. 56-57, 1984 (12 issues) ..... \$560

**SOVIET JOURNAL OF GLASS PHYSICS AND CHEMISTRY**

*Fizika i Khimiya Stekla*  
Vol. 10, 1984 (6 issues) ..... \$235

**SOVIET JOURNAL OF NONDESTRUCTIVE TESTING**

*Defektoskopiya*  
Vol. 20, 1984 (12 issues) ..... \$615

**SOVIET MATERIALS SCIENCE**

*Fiziko-khimicheskaya Mekhanika Materialov*  
Vol. 20, 1984 (6 issues) ..... \$445

**SOVIET MICROELECTRONICS**

*Mikroelektronika*  
Vol. 13, 1984 (6 issues) ..... \$255

**SOVIET MINING SCIENCE**

*Fiziko-tehnicheskie Problemy Razrabotki Poleznykh Iskopaemykh*  
Vol. 20, 1984 (6 issues) ..... \$540

**SOVIET PHYSICS JOURNAL**

*Izvestiya Vysshikh Uchebnykh Zavedenii, Fizika*  
Vol. 27, 1984 (12 issues) ..... \$520

**SOVIET POWDER METALLURGY AND METAL CERAMICS**

*Poroshkovaya Metallurgiya*  
Vol. 23, 1984 (12 issues) ..... \$555

**STRENGTH OF MATERIALS**

*Problemy Prochnosti*  
Vol. 16, 1984 (12 issues) ..... \$625

**THEORETICAL AND MATHEMATICAL PHYSICS**

*Teoreticheskaya i Matematicheskaya Fizika*  
Vol. 58-61, 1984 (12 issues) ..... \$500

**UKRAINIAN MATHEMATICAL JOURNAL**

*Ukrainskii Matematicheskii Zhurnal*  
Vol. 36, 1984 (6 issues) ..... \$500

**Send for Your Free Examination Copy**

**Plenum Publishing Corporation, 233 Spring St., New York, N.Y. 10013**

**In United Kingdom: 88/90 Middlesex St., London E1 7EZ, England**

Prices slightly higher outside the U.S. Prices subject to change without notice.

# JOURNALS IN THE PHYSICAL MATHEMATICAL SCIENCES

1

AVAILABLE IN ENGLISH TRANSLATION

**ALGEBRA AND LOGIC***Algebra i Logika*

Vol. 23, 1984 (6 issues) ..... \$360

**ASTROPHYSICS***Astrofizika*

Vol. 20, 1984 (4 issues) ..... \$420

**AUTOMATION AND REMOTE CONTROL***Avtomatika i Telemekhanika*

Vol. 45, 1984 (24 issues) ..... \$625

**COMBUSTION, EXPLOSION, AND SHOCK WAVES***Fizika Goreniya i Vzryva*

Vol. 20, 1984 (6 issues) ..... \$445

**COSMIC RESEARCH***Kosmicheskie Issledovaniya*

Vol. 22, 1984 (6 issues) ..... \$545

**CYBERNETICS***Kibernetika*

Vol. 20, 1984 (6 issues) ..... \$445

**DIFFERENTIAL EQUATIONS***Differentsial'nye Uravneniya*

Vol. 20, 1984 (12 issues) ..... \$505

**DOKLADY BIOPHYSICS***Doklady Akademii Nauk SSSR*

Vols. 274-279, 1984 (2 issues) ..... \$145

**FLUID DYNAMICS***Izvestiya Akademii Nauk SSSR,**Mekhanika Zhidkosti i Gaza*

Vol. 19, 1984 (6 issues) ..... \$500

**FUNCTIONAL ANALYSIS AND  
ITS APPLICATIONS***Funktsional'nyi Analiz i Ego Prilozheniya*

Vol. 18, 1984 (4 issues) ..... \$410

**GLASS AND CERAMICS***Steklo i Keramika*

Vol. 41, 1984 (6 issues) ..... \$590

**HIGH TEMPERATURE***Teplofizika Vysokikh Temperatur*

Vol. 22, 1984 (6 issues) ..... \$520

**HYDROTECHNICAL CONSTRUCTION***Gidrotekhnicheskoe Stroitel'stvo*

Vol. 18, 1984 (12 issues) ..... \$385

**INDUSTRIAL LABORATORY***Zavodskaya Laboratoriya*

Vol. 50, 1984 (12 issues) ..... \$520

**INSTRUMENTS AND  
EXPERIMENTAL TECHNIQUES***Pribory i Tekhnika Eksperimenta*

Vol. 27, 1984 (12 issues) ..... \$590

**JOURNAL OF APPLIED MECHANICS  
AND TECHNICAL PHYSICS***Zhurnal Prikladnoi Mekhaniki i Tekhnicheskoi Fiziki*

Vol. 25, 1984 (6 issues) ..... \$540

**JOURNAL OF APPLIED SPECTROSCOPY***Zhurnal Prikladnoi Spektroskopii*

Vols. 40-41, 1984 (12 issues) ..... \$540

**JOURNAL OF ENGINEERING PHYSICS***Inzhenerno-fizicheskii Zhurnal*

Vols. 46-47, 1984 (12 issues) ..... \$540

**JOURNAL OF SOVIET LASER RESEARCH***A translation of articles based on the best Soviet research in the  
field of lasers*

Vol. 5, 1984 (6 issues) ..... \$180

**JOURNAL OF SOVIET MATHEMATICS***A translation of Itogi Nauki i Tekhniki and Zapiski**Nauchnykh Seminarov Leningradskogo Otdeleniya**Matematicheskogo Instituta im. V. A. Steklova AN SSSR*

Vols. 24-27, 1984 (24 issues) ..... \$1035

**LITHOLOGY AND MINERAL RESOURCES***Litologiya i Poleznye Iskopaemye*

Vol. 19, 1984 (6 issues) ..... \$540

**LITHUANIAN MATHEMATICAL JOURNAL***Litovskii Matematicheskii Sbornik*

Vol. 24, 1984 (4 issues) ..... \$255

**MAGNETOHYDRODYNAMICS***Magnitnaya Gidrodinamika*

Vol. 20, 1984 (4 issues) ..... \$415

**MATHEMATICAL NOTES***Matematicheskie Zametki*

Vols. 35-36, 1984 (12 issues) ..... \$520

continued on inside back cover